

EFFECT OF ASPHALTENES ON THE
PERFORMANCE OF HDS CATALYSTS
USED IN GRADED BEDS

By

RAUL ADARME
//

Diploma of Chemical Engineering
Industrial University of Santander
Bucaramanga, Colombia
1983

Master of Science
Oklahoma State University
Stillwater, Oklahoma
1986

Submitted to the Faculty of the
Graduate College of the
Oklahoma State University
in partial fulfillment of
the requirements for
the degree of
DOCTOR OF PHILOSOPHY
December, 1989

1989, 1989, 1989, 1989

Thesis
1989D
A221e
cop. 2

EFFECT OF ASPHALTENES ON THE
PERFORMANCE OF HDS CATALYSTS
USED IN GRADED BEDS

Thesis Approved:

M M Johnson

Thesis Adviser

E L Eugene II

D. J. Stego

Horacio A Mottola

Arund H. Johannes

Darryl L Foutch

Norman N. Durham

Dean of the Graduate College

ACKNOWLEDGMENTS

I wish to express my appreciation to all the people that made this project and this degree possible. I am specially indebted to my advisor Dr. Marvin M. Johnson for his enlightening ideas and cooperation in all the stages of the program, for his friendship, patience, and support. Also, I am mostly grateful to Dr. Ed Sughrue for his invaluable guidance in the project, for introducing me into the meaning of industrial research and for his cooperation and understanding. Special thanks to Dr. Arland H. Johanness, Dr. Gary L. Foutch, Dr. Daniel J. Strobe, and Dr. Horacio A. Mottola for their valuable assistance as members of the advisory committee.

A special note of thanks to Oklahoma State University and Phillips Petroleum Co. for the financial support that made this project possible. I am indebted to all of my professors at Oklahoma State University for their valuable contribution to my education.

Thanks are due to all the people in Phillips that were involved in the project. To Alan Witt and Kendall Smith for the excellent operation of the reactor equipment, to Mary Little for the plasma analysis of so many samples, to Dean Phillips for working with me in the microprobe analysis on

the catalysts samples and for his friendly help, to Dr. Charlie Lord for the guidance during the operation of the LC-ICP equipment, to Sue Grayson and Bobby Dodd for all the help and good times in the laboratory. I am grateful to a number of professionals in the Phillips Catalyst Laboratory section: Larry Lew, Dee Johnston, Art Aldag, Dennis R. Kidd, Frank N. Lin, Steve L. Parrott, Mike M. Briggs, Alan Eastman, Patricia A. Tooley and the whole group of technicians for their great help and friendship that made my stay at the Phillips R&D Center so enjoyable.

I dedicate this thesis specially to my wife Maribel who inspired and understood the meaning of this work. She has been a great companion and a believer in my abilities. She always encourages me to keep moving even when things do not seem to go in the right direction. Her love, friendship and cooperation is invaluable to me. My parents Efrain and Mery and my brothers and sisters always supported and motivated me, so this work is also dedicated to them. Great friends like Hassan, Ricardo, Anoushtakin, Erardo and Martha, Edgardo and Gloria, Raul and Claudia, Gabriel and Melissa made the duration of this work joyful. I extend my sincere gratitude and friendship to them and so many others who are not explicitly named here but are sincerely appreciated.

TABLE OF CONTENTS

Chapter	Page
I. INTRODUCTION/LITERATURE REVIEW.	1
Graded Beds.	1
Hydrodemetallization vs. Hydrodesulfurization Activity . . .	4
Commercial Applications	5
Severity of Operation	5
Catalyst Deactivation.	7
Deactivation by Metals and Coke . . .	7
Metals Deposition Profile and Distribution Factor	10
Deactivation Models	14
Characterization of Residua.	20
Asphaltenes	23
Asphaltenes Reactions	26
Objectives and Strategy.	34
II. EXPERIMENTAL AND ANALYTICAL PROCEDURES.	38
Experimental Technique	38
Oil Analyses	41
Plasma Analyses	41
Liquid Chromatography with Inductively Coupled PLasma (LC-ICP) Detector Analyses	41
Asphaltenes Precipitation	41
Catalyst Analyses.	43
Soxhlet Extraction.	43
Electron Scanning Microprobe.	43
Feedstock.	46
Fresh Catalyst	50
III. EXPERIMENTAL RESULTS.	52
Description and Results from Reactor Experiments.	52
Hondo Experiments	55
Oriente Experiments	60
Caño Limon Experiments.	63
Asphaltenes Determination.	71
Analyses of Catalyst	71
Distribution Factors.	74

Chapter	Page
Results from Hg Porosimetry	
Analyses	78
LC-ICP Results	79
IV. DISCUSSION OF RESULTS	87
Asphaltenes Conversion and HDM	87
Interaction of Thermal and Catalytic	
Metals Removal	92
Qualitative Solution of Modified Delaware	
Mechanism.	98
Catalyst Deactivation.	104
Deactivation for Hondo Tests	104
760-710 Results.	104
710-710 Results.	105
Activity for Different Residues.	109
Discussion of Microprobe Results	116
LC-ICP Results Modelling	116
V. CONCLUSIONS AND RECOMMENDATIONS	134
Conclusions.	134
Recommendations	136
BIBLIOGRAPHY.	138
APPENDIXES.	144
APPENDIX A - REACTOR EXPERIMENTAL DATA.	145
APPENDIX B - MICROPROBE DATA.	160

LIST OF TABLES

Table	Page
1. Effect of Crude Source on Metal Penetration Factor.	12
2. Typical Residue Properties.	21
3. Properties of Asphaltenes	24
4. Hondo Properties.	47
5. Oriente Properties.	48
6. Caño Limon Properties	49
7. VPO MW and NMR Properties of Asphaltenes.	51
8. Numbers for each Run.	53
9 Asphaltene Content (wt%) as Function of Reactor Conditions.	72
10. Analytical Results for Middle Zone Catalysts.	73
11. Qv at Different Metals Loading.	75
12 Average penetration Factors	77
13. Results from Statistic Analysis	77
14. Spent Catalyst Properties	78
15. Average Percent HDM Conversion as Function of Reaction Conditions	88
16. Percent Asphaltene Conversion as Function of Reaction Conditions	90
17. Vanadium Concentration in Asphaltenes	93
18. Kinetic Equations and Analytical Solution for Asphaltene Decomposition Model.	99
19. Fitting Model Parameters for Hondo, Oriente and Caño Limon.	131

Table	Page
20. Activity Data for Run 01.	148
21. Activity Data for Run 02.	149
22. Activity Data for Run 03.	150
23. Activity Data for Run 04.	151
24. Activity Data for Run 05.	152
25. Activity Data for Run 06.	153
26. Activity Data for Run 07.	154
27. Activity Data for Run 08.	155
28. Activity Data for Run 09.	156
29. Activity Data for Run 10.	157
30. Activity Data for Run 11.	159
31. Sample of Microprobe Data for Run 03.	163
32. V/Al ₂ O ₃ Values for Run 01, Hondo 10%, 760-710, Top of Bed	165
33. V/Al ₂ O ₃ Values for Run 01, Hondo 10%, 760-710, Bottom of Bed	166
34. V/Al ₂ O ₃ Values for Run 02, Hondo 10%, 710-710, Top of Bed	167
35. V/Al ₂ O ₃ Values for Run 02, Hondo 10%, 710-710, Bottom of Bed	168
36. V/Al ₂ O ₃ Values for Run 03, Hondo 5%, 760-710, Top of Bed	169
37. V/Al ₂ O ₃ Values for Run 03, Hondo 5%, 760-710, Bottom of Bed	170
38. V/Al ₂ O ₃ Values for Run 04, Hondo 5%, 710-710, Top of Bed	171
39. V/Al ₂ O ₃ Values for Run 04, Hondo 5%, 710-710, Bottom of Bed	172
40. V/Al ₂ O ₃ Values for Run 06, Oriente 5%, 760-710, Top of Bed	173
41. V/Al ₂ O ₃ Values for Run 06, Oriente 5%, 760-710, Bottom of Bed	174

Table	Page
42. V/Al ₂ O ₃ Values for Run 07, Oriente 5%, 710-710, Top of Bed	175
43. V/Al ₂ O ₃ Values for Run 07, Oriente 5%, 710-710, Bottom of Bed	176
44. V/Al ₂ O ₃ Values for Run 09, Caño Limon 5%, 760-710, Top of Bed	177
45. V/Al ₂ O ₃ Values for Run 09, Caño Limon 5%, 760-710, Bottom of Bed	178
46. V/Al ₂ O ₃ Values for Run 10, Caño Limon 5%, 710-710, Top of Bed	179
47. V/Al ₂ O ₃ Values for Run 10, Caño Limon 5%, 710-710, Bottom of Bed	180

LIST OF FIGURES

Figure	Page
1. Representation of a Graded Bed for Residua Hydrotreating	3
2. Catalyst Deactivation as Function of Pore Size.	9
3. Cross Sectional View of an Asphaltene Model . .	27
4. Mechanism of Asphaltene Cracking	33
5. Diagram of the Hydrotreating Unit	39
6. Schematic of Experimental Conditions.	54
7. HDT Results for Run 01.	57
8. HDT Results for Run 02.	58
9. HDT Results for Run 03.	59
10. HDT Results for Run 04.	61
11. HDT Results for Run 05.	62
12. HDT Results for Run 06.	64
13. HDT Results for Run 07.	65
14. HDT Results for Run 08.	66
15. HDT Results for Run 09.	68
16. HDT Results for Run 10.	69
17. HDT Results for Run 11.	70
18. LC-ICP Molecular Size Distribution for Vanadium in a Hondo Residue	80
19. Molecular Size Distribution of V for Hondo as function of Reaction Conditions.	81
20. Molecular Size Distribution of V for Oriente as Function of Reaction Conditions.	83

Figure	Page
21. Molecular Size Distribution of V for Caño Limon as Function of Reaction Conditions. . .	85
22. HDM vs Asphaltene Conversion for Catalytic and Thermal Tests	91
23. Molecular Size Distribution of V for Hondo at Thermal Conditions	95
24. Mechanism for Asphaltene Decomposition	97
25. Asphaltene Conversion and Coking Tendency for Hondo	101
26. Asphaltene Conversion and Coking Tendency for Caño Limon.	102
27. Asphaltene Conversion and Coking Tendency for Oriente	103
28. HDM Activity for Hondo (Runs 01 and 03)	106
29. HDS Activity for Hondo (Runs 01 and 03)	107
30. HDM Activity for Hondo (Runs 02 and 04)	108
31. HDS Activity for Hondo (Runs 02 and 04)	109
32. HDM Activity for Hondo, Oriente and Caño Limon (Runs 04, 07 and 10).	111
33. HDM Activity for Hondo, Oriente and Caño Limon (Runs 03, 06 and 09).	112
34. HDS Activity for Hondo, Oriente and Caño Limon (Runs 04, 07 and 10).	113
35. HDM Activity for Hondo, Oriente and Caño Limon (Runs 03, 06 and 09).	114
36. Equations Representing the Asphaltene Decomposition Model	118
37. Model Fit of LC-ICP Data Using Diffusion-Reaction Only	122
38. Model Fit of Product from Pretreatment Reactor for Hondo	123
39. Model Fit of Product from Up-Flow Reactor at 710F for Hondo	124

Figure	Page
40. Model Fit of Product from Up-Flow Reactor at 760F Thermal - 710F Catalytic for Hondo.	125
41. Model Fit of Product from Pretreatment Reactor for Oriente	126
42. Model Fit of Product from Up-Flow Reactor at 710F for Oriente	127
43. Model Fit of Product from Pretreatment Reactor for Caño Limon.	128
44. Model Fit of Product from Up-Flow Reactor at 710F for Caño Limon.	129
45. Model Fit of Product from Up-Flow Reactor at 760F Thermal - 710F Catalytic for Caño Limon.	130

CHAPTER I

INTRODUCTION/LITERATURE REVIEW

Residual oil hydrotreating has become an important front end process in commercial oil upgrading schemes because of tighter environmental regulations and the continuing trend toward processing heavier crudes. Hydrotreating (HDT) allows the conversion of the bottom of the barrel into suitable feedstock for downstream processes such as fluid catalytic cracking (FCC) or heavy oil cracking (HOC). During hydrotreating, residual oil reacts catalytically over a fixed bed reactor in the presence of hydrogen at high temperatures and pressures. The general objective of HDT is the removal of sulfur, nitrogen, and metals (mainly Ni and V) coupled with a reduction in carbon residue to reduce catalyst deactivation and to improve yields in the downstream processes.

Graded Beds

Extensive research efforts directed towards the improvement of HDT technology have resulted in increased flexibility of refineries to process different feedstocks. As a result, the refiner of today has a better range of catalysts and reactor systems available. It is widely

recognized that catalyst activity is a function of promoter-loading and pore size distribution. Small pore, high promoter-loading catalysts show good removal rates for sulfur whereas large pore, low promoter-loading catalysts display good tolerance for metals deposition but limited activity for sulfur removal. The availability of new "tailor-made" catalysts allows refiners to configure or grade their catalyst beds for better performance. Figure 1 is a general representation of a hydrotreating unit which can be several reactors in series. The top of the unit is loaded with a large pore, low promoted catalyst that has high tolerance for metals deposition but low activity for sulfur removal. The catalyst in the next section, known as a transition catalyst, has smaller pore diameter, slightly higher level of promoters, still acceptable tolerance for deposition of metals and somewhat better activity for hydrodesulfurization (HDS). The last section is loaded with a small pore, high surface area, and highly promoted catalyst that has high activity for HDS but is more sensitive towards deactivation by deposition of metals. With this catalyst combination in graded beds, large pore catalysts with low HDS activity and high metals capacity at the top of the reactor protect the small pore catalysts having high HDS activity and low metals tolerance at the bottom part of the reactor by avoiding pore plugging of the active small pores and taking advantage of the metals

HYDROTREATER

CATALYST LOADING

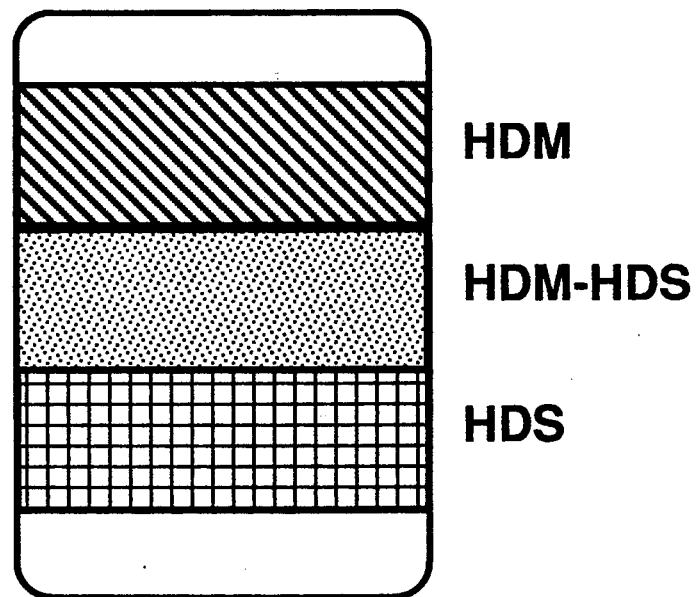


Figure 1. Representation of a Graded Bed for Residua Hydrotreating

capacity of large pores. (Jacobsen et al., 1983; Hannerup and Jacobsen, 1983).

Hydrodemetallization vs. Hydrodesulfurization

Activity

Using graded beds, HDT can be adapted to upgrade different feeds or to obtain a certain degree of desulfurization and/or demetallization. HDS activity correlates with catalytic metals present in the micropore structure, 5 to 15 nm diameter, whereas hydrodemetallization (HDM) correlates with mesopore structure, 10 to 50 nm diameter (Christman et al., 1985). So, graded beds allow a balance between metals removal and HDS activity. This balance results in higher conversion and longer run length. Activity of the bed decreases for HDM and increases for HDS from top to bottom of the reactor (Higashi et al., 1985; Gibson et al., 1983).

Optimum catalyst combination depends on feedstock, operating conditions, and catalyst properties. A rule of thumb uses dual catalyst systems for residua having 25-50 ppm metals, and triple catalyst beds when the metals are in the range of 50-100 ppm. When metals are higher than 100 ppm, on stream catalyst replacement is advised (Kwant et al., 1984). Jacobsen et al. (1983) found that at lower pressures, higher severity, a triple catalyst system with an intermediate transition catalyst is better than a dual

system of large and small pore catalyst. As mentioned before, the best conditions depend on particular applications. Experience in actual commercial or pilot plant operation with the same type of feedstock is usually required to make the correct selection.

Commercial Applications

Commercial applications of graded beds include Exxon RESIDfining process, UNOCAL Unicracking/RDS process, Shell's RDS process, UOP's RCD/BOC Unibon, and Chevron/Gulf RDS/VRDS/RHDS process (Shah et al., 1979; Hydrocarbon Processing, 1984; Kwant et al., 1984; Sikonia, 1980; Howell et al., 1985). In some applications HDM catalyst placed in a guard reactor, as in the RESIDfining process, can be replaced without disturbing the system by bypassing the feed around the guard bed (Shah et al., 1979).

Severity of Operation

The selection of operating conditions relies on the degree of HDS and HDM desired, the expected catalyst performance, and the type of feedstock. Typically, pressure ranges from 5.5 to 20.7 MPa (800 to 3,000 psig). At low operating pressure and higher temperatures cracking and coking reactions are promoted whereas HDM and HDS activities are reduced. On the other hand, increasing pressure results in higher deactivation by metals deposited

on the catalyst (Sakabe and Yagi, 1979; Tamm et al., 1981; Pazos et al., 1983).

In practice, HDT units do not operate at constant temperature. The temperature is progressively increased to offset catalyst deactivation and to maintain constant HDS or HDM activity. Reaction severity determines the start of run (SOR) temperature (Nielsen et al., 1981; Tamm et al., 1981). On the other hand, typical end of run (EOR) values range from 400⁰ to 440⁰C (758⁰ to 824⁰F) and are limited by changes in product properties, and/or metallurgy restrictions. At the higher EOR temperatures, thermal cracking and other undesired reactions accelerate catalyst deactivation by increasing coke deposition (Jacobsen et al., 1983; Hohnholt and Fausto, 1985).

Reported Liquid Hourly Space Velocities (LHSV) are in the range from 0.2 to 3.0 h⁻¹. Brunn et al. (1975) observed a decrease in deactivation with increasing LHSV. For heavier feeds and deep desulfurization lower LHSV's are required to sustain adequate HDS (Hohnholt and Fausto, 1984). The hydrogen consumption in residua HDT depends on activity and selectivity of the catalyst, temperature, and hydrogen partial pressure. The hydrogen consumption range from 53.4 to 267 standard m³ H₂/m³ oil, and the corresponding rates from 890 to 1,780 standard m³ H₂/m³ oil, respectively (Ebel, 1972; Brunn et al., 1975; Billon et al., 1977; Nielsen et al., 1981; Van Driesen et al., 1985).

Catalyst Deactivation

It is recognized that catalyst activity is a tradeoff between decreasing surface area and increased rates of diffusion as average catalyst pore diameter increases. However, all catalysts deactivate during hydroprocessing and the way they deactivate determines the useful life of the catalyst beds. For fixed-bed commercial operations long catalyst life, typically a year, is important. The catalyst life, or the way the catalyst deactivates depends heavily on the feed choice, the severity of operation and the feed properties.

Deactivation by Metals and Coke

Deactivation is commonly attributed to both coke and metals deposition. Coking reactions are associated with decomposition and condensation of heavy asphaltenic molecules, whereas metals deposition relates well to reaction of organometallic compounds. Coke is thought to be important primarily during the first 100 h of the run whereas metals deposition is more important during long term deactivation (Agrawal and Wei, 1984). The coke deposited diminishes the activity of the active sites and reduces the catalyst pore volume needed for metals accumulation.

Metal deposits cause deactivation by two mechanisms: coverage of the active catalytic metals reducing the

activity of the catalyst surface, and pore mouth plugging decreasing the reactant's rate of diffusion within the catalyst pores (Tamm et al., 1981; Ahn and Smith, 1984). Surface poisoning and pore plugging are distinct but not independent mechanisms. The more extensive the surface poisoning the more gradual the pore plugging may be (Tamm et al., 1981; Newson, 1975).

As expected, catalyst deactivation is a function of catalyst pore size. For small pore catalysts, metals deposit predominately on the external surface of the catalyst causing little internal surface poisoning, but pore mouth plugging. On the other hand, penetration is deeper with large pores. Thus, large pore HDT catalysts usually take longer to deactivate by pore plugging (Pazos et al., 1983).

Figure 2 illustrates how a hydrotreater operates to maintain a given degree of desulfurization. An increase in temperature is used to offset the reduction in catalyst activity. Small pore catalysts require an exponential increase of temperature with time. This is a representation of pore mouth poisoning. They maintain high activity longer because they do not see initial surface poisoning (no metals penetration). On the other hand, large pore catalysts follow three well defined periods of deactivation:

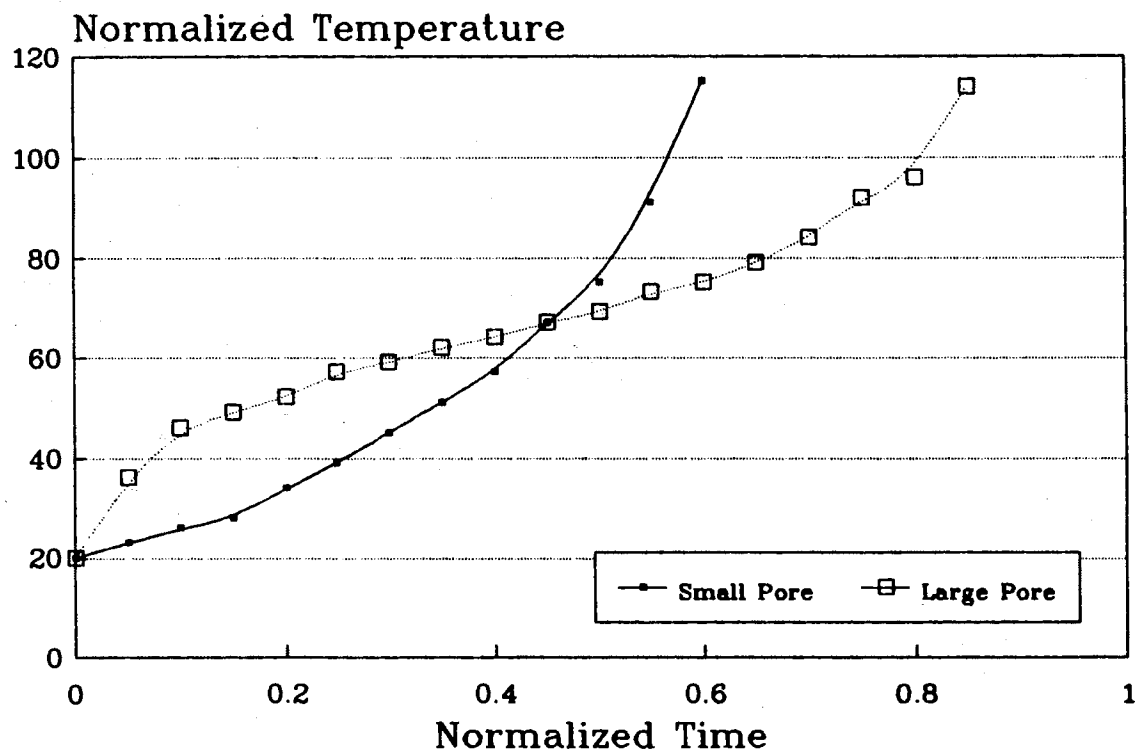


Figure 2. Catalyst Deactivation as Function of Pore Size

1. Initially, a rapid deactivation attributed to surface poisoning by metals and coke (Tamm et al., 1981; Hannerup and Jacobsen, 1983).
2. After that, a more gradual deactivation caused by moderate plugging of the pores by feed metals. The build up of metal sulfides within the pores reduces the rate of diffusion of metal-containing molecules. This determines the metal distribution in the catalyst particles (Sie, 1980; Pazos et al., 1983; Hannerup and Jacobsen, 1983).
3. Finally, a fast deactivation period. This accelerated deactivation near the end of the run occurs when the reduced pore size approaches the size of the molecules and hindered diffusion becomes more important. Periods 2 and 3 represent the pore plugging mechanism of deactivation.

In fixed beds the final deactivation occurs as a wave moving downwards from the reactor inlet. The top of the bed is plugged first and, as a result, more and more metals are able to reach the lower portions of the catalyst bed (Sie, 1980; Beuther et al., 1980).

Metals Deposition Profile and Distribution Factor

New and sophisticated analytical techniques, such as Electron Microprobe have been applied to HDT to obtain a

more accurate picture of the catalyst-feedstock interaction. From electron microprobe results Tamm et al. (1981) defined a distribution factor (Q_v) for cylindrical catalysts as:

$$Q_v = \frac{\int_0^r M(r) r dr}{M_{\max} \int_0^r r dr} = \frac{\text{average metal concentration}}{\text{maximum metal concentration}}$$

This distribution factor is analogous to the effectiveness factor for the run and relates to effective use of the catalyst capacity for metals deposition. High distribution factors represent high penetration (more uniform distribution) of metals deposited in the pores. On the other hand, low values of Q_v indicate low penetration of the metals deposited. Therefore, catalysts with low distribution factors deactivate mainly by the pore plugging mechanism. This distribution factor can take values from zero to one. A value of one represents an even radial distribution of metals throughout the catalyst while a value close to zero is characteristic of deposits concentrated on the mouth of the pores.

Table 1 summarizes the distribution parameter values reported for several residua. These values indicate that deposition profiles are a function of the crude source because of differences in reactivity of the metal-bearing molecules from crude to crude. The data from Table I suggest that a catalyst processing Maya, $Q_v = 0.23$,

deactivates more by pore plugging than by active surface poisoning (small penetration). Conversely, a catalyst treating Kern River, $Q_v = 0.52$, loses more activity by surface poisoning than by pore plugging (high penetration).

TABLE 1
EFFECT OF CRUDE SOURCE ON METAL PENETRATION FACTOR

Crude Source	Distribution Factor Q_v
Maya	0.23
Manifa/Ratawi	0.23
Kuwait	0.25
Arabian Heavy	0.31 0.33 ^a
North Slope	0.38 0.48 ^a
Kern River	0.52

^a The Q_v values are reported by Hung et al. (1986). The values indicated by ^a are reported by Tamm et al. (1981).

There is little literature available relating Q_v to axial position within catalyst beds. Tamm et al. (1981) studied an Arabian Heavy residuum and reported that Q_v decreases from inlet to outlet of reactor at the start-of-run (SOR). But, at the end-of-run the inlet Q_v decreases

approaching the value for the outlet which is fairly constant with time on stream. Asaoka et al. (1987) also reported a decrease in metal deposits along the reactor axis. On the other hand, Hung et al. (1986) observed an increase in the vanadium distribution factor from inlet to outlet of the reactor while processing Maya residuum. Using model compounds Agrawal and Wei (1984) reported a maximum vanadium deposition at interior positions along the reactor axis. Even though different publications disagree on the direction of the axial variation of Q_v , the information available suggests that the distribution parameter is a function of the feed source, pore size distribution of the catalyst, time on stream, and location in the catalyst bed.

The maximum metal concentration is usually at the catalyst surface. However, Tamm et al. (1981) reported maximum concentration inside the catalyst and explained it as HDM promoted by the presence of H_2S in the reacting stream. Asaoka et al. (1987) also reported a decrease in metal deposits towards the pellet center. Ware and Wei (1985) observed radial profiles with internal maxima at the reactor entrance shifting to the external maxima at the reactor outlet. They explain this by consecutive HDM reactions in which the metal-containing compounds must go through an intermediate before they deposit on the catalyst internal surface. At the reactor outlet there is usually a sufficient concentration of intermediates in the oil that

readily deposit near the entrance of the catalyst pores and Q_v is usually low.

Deactivation Models

Numerous models have been developed to simulate and quantify the HDM and HDS reactions and catalyst deactivation in residua HDT. These models are important tools for prediction of catalyst life and for catalysts and processes optimization and development. They also contribute to the understanding of deactivation by metals and coke deposition in porous catalysts. Diffusion theory has been the basis for the development of most of the models available today. Diffusion limitations are inherent to the process since the diameter of the metal-bearing molecules is comparable to the diameter of the catalyst pores common in HDT operations. These molecules must diffuse inside the pores before they react depositing the metals as sulfides on the catalyst surface and converting sulfur containing molecules to H_2S and hydrocarbons.

Configuration of Pores. The physical configuration of the pores is complex and the analytical tools required to uncover important characteristics of the porous structures do not exist at this stage in the development. Therefore any assumptions taken in this area are difficult to test. The approach taken to represent the pore size distribution of the catalyst varies from a simple single pore or

assembly of parallel pores (Newson, 1975) to more complicated stochastic representations such as random networks of pores (Gonzalez and Galiasso, 1983; Reyes and Jensen, 1985).

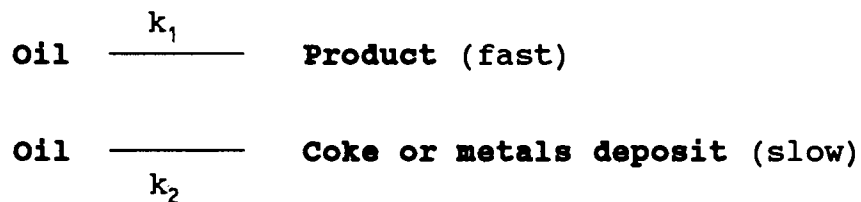
Other approaches taken to represent pores configuration include nonintersecting pores with variable pore lengths and bidispersed structured catalysts to analyze the effects of macro and micro-pores (Rajagopalan and Luss, 1979; Leung and Haynes, 1984). Tsakalis et al. (1984) used two pore structure models: single pore and parallel bundle of pores to study the effect of pore size distribution on deactivation.

Intrinsic Activity and Deactivation Mode. Another aspect in modelling is to visualize how the deposition of metals and coke affect the activity for sulfur and metals removal. Most of the models neglect the effect of coke on activity or consider it as a fixed effect, applicable only to the initial deactivation period. However, Leung and Haynes (1984) found coke deposition to be the main cause of deactivation when applying their model to coal liquefaction. Pazos et al. (1983) correlated experimental data on deactivation and concluded that deactivation by coke correlates with the physical properties of the catalyst whereas deactivation by metals correlate better with the increased diffusion restrictions.

Nitta et al. (1980) assumed that both the effective

surface areas for HDS and HDM and the effective diffusivity of the sulfur and metal compounds are reduced by the deposition of metals and coke. They included coking as a reversible reaction in their deactivation model. Deactivation by metals deposition is modeled as surface coverage and/or pore plugging. Newson (1975) presented the first model using pore plugging. He showed that the size of the pores had a great impact on catalyst life. Rajagopalan and Luss (1979), using a more rigorous approach, incorporated in their model the effects of pore plugging and active site poisoning. They considered intrinsic activity unaffected by surface coverage. Prediction of catalyst life was based on the rate of demetallization, including the influence of pore size.

Other investigators considered that effective surface area and effective diffusivity of reactants decrease, proportionally to the total amount of metals and coke deposited (Nitta et al., 1979; Kodama, 1980; Leung and Haynes, 1984). Yorstos and Tsotsis (1984) found that pore blockage can be more detrimental to catalyst life than site coverage using a parallel poisoning mechanism in their model. Other authors (Tsakalis et al., 1984; Leung and Haynes, 1984) also use the parallel type deactivation in their models. In this mechanism the main reaction occurs simultaneously with the poisoning reaction:



Ahn and Smith (1984) expanded previous deactivation models assuming two deactivation rates: a fast initial surface-deactivation due to progressive poisoning from the pore mouth to the interior of the pore and a slow deactivation due to physical deposition of metal products which eventually lead to pore plugging. The initial fast deactivation step makes the model more realistic. The model was restricted to isothermal operation and a uniform pore size distribution.

Diffusion and Reaction Representation. The reduction in pore size due to deposition of metal sulfides and coke increases the resistance to the diffusion of the reactants inside the pores. Spry and Sawyer (1975) developed an expression that relates the effective diffusivity to the bulk diffusivity and the ratio of molecular diameter to pore diameter:

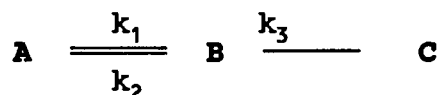
$$D_e = \epsilon_p D_0 / \Gamma * (1 - r_m / r_p)^4 \quad (1)$$

where D_e is the effective diffusivity under transport restrictions, D_0 is the bulk diffusivity, ϵ_p is the catalyst

particle porosity, Γ is the tortuosity factor and r_m / r_p is the ratio of molecule to pore size.

Reaction Kinetics. Because of the complexity and the large number of reactions occurring in hydrotreating, the most common approach is to lump the reactions and assume overall kinetics for the system. The assumptions range from first order kinetics for HDM and HDS (Ahn and Smith, 1984) to second order kinetics for both HDM and HDS (Nitta et al., 1979; Kodama, 1980). The validity of these assumptions has been tested experimentally to a certain degree but the issue is not settled yet. For instance Inoguchi et al. (1971) reported both first and second order kinetics for HDM of Kuwait and Khafji atmospheric residua, Galiasso et al. (1985) hydrotreated resin and asphaltene fractions from a Jobo crude and represented the HDM process by first order kinetics for both fractions and for vanadium and nickel.

Agrawal and Wei (1984) and Ware and Wei (1985) used more complicated kinetics and proposed a theory of coupled, multicomponent first order reaction and diffusion. Instead of lumping the kinetics into a single reactant species they consider HDM as a sequential reaction in which the reactants go through an intermediate by a hydrogenation step before they can deposit on the catalyst:



With this mechanism implemented in the model they were able to predict the internal maxima observed experimentally for the metal deposition profile (Agrawal and Wei, 1984; Ware and Wei, 1985).

Catalyst life versus Penetration Factor. One important application of the model is to predict the useful catalyst life of an actual HDT operation. For this purpose, the model should correlate life with measurable properties of the catalyst, or include parameters that can be fit with experimental data. Following this line of applications Hannerup and Jacobsen (1983) developed a semi-empirical model that correlates catalyst activity to the metals deposited on the catalyst:

$$K_N(t) = K_{N0} [1 - (U_V(t)/U_{max})^2] \quad (2)$$

where K_{N0} is the normalized second order reaction rate constant for HDS after the initial deactivation period, $K_N(t)$ is the normalized rate constant at the time of the prediction, $U_V(t)$ is the amount of metals deposited on the catalyst by the time of interest, and U_{max} is the maximum catalyst capacity for deposition of metals. They defined U_{max} as the maximum amount of metals, relative to a unit mass of fresh catalyst, accumulated in a pellet until the catalyst's residual activity becomes zero. They related the parameters contained in the model to physical and chemical

properties of the catalyst. With the model expression given by eq. 2 they fit extensive experimental data for catalyst deactivation. They obtained a good fit for the deactivation curves after the initial deactivation period.

Toulhoat et al. (1987) included in their demetallization model a parameter named ultimate storage capacity (USC) of the catalyst which is equivalent to the parameter U_{\max} defined by Hannerup and Jacobsen (1983). Both groups of researchers presented equations to relate this parameter to measurable catalyst properties. Toulhoat et al. (1987) using their model predicted penetration factors and final metals uptake in agreement with experimental values from their CSTR experiments. Although there is a number of theoretically developed deactivation models, there is still a lack of experimental data to test them. Especially lacking are data related to HDT of residual oils. These data are important to test the validity and to improve existing models.

Characterization of Residua

The differences between residua can make a major impact on operation and catalyst life of residual oil hydrotreaters. When a large variety of crudes is available, selection of the best crudes to process is not a trivial task. Table 2 shows the large variation on bulk properties that have a critical effect on catalyst life. The sulfur

content varies between 2 and 6%, the metals content could be as high as 600 ppm or higher, as is the case for a few Latin American residua. Asphaltenes and carbon residue also have a wide range of variability and the same can be said for nitrogen. This large variation complicates the classification of residua by ease of processing. For example, a residuum that is low in sulfur and metals is likely to be easier to process than another that is high in sulfur and metals. However, it will be more difficult to rank two residua when the first is low in sulfur but high in metals and the other is low in metals but high in sulfur. Then other properties such as the level of asphaltenes or the aromaticity of the residua become important.

TABLE 2
TYPICAL RESIDUA PROPERTIES

Sulfur, wt%	2 - 6
Ni + V, ppm	100 - 600
Carbon Residue, wt%	5 - 15
Asphaltenes, wt%	5 - 25
Nitrogen, wt%	0.1 - 0.5

However, it has been found difficult to quantify the ease of processing residua based on bulk properties.

Dolbear et al. (1987) studied the hydrotreatment of five atmospheric residua at pilot plant scale and reported that there is no correlation of HDM and HDS activities with the feed sulfur or metal levels.

Hence, researchers have focused their efforts on new techniques of characterization. The oldest and most used technique focuses on the separation of the residuum into classes of compounds based on solubility. This separation describes the residua as a mixture of asphaltenes: benzene soluble and n-C₅ insoluble, maltenes: soluble in both n-C₅ and benzene, resins: n-C₅ soluble and propane insoluble, and oils: soluble in both n-C₅ and propane (Jewell et al., 1972; Yen, 1972; Murphy et al., 1979).

More recent characterization schemes provide information on molecular weight distributions and classification by compound class and acid-base relations rather than solubility class. New instrumentation such as the use of Wiped Film Still has measured boiling point distributions at higher temperatures such as 1300⁰F (Drushel, 1972; Boduszynski et al., 1985; McKay and Lathan, 1981).

One method that has received particular attention for determination of molecular size distribution of heteroatom contaminants is size exclusion liquid chromatography

directly interfaced with specific element detection by inductively coupled plasma (SEC-ICP) or by graphite furnace atomic absorption (SEC-GFAA). These techniques provide a size distribution of molecules containing elements such as V, Ni, and S. The technique has proven useful to follow how the heteroatom-containing molecules change size during hydroprocessing. This is extremely important in catalytic processes where the size of the pores creates a resistance to the diffusion of large molecules into the catalyst (Reynolds, 1985; Hausler and Carson, 1985; Sughrue et al., 1988). Other analytical techniques such as nuclear magnetic resonance (NMR), X-ray diffraction (XRD), small angle X-ray scattering (XRS), electron spin resonance (ESR), and vapor pressure osmometry (VPO), have also contributed to better heavy oils characterization.

Asphaltenes

Asphaltenes are the most difficult fraction to process. Research has shown that when the residua are hydrotreated at high conversions, the less reactive sulfur and metals (Ni and V) concentrate on the asphaltene fraction of the product (Speight, 1987; Le Page et al., 1987). Asphaltenes are complex large molecules or molecular aggregates dispersed in the oil. Table 3, from Baltus and Anderson (1983), summarizes asphaltene properties reported in the literature.

TABLE 3
PROPERTIES OF ASPHALTENES

5 to 20 wt% of petroleum residuum (b.p. > 600⁰F)
n-pentane (or n-heptane) insoluble
Soluble in benzene, toluene, tetrahydrofuran (THF)
Hydrogen/carbon atomic ratio: 1.0-1.2
Contain sulfur, nitrogen, oxygen and metals
Polydisperse: weight avg. MW >> number avg. MW
Microstructure (5-40 Å)
Macrostructure (40 -1000 Å)
Colloidal nature
Degree of subunit, molecular, association depends on
solvent, temperature, and asphaltene concentration.

Yan (1987) considers that asphaltenes are peptized and held in suspension, as a colloidal dispersion, in the oil phase by aromatic hydrocarbons and resins. Koots and Speight (1975) supported this by separating the asphaltene, maltene and oil fractions and recombining them. They showed that the asphaltene fraction was only soluble in the presence of the resin fraction.

From the information in Table 3, it is natural to infer that the heterogeneity and complexity of the

asphaltene molecules makes any characterization attempt difficult. The techniques used are highly sensitive to the conditions and reagents used.

Speight et al. (1984) reviewed several methods for asphaltene precipitation. They found that precipitant/oil ratio, precipitant-type and aging time influence the characteristics of the asphaltenes. They concluded that to obtain "stable" asphaltenes it is necessary to contact the oil for approximately 10 h with more than 30 mL of pentane or heptane per gram of oil.

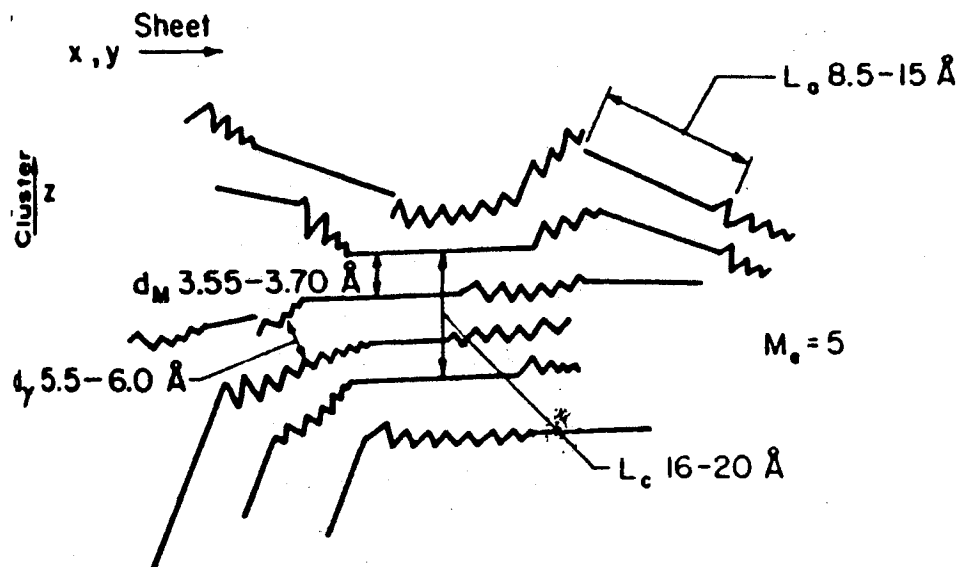
The determined average molecular weight of an asphaltene fraction is also sensitive to the analytical procedure used. Values reported range from 600 to 140,000 g/mole (Speight, 1980). Analogously, asphaltene diameters extend from 10^{-9} to 10^{-7} m (10 to 1000 Å). Molecular weights larger than 2000 are attributed to the association of asphaltenes into macromolecules or clusters.

Asphaltene Structure. Numerous investigations have been devoted to depicting the structure of asphaltenes. The complexity of asphaltenes has contributed to the existing controversy about their chemical structure. Despite the inherent limitations, researchers have proposed average asphaltene structures based on spectroscopic methods. Yen and Pollack proposed one asphaltene structure in 1961. Since then, it has been supported with minor modifications by many other investigators. On this basis, asphaltene

structures are defined as units with a large central polynuclear aromatic system linked by aliphatic, naphthenic, or heteroatomic functionalities. The perimeters of these aromatic sheets are highly substituted by similar moieties (Speight, 1981; Yen et al., 1979; Yen et al., 1984; Savage et al., 1988). An average of five to seven units form a macromolecule such as particles or micelles (Drushel, 1972; Yen, 1972; Shiroto et al., 1983). Figure 3 is a cross sectional view of an asphaltene model as proposed by Yen and coworkers. Straight lines symbolize the edge of flat sheets of continuous aromatic rings and the zig-zag lines represent saturated chains or groups of naphthenic rings (Dickie and Yen, 1967; Yen, 1972). However, recently Speight (1989) shows evidence of asphaltenes as distributions of molecular and functional types in a much more open, rather than highly condensed, structure.

Asphaltenes Reactions

Asphaltenes are extremely large molecules having effective diameters in the range of pore sizes common in HDT catalysts and larger. Thus, there must be a reduction in molecular size of asphaltenes before they can enter the pores to undergo catalytic HDM. Over the years HDM of residua has been considered basically a catalytic process. Nonetheless, thermal effects in HDM have recently received



Cross Sectional View of an Asphaltene Model



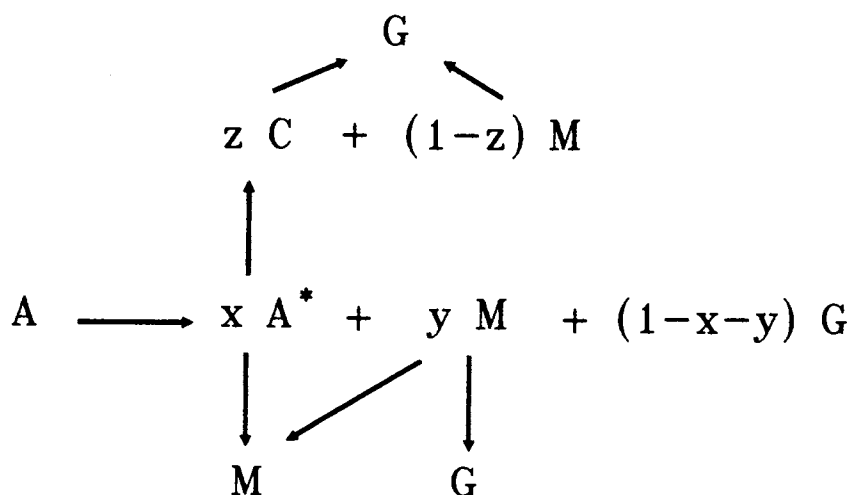
-  represents the zig-zag configuration of a saturated carbon chain or loose net of naphthenic rings
 represents the edge of flat sheets of condensed aromatic rings

Figure 3. Cross Sectional View of an Asphaltene Model

significant attention because they are associated with breakdown of large molecules and increased coke formation.

The mechanism of HDM is complex due to the different types and sizes of molecules involved. Because metals are concentrated on the asphaltenes, mechanisms for asphaltene decomposition are important in HDM of residua and heavy oils. Savage et al. (1988) propose a mechanism for asphaltene decomposition based on thermal and catalytic studies. Basically they consider that asphaltenes will decompose thermally into some intermediates, maltenes, and gases. The intermediates undergo catalytic hydrogenation to maltenes or they are thermally degraded into coke, additional maltenes and gases. The following is a diagram of the mechanism proposed by Savage and coworkers (1988):



Where A represents the asphaltene molecules, A* the intermediate asphaltenes, M the maltenes, G the gases, C the coke, and x, y, z the fractions.

Coking Reactions. Coke formation is associated with thermal decomposition of asphaltenes. Speight (1987) reviewed the literature on coke formation and described how initial coking reactions involve thermolysis of aromatic-alkyl bonds to produce volatile species (paraffins, olefins) and non-volatile species (aromatics). Nitrogen species were found to enhance the initial coking reactions. Secondary reactions for the formation of coke include aromatization of naphthenic species and condensation of the aromatic ring systems. Savage et al. (1988) agree that coke formation is a primary product of asphaltene thermolysis. They suggest that coke is formed by stripping the asphaltenic core of its hydrogen-rich peripheral substituents and perhaps by aromatizing the core. The presence of catalyst and solvents inhibits the formation of coke.

In HDM by coking, severity of operation is important. Reynolds et al. (1987) conclude that residence time over a wide range of severity at a given temperature and pressure affects the amount removed but has little effect on the size change of the molecules. They operated their experiments over a wide range of severity. Savage et al. (1988) studied the effects of H₂ donor and catalyst in the

pyrolysis of asphaltenes. In the absence of hydrogen they obtained high conversion of asphaltenes and also high yields of coke. When H₂ was present they observed a slower but more selective conversion to maltenes and also high yields of coke. Coke formation was inhibited in the presence of a catalyst which results in high conversion and high selectivity to maltenes.

Catalytic HDM. Catalytic HDT preferentially removes the metal-containing molecules in the size range of the catalyst pores. Reynolds et al. (1987) treated asphaltenes from several residua over small and large pore catalysts. They found that molecules that fit the pores are easily removed. As expected, removal of metals occurred in all size ranges for large pore catalysts. They concluded that catalytic treatment depends heavily on pore size distribution and that the molecules bigger than catalyst pores require a different demetallization mechanism. Additionally, Carbognani et al. (1987) suggest that, rather than total metals, the distribution according to molecular size may control the degree of HDM.

Thermal HDM. The molecular size of asphaltene structures range from 10^{-9} to 10^{-7} m (10 to 1000 Å). These molecules are too large to enter pores from 50 to 200 Å which are common in hydrotreating catalysts. Therefore, for HDM of asphaltene molecules some kind of size reduction is

required. Literature reports indicate that at temperatures approaching reaction temperature the asphaltenes are dissociated, or depolymerized into smaller units which are able to penetrate inside the catalyst pores (Reynolds et al., 1987; Savage et al., 1988; Bridge and Green, 1979; Richardson and Alley, 1975). Asaoka et al. (1983) also concluded that asphaltenes depolymerize into the basic unit sheets during cracking.

What is not clear yet is the effect of thermal breakdown in reactivity of the metal bearing species. Are the new smaller molecules more reactive or more refractory than the originals? Yan (1987) states that thermal processing could lead to either breaking of the asphaltene molecules into more reactive products or to condensation of the asphaltenes into the smaller more aromatic core. Savage et al. (1988) favor the idea of thermal conversion of asphaltene into its less soluble core which is more refractory and a promoter of coke formation.

Thermal + Catalytic HDM. Some researchers give equal importance to both thermal and catalytic steps during HDT. Asaoka et al. (1987) hypothesizes that HDM of asphaltenes involves both thermal and catalytic steps. The asphaltenes micelles are broken down thermally into smaller molecules. This thermal reduction in size allows molecules to penetrate catalyst pores where HDM occurs. Savage et al. (1988) found that some V in the asphaltenes is present as

thermally stable, high molecular weight moieties.

Therefore, only large pore size catalytic treatment could achieve complete HDM.

Correlations between sulfur and metals removal, both thermal and catalytic, have been suggested by several authors. Reynolds and Biggs (1987) using an LC-ICP technique showed a correlation between V and S peaks in the larger molecular size ranges for the asphaltenes. They suggest that larger V compounds may have some type of S incorporated into the ligation structure.

Asaoka et al. (1983) claimed that destruction of micelles strongly interacts with metals removal from the asphaltenes whereas depolymerization of asphaltene molecules is coupled with sulfur and nitrogen removal. They concluded that vanadium plays a major role in the association of asphaltene molecules. Figure 4 represents their model for asphaltene cracking. In this mechanism the micelle decomposes promoting metals removal. Additional breakdown of the particles results in removal of heteroatoms.

Galiasso et al. (1985) proposed an HDM mechanism consistent with Yen's definition of asphaltenes. They suggest that HDM at high temperature involves separation of the micelles, selective removal of metals, and some cracking and dealkylation reactions. After cooling, the product associates again forming a partially demetallized

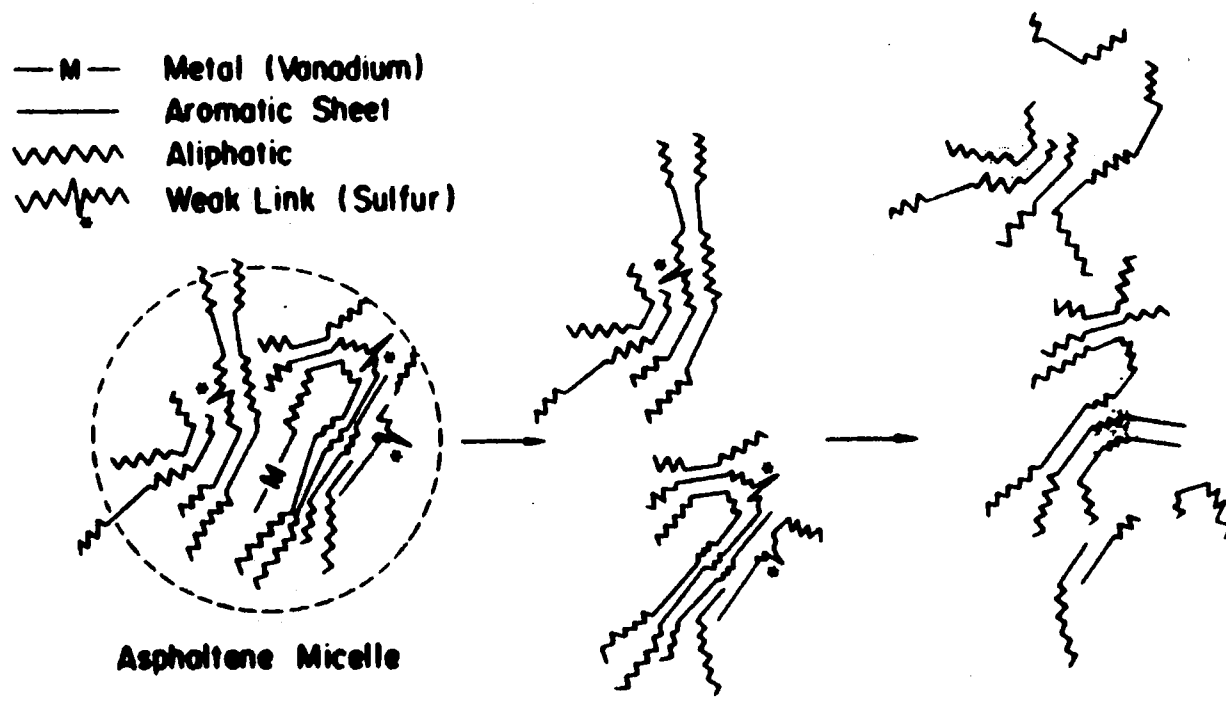


Figure 4. Mechanism of Asphaltene Cracking

and smaller asphaltene or resin. These mechanisms are very similar and they suggest that asphaltenes must dealkylate or break into smaller molecules that can enter the catalyst pores where they are demetallized.

Objectives and Strategy

The first objective of this study is to find out how the dissociation of asphaltenes from different residua feeds affects the back end HDS catalysts used in graded hydrotreaters. Typically, the catalyst at the bottom of the bed only accumulates a small percentage of the metals deposited in the overall bed and deactivates mainly by coverage of the active surface. Therefore, if the metals in the asphaltenes do not penetrate into the catalyst, the catalyst will lose only a small amount of activity due to internal surface poisoning. However, if the metals do penetrate, the catalyst will display a rapid loss of activity due to poisoning of the catalyst surface that ordinarily occurs only in large pore catalysts that precede the small pore HDS catalyst in the reactor train. If high penetration of contaminant metals occurs, the advantage of having small pore, high activity catalysts at the bottom of the bed is lost. This can and has occurred and feedstocks are selected after long term pilot plant scale tests to limit this possibility. Little is known however about the HDS catalyst deactivation that results from metals

deposition and the effects of varying chemical composition in this process.

Residua from Hondo, Oriente and Caño Limon crudes were selected for this study. Previous work at Phillips Petroleum indicates that Hondo, Oriente and Caño Limon represent wide ranges in residual oil processability and that they are not ideal candidates for processing in the atmospheric residua desulfurization (ARDS) unit. Hondo which has high sulfur, nitrogen and metals content, has shown very high HDM rates and its asphaltene fraction is thought to be highly aliphatic. Oriente has high metals content and medium levels of sulfur and nitrogen. Caño Limon has the lowest level of metals, sulfur and nitrogen of the three residua. Oriente and Caño Limon have high proportions of metals in the asphaltene fraction and both have shown very low reactivity for HDM (Sughrue, 1989).

To simulate what happens in the top section of the graded beds the residual oils will first be hydrotreated at mild conditions over a small pore catalyst to remove very reactive metals and concentrate the metals in the asphaltene fraction. A small pore catalyst with high levels of promoters, equivalent to a high activity HDS catalyst, will be prepared to contact the pretreated residua. The changes in size and distribution of the vanadium-containing molecules and the catalyst deactivation will be followed to study the effect of asphaltenes from Hondo, Oriente, and

Caño Limon on the bottom section of a graded hydrotreater.

Molecular size distribution for the vanadium in the asphaltenes will be determined using LC-ICP, and Penetration Factors of metals inside the catalyst will be determined using microprobe analyses. Results of these analyses from tests at different temperatures and with different feeds will be used to study how the asphaltene molecules react, how far they penetrate into the catalyst and how this impacts HDS activity. If asphaltenes decompose as suggested, a series mechanism combining thermal cleavage outside the catalyst with diffusion of the molecules into the pores and a parallel first order reaction mechanism within the pores could be used to determine how asphaltene cracking interacts with catalytic HDM on small pore catalysts.

From the information developed in this study it should be possible to:

1. Verify the existing mechanisms of asphaltene thermal decomposition.
2. Determine the extent to which existing and formed small molecules contribute to the penetration of the metals inside the catalyst and contribute to the catalyst deactivation for sulfur removal.
3. Determine whether or not all these tests combined could be used as a screening tool for better selection of crudes to be processed in an ARDS unit. There is a large

number of crudes available in the world oil market and prices and quality vary widely. Therefore, the better the selection process, the more advantage can be taken of the range of candidate crudes to optimize refinery operations and profitability. While this screening test could take three to four weeks , certainly it could be a very useful and insightful tool for better crude selection. It will be shorter and less expensive than the existing pilot plant tests now used to select feedstocks.

CHAPTER II

EXPERIMENTAL AND ANALYTICAL PROCEDURES

Experimental Technique

Reactor studies were done in the catalyst laboratory at the R&D Center of Phillips Petroleum Co. in Bartlesville, Oklahoma. Figure 5 shows a schematic diagram of a reactor system used. A description of this oil hydroprocessing unit is given elsewhere (Johnston et al., 1983). The reactor is a 71 cm (28 in) long and 1.9 cm (0.75 in) ID stainless steel tubing suited with a 0.635 cm (1/4 in) OD axial thermowell. An electrical three zone furnace provides uniform heat distribution and good control over the temperature profile across the bed. A high pressure vessel separates the gas from the liquid product. The gases can be vented to a flare system or they can be analyzed by an on-line chromatograph before venting. The liquid from the pressure vessel goes to a sample loop or to a product accumulator.

The reactor is packed as follows: A 40.6 cm (16 in) non-catalytic zone followed by a 10.2 cm (4 in) catalytic zone. An additional 19 cm (7.5 in) zone of inert is placed above the bed to reduce end effects. The non-catalytic zone

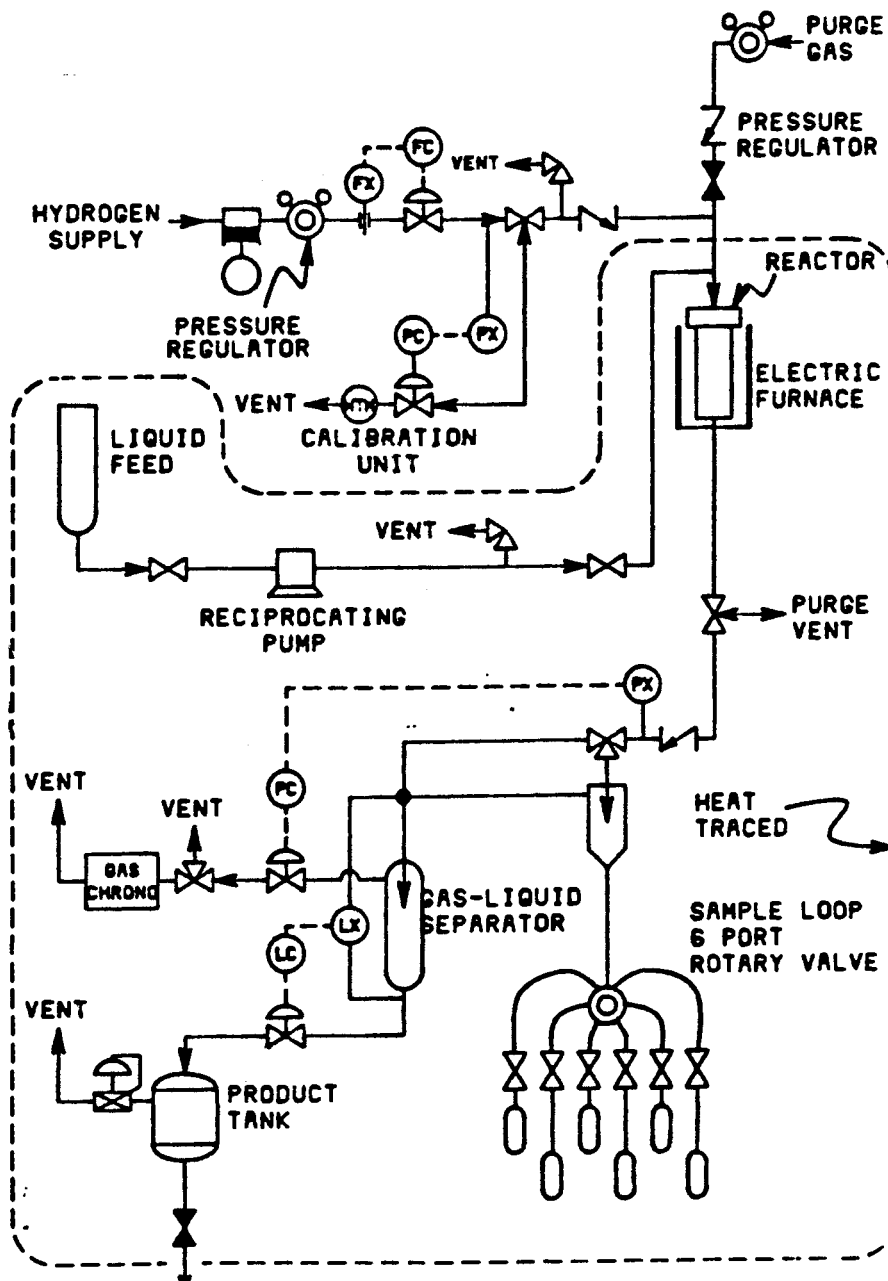


Figure 5. Diagram of the Hydrotreating Unit

consists of 0.38 cm (1/8") alundum spherical particles. The catalyst zone consists of 10 cc of catalyst diluted with 20 cc of 36-mesh alundum. Catalyst dilution improves the system hydrodynamic properties by minimizing bypassing. After packing, the reactor is pressure tested.

The packed catalyst bed is sulfided in a computer controlled unit with a 10% H₂S/H₂ mixture over the temperature range from 200 to 370⁰C. This sulfiding procedure provides the catalyst with three times the amount needed for complete sulfiding of the nickel and molybdenum present. After cooling, the sulfided reactor is placed in the HDT unit ready for start-up.

A Whitey Model LP-10 positive displacement pump supplies a continuous oil flow rate of 25 cm³/h from a feedstock buret. Hydrogen tanks supply the gas at a rate of 5000 SCF(H₂)/BBL(Oil) and a pressure of 2000 psig. The oil and hydrogen move concurrently up-flow through the bed. The up-flow system has been selected to insure good catalyst wetting. The liquid hourly space velocity (LHSV) is 2.5 based on the catalyst volume. The temperature of the catalytic zone is constant at 377⁰C (710⁰F), while the non-catalytic zone is also constant but at 377 or 404⁰C (710 or 760⁰F) depending on the test. After the system is taken to steady state, a computer system maintains and controls the reactor operation. Liquid samples are taken every 24 h to monitor the operation. After completion of each test, the reactors were unloaded and the catalyst zone is unpacked

and divided into three sections: top, middle, and bottom. The top and bottom sections are used for microprobe analysis in the Phillips Microprobe Laboratory and the middle section for bulk analysis in the Phillips Analytical Branch. The reactor operation is up-flow so the bottom catalyst section contacts the oil first.

Oil Analyses

Plasma Analyses

A Bausch and Lomb Model 3510 inductively coupled plasma (ICP) emission spectrometer is used to determine the vanadium, nickel, and sulfur content for the feedstock and products. The system was calibrated for Ni, V and Mo using Standard S-21 from Conostan, and for S using Standard 1634b from the National Bureau of Standards. Mary Little from Phillips Catalyst Laboratory provided us with these analyses.

Liquid Chromatography with Inductively Coupled Plasma (LC-ICP) Detector Analyses

The LC-ICP unit consists of liquid chromatograph columns in the size exclusion mode interfaced with an ICP spectrometer. This technique provides a molecular size distribution of metals and sulfur in the oil. Standard procedures and techniques were used to run the LC-ICP tests. LC columns loaded with a Waters μ styragel packing

allow separation on the basis of molecular size, while the ICP detector measures selected elements simultaneously as function of elution time. Four columns, 7.8 mm ID, 30 cm long, are used in series. The nominal pore sizes of the columns are 10,000, 1,000, 500, and 100 angstrom. The packing material is a fully porous highly cross-linked styrene divinylbenzene copolymer with particle size of about 10 microns.

The analysis requires 0.1 to 0.2 g of sample. All samples are diluted approximately 1:10 in the mobile phase and placed in a shaker to promote dissolution. To remove any suspended matter, samples are filtered through a Millex-SR 0.5 μm filter.

For detection, 0.25-0.50 mL of liquid sample is injected into the system. The mobile phase, a xylene mixture of 20% pyridine and 0.5% cresol in xylene, flows at 1.0 mL/min. The analysis of one sample takes approximately 1 hr.

Asphaltenes Precipitation

The asphaltenes of the original residua, feedstocks, and products are precipitated using 40 cm^3 of n-pentane per gram of oil. The mixture is stirred for 16 h, and then left standing for one hour to facilitate filtration. The mixture is filtered using a Buchner funnel apparatus over a medium speed, number 40, filter. The asphaltenes are then dried under vacuum for one hour at 125⁰C and are redissolved

in xylene for LC-ICP and Plasma analyses.

Catalyst Analyses

Soxhlet Extraction

The used catalyst particles are Soxhlet-extracted with tetrahydrofuran (THF) for 24 h at 175⁰C (347⁰F). Then, they are washed with n-pentane to remove the THF, and dried at 150⁰C (302⁰F) for 8 h under vacuum of 30 in Hg to remove any adsorbed materials.

Electron Scanning Microprobe

Selected catalyst pellets from the top and bottom sections of the catalytic zone are analyzed for metals, sulfur, and carbon content and distribution profile across the pellets using electron scanning microprobe (ESM). The electron microprobe is a JEOL model 733 with 5500 data handling system and 5600 instrument automation. The microprobe is equipped with three wavelength and one energy dispersive spectrometers (WDS and EDS respectively).

Soxhlet extracted pellets from the top and bottom sections of the catalyst bed are imbedded on end in epoxy resin. After the epoxy is cured, a length equal to the pellet diameter is ground off of the ends of the embedded samples to obtain a representative cross-sectional elemental profile free of the effects of metals penetration from the pellet end. Silica carbide paper (600 grit) is

used to remove the deep scratches that remained after this grinding step. Subsequent polishing steps involve 9 microns alumina followed by 3 micron silica carbide Fibrmet disks. Each change in grit size is followed by cleaning of the samples with methanol in an ultrasonic cleaner. Mastermet colloidal silica (submicron particle size) is used with a Mastertex polishing cloth as the final polishing step. The samples are then cleaned with water in an ultrasonic bath and dried.

The polished surface is then coated with a thin layer of carbon in a JEOL 4A vacuum evaporator to provide a conductive coating for microprobe analysis. All polishing equipment and supplies are purchased from Buehler Ltd.

For each sample, ten pellets are viewed in the electron microprobe using backscatter electron imaging to compare the uniformity of metals deposition. Three pellets are chosen for analysis to determine deposition profiles for selected elements. And four quantitative traverses are done on each of these pellets at 90 degree angles to one another. Each traverse involves 30 analysis points, beginning at the pellet rim and ending at the center. The first ten points are spaced 5 microns apart, the second ten points are 15 microns, and the final ten points have to be spaced 65 microns to reach the center.

The microprobe is operated with a focussed beam (approximately 1 micron diameter) at 15 kV accelerating voltage and 20 nA beam current for calibration of the

instrument and quantitative analysis of the samples. Aluminum and silicon are analyzed with EDS and are calibrated using alumina and silica standards. All of the other elements are analyzed with WDS. The first WDS spectrometer is calibrated for carbon and oxygen using a lead stearate (STE) crystal and carbon and alumina standards. The second WDS spectrometer is calibrated for nickel and vanadium using a lithium fluoride (LiF) crystal and nickel and vanadium metal standards. The third WDS spectrometer is calibrated for molybdenum and sulfur using a pentaerythritol (PET) crystal and molybdenum metal and zinc sulfide standards. The standards are obtained from either JEOL or C. M. Taylor Corporation.

Since analysis of each of the samples requires approximately 20 hours, the instrument is set up to run in unattended mode under computer control. Beam alignment and beam current stabilizer controls are used to insure that analysis conditions remain constant. The reproducibility of the stage for movement to the various pellet rim coordinates is plus or minus one micron. Counting time for EDS is set at 20 seconds, and WDS is set for a maximum of 40 seconds. The characteristic x-ray counts at each analysis point on the samples are corrected for matrix effects using the ZAF correction program provided in the Tracor Northern software.

The results are stored as elemental weight percents and transferred electronically to a Macintosh SE to be

incorporated into an EXCEL spreadsheet for further data handling, i.e. plotting, Q value determination, etc. The microprobe is calibrated regularly to insure proper quantitative analysis.

Feedstock

Residua from Hondo, Oriente and Caño Limon crudes were selected for this study. These crudes contain relatively high levels of asphaltene and metals. Previous work at Phillips Petroleum indicates that Hondo, Oriente and Caño Limon represent wide ranges in residual oil processability. Hondo is an offshore California residuum with high sulfur, nitrogen and metals content. Hondo has shown very high HDM rates and its asphaltene fraction is thought to be highly aliphatic. Oriente from Ecuador has high metals content and medium levels of sulfur and nitrogen. Caño Limon has the lowest level of metals, sulfur and nitrogen from the three residua. Oriente and Caño Limon have high proportions of metals in the asphaltenes and have shown very low reactivity for HDM (Sughrue, 1989).

In order to simulate the feedstock that contacts the high activity HDS catalyst at the bottom of commercial HDT units the residual oils are hydrotreated at mild conditions over a small pore catalyst to remove very reactive metals and concentrate the metals in the asphaltene fraction. Tables 4 through 6 list the properties of the residua and the corresponding mildly hydrotreated product. The data

TABLE 4
HONDO PROPERTIES

PROPERTY	HONDO RESID	HYDROTREATED HONDO RESID
V ppm	213	94.50 (119.6) ^a
Ni ppm	92.2	42.03 (51.38)
S wt%	5.7	1.40 (2.04)
N wt%	0.766	0.483
Basic N wt%	0.17	0.14
CR Ramsbottom wt%	11.2	6.45
API	12.8	22.6
H (NMR)	10.6	12.11
SG 38.5 ⁰ C	0.9649	0.9018
Asphaltenes wt%	16	10
Metals in Asph. %	80	85

^a Properties of the second batch of residuum prepared.

TABLE 5
ORIENTE PROPERTIES

PROPERTY	ORIENTE RESID	HYDROTREATED ORIENTE RESID
V ppm	143.56	125.74
Ni ppm	69.57	58.63
S wt%	1.61	1.02
N wt%	0.457	0.326
Basic N ppm	955	713
CR Ramsbottom wt%	11.1	9.99
API	15.2	18.1
H (NMR)	10.84	11.37
SG 38.5 ⁰ C	0.9488	0.9297
Asphaltenes wt%	12.5	11.1
Metals in Asph. %	90	98

TABLE 6
CANO LIMON PROPERTIES

PROPERTY	CANO LIMON RESID	HYDROTREATED CAÑO LIMON RESID
V ppm	17.04	13.613
Ni ppm	51.15	39.251
S wt%	0.6615	0.3986
N wt%	0.269	
Basic N ppm	843	903
CR Ramsbottom	6.85	5.88
API	23.6	25.5
H (NMR)	12.25	12.53
SG 38.5 ⁰ C	0.8957	0.8847
Asphaltenes wt%	9.5	7.5
Metals in Asph. %	90	98

shows that during pretreatment the metals in the asphaltenes concentrate to 85% of the total metals for Hondo, and to 98% for Oriente and Caño Limon. Also the conversion of asphaltenes was high for Hondo, followed by Caño Limon and then Oriente. The Hondo feed was accumulated in two separate vessels and the metals and sulfur properties varied slightly as indicated in Table 4 by the values in parenthesis. Table 7 shows some data from previous work at Phillips Petroleum (J. W. Shaw, 1989) on molecular weight and NMR properties of asphaltenes for the selected crudes. The data indicate that Hondo is more aliphatic and has lower molecular weight than Oriente and Caño Limon.

Fresh Catalyst

The support for the catalyst used in this study is a 1.6 mm (1/16") alumina cylindrical extrudate manufactured by ArmaK Ketjen Catalysts. These pellets have an average pore diameter of 7.8 nm (78 Å), an average pore volume of $0.50 \times 10^{-3} \text{ m}^3/\text{kg}$ ($0.50 \text{ cm}^3/\text{g}$), and an average surface area of $270 \times 10^3 \text{ m}^2/\text{kg}$ ($270 \text{ m}^2/\text{g}$). The support was impregnated using an incipient wetness technique at Phillips Laboratories with a solution of molybdenum oxide (MoO_3) and nickel carbonate in ammonia to load the catalyst with 3 wt% Ni and 10 wt% Mo. The catalyst was dried in open air overnight and then calcined at 500°C for 8 h. The catalyst impregnated has promoters load and pore size similar to an HDS catalyst

used in the lower section of an HDM-HDS unit.

TABLE 7
VPO MW AND NMR PROPERTIES OF ASPHALTENES

PROPERTY	HONDO	ORIENTE	CAÑO LIMON
VPO Average Molecular Weight	2060	3360	3110
Aromatic Carbon wt%	29.5	48.2	56
No of Fused Aromatic Rings per Molecule	12.2	41.9	49
Ratio of Saturated Substituents to No of Fused Rings per Molecule	1.43	0.54	0.39

CHAPTER III

EXPERIMENTAL RESULTS

Description and Results from Reactor Experiments

To prepare the feedstock for this study, each residuum was pretreated over a trickle bed reactor loaded with a commercial catalyst operated at 655 K (720⁰F), 13.79 MPa (2000 psig) and 0.8 LHSV based on catalyst volume. Three reactor tests were made with each hydrotreated residuum (Table 8). The experiments were designed to study thermal and catalytic effects on HDM of asphaltenes. The oil in these tests moves up-flow through two zones in the reactor: First, a thermal zone where the oil stays for approximately 60 minutes followed by a catalyst zone where the oils stays for approximately 30 minutes (Figure 6).

Thermal effect was studied at two temperature levels: 650 and 678 K (710 and 760⁰F). The 650 K (710⁰F) value, which is lower than the pretreatment temperature, should provide little additional thermal cracking. On the other hand the high temperature level of 678 K (760⁰F) should relate the importance of thermal severity on breakdown and HDM of the asphaltenic portion of the oil. The catalyst

TABLE 8
NUMBERS FOR EACH RUN

CONDITIONS ZONE1-ZONE2	CRUDE SOURCE			
	HONDO	HONDO	ORIENTE	CAÑO LIMON
THER - CAT ^a				
760 - 710	1	3	6	9
710 - 710	2	4	7	10
THER - THER				
710 & 760		5	8	11
MET ON CAT ^a				
	10%	5%	5%	5%

^a THER : Thermal zone temperature
CAT : Catalyst zone temperature
MET ON CAT : Desired metals level to be deposited on
the catalyst
Each number in this table represents an experiment
and the results are presented in this chapter.

zone was kept at 650 K (710⁰F) for both experiments. The third experiment for each feedstock was thermal only. In this experiment the catalyst was replaced with the alundum spheres. This thermal test was run at 650 K (710⁰F) in the whole bed during 150 h. Then, the temperature of the bottom section of the reactor, equivalent at the thermal zone in the catalytic experiments, was raised to 678 K (760⁰F) and run for an additional 150 h. The objective of this experiment was to examine the thermal effect on asphaltene and HDM.

Initially, the length of each catalyst run was defined as the time necessary to deposit 10 wt% metals on the catalyst. However, low HDM levels for Oriente and Caño Limon mandated that the length of the experiments be equal to the time required to deposit 5 wt% metals on the catalyst. As indicated in Table 8, Hondo was run at both 10% and 5% metals level. This facilitated the study of the effect of different metals loading on the radial distribution profiles inside the catalyst and provided some insight into the experimental reproducibility.

Hondo Experiments

Run 01 (Hondo 760-710 10%). The first experiment was run using the high temperature level for the thermal zone: 760⁰F. The catalyst zone temperature was 710⁰F. Pretreated Hondo (see Table 4 in Chapter II) was fed at 25 cm³/h for 382 hours. The metals removed were assumed to be deposited

on the catalyst. The calculated metals deposited in the catalyst zone was 10.13 wt%. Under the conditions used the reactor showed a HDM level of approximately 47% whereas HDS varied from 66 to 44% as indicated in Figure 7.

Run 02 (Hondo 710-710 10%) In this experiment the temperature of the thermal and catalytic zones was kept at 710⁰F. Pretreated Hondo was fed at 25 cm³/h for 359 hours. Then, Hondo from the second container (properties in parenthesis in Table 4) was charged to the unit and run for additional 215 hours and this is also the Hondo used for Runs 03 and 04. As expected at the lower thermal temperature the conversion for HDM and HDS was lower. As shown in Figure 8, the level of HDM was 30% for the first 359 h and increased to 39% for the new feed. HDS varied from 47 to 32% and the change in feed did not change the HDS trend. The calculated metals deposited on the catalyst was 11.24 wt%.

Run 03 (Hondo, 760-710, 5 wt%). This experiment was a duplicate of Run 1 except for the lower amount of deposited metals. The run lasted 190 h and deposited 5.99 wt% metals on the catalyst using pretreated Hondo. HDM stayed in the range from 47 to 50%, whereas HDS ranged from 62 to 57% (Figure 9).

Run 04 (Hondo, 710-710, 5 wt%). This test was operated at the conditions of Run 2 with the new level of metals

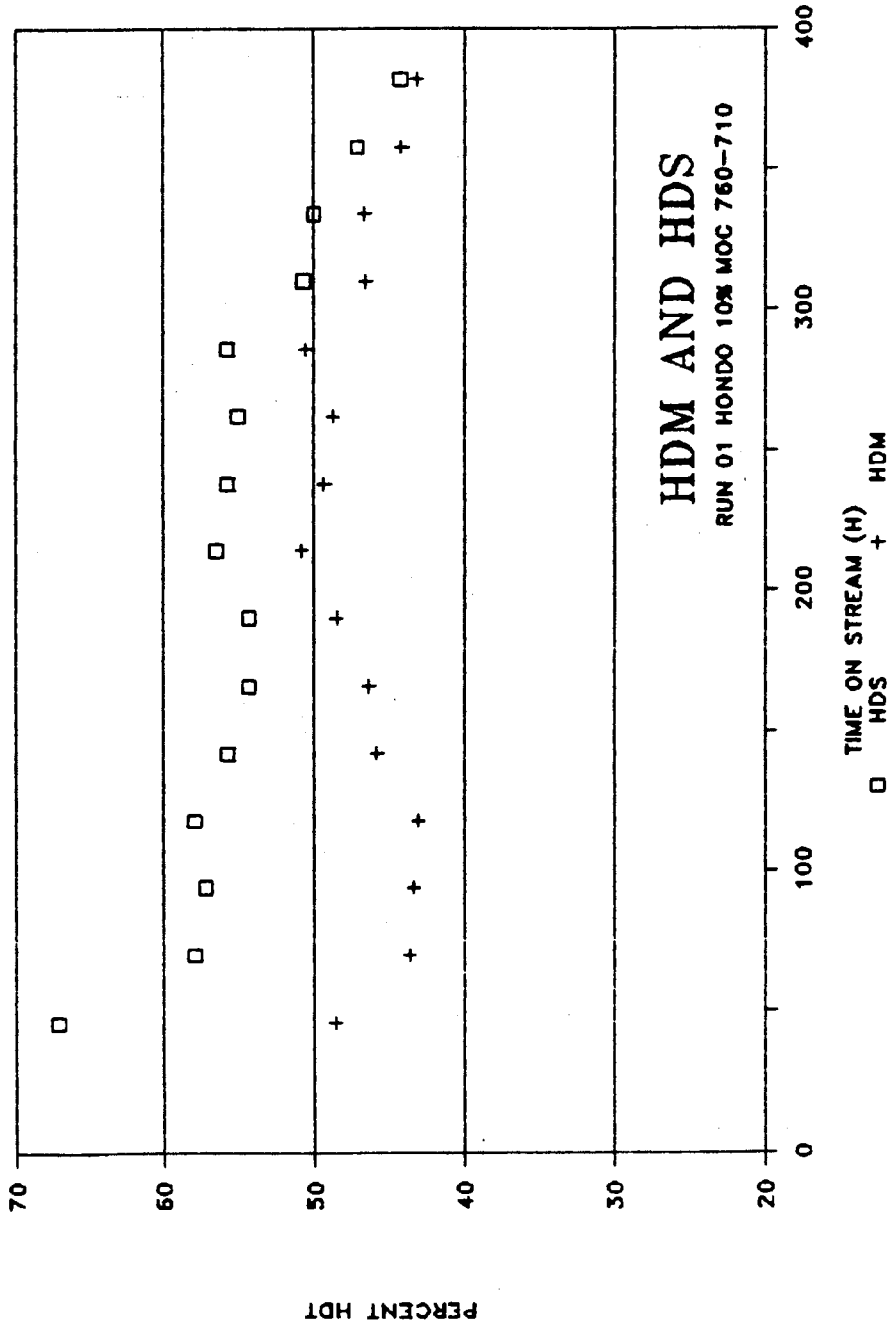


Figure 7. HDT Results for Run 01

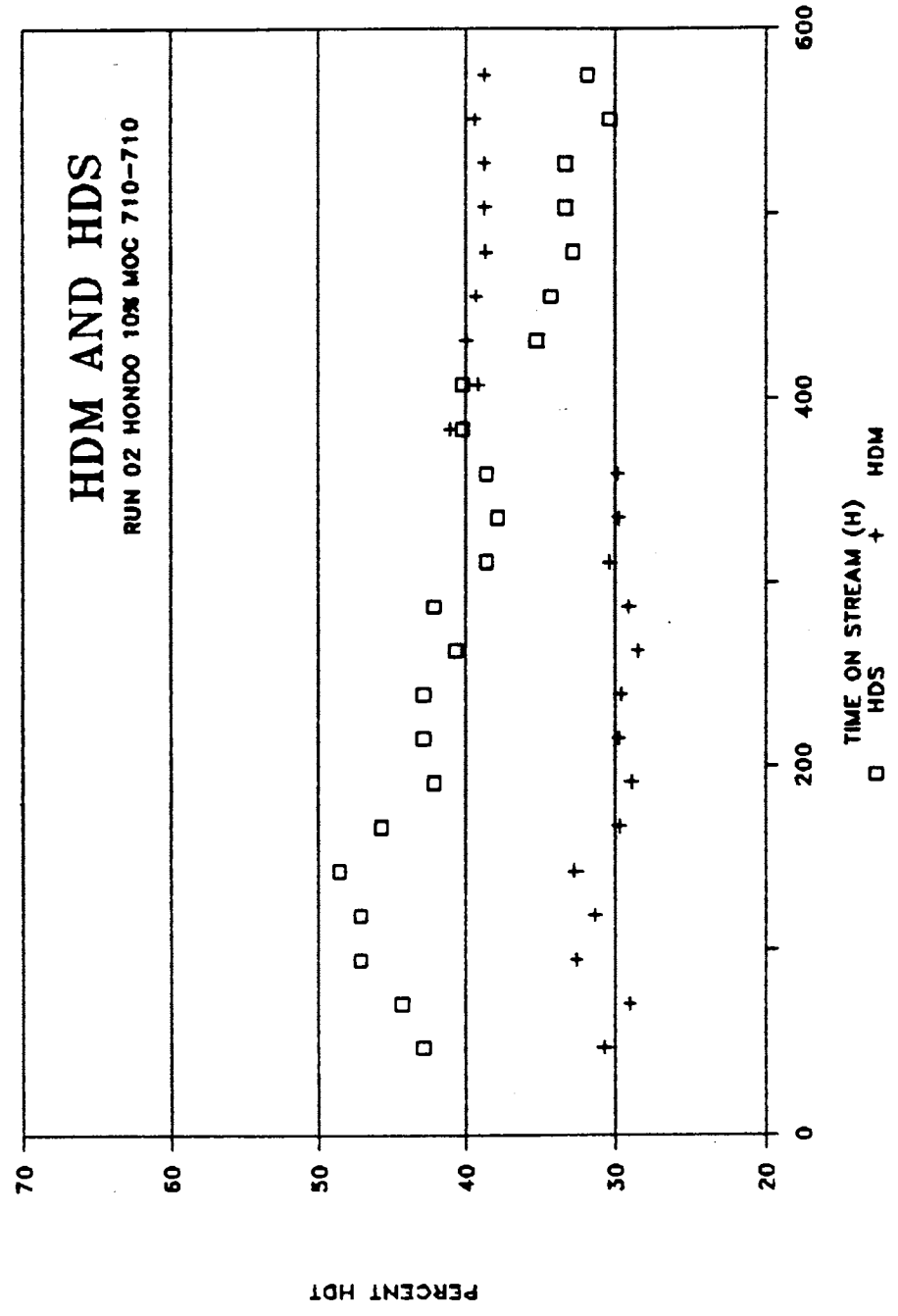


Figure 8. HDT Results for Run 02

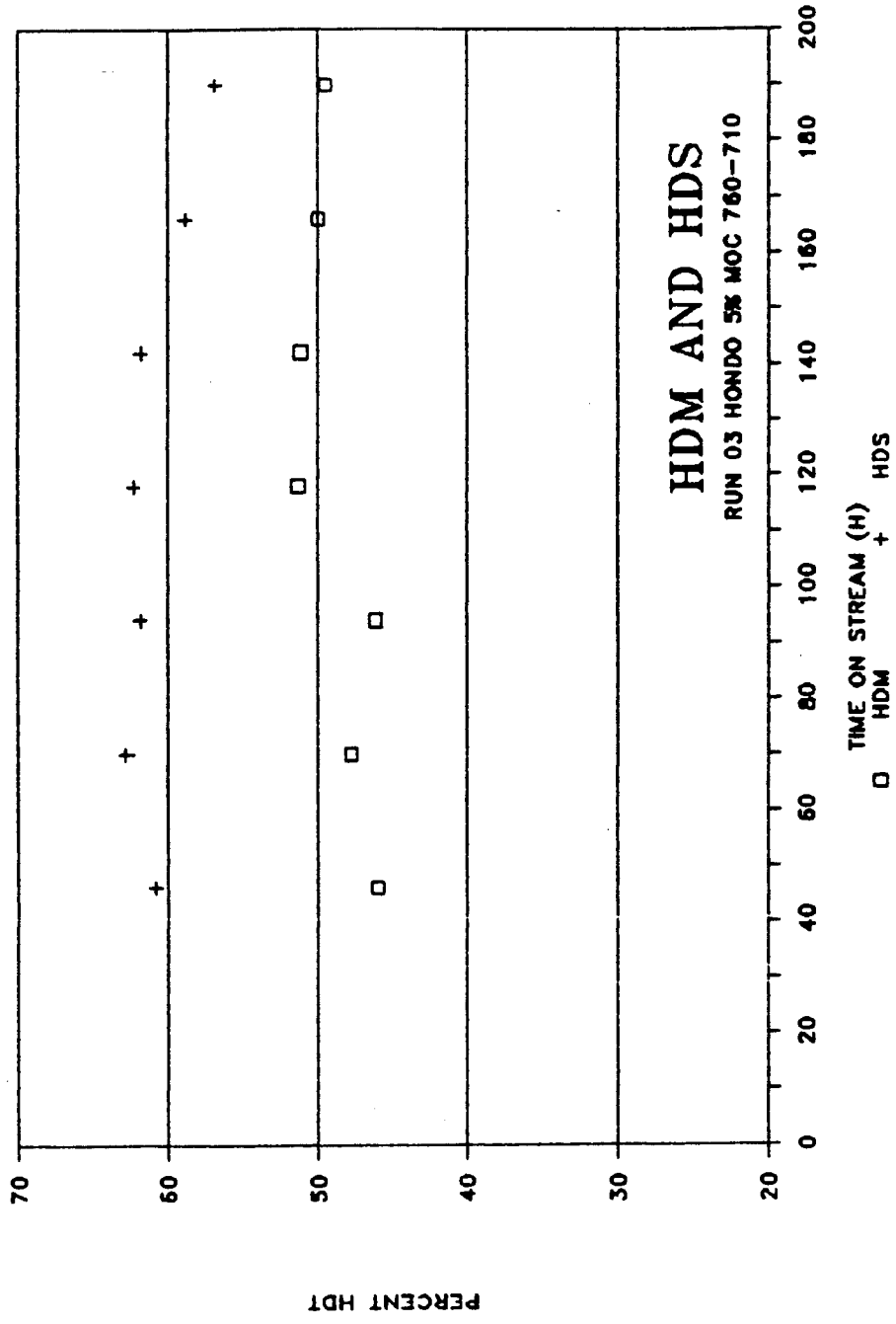


Figure 9. HDT Results for Run 03

loaded on the catalyst at 5 wt%. Pretreated Hondo was run for 213 h to deposit 5.33 wt% metals on the catalyst. HDM varied between 37 and 42% as indicated in Figure 10. HDS declined with time on stream from 54 to 44%. There is a larger difference in percent removal between Runs 01 and 02 than between Runs 03 and 04. This difference is attributed to the change in the properties of the pretreated residua rather than to changes in catalyst activity. This observation is corroborated in the next chapter where a normalization in activity indicates that the data follows the same deactivation trend.

Run 05 (Hondo, Thermal). This experiment was run to elucidate the role of thermal effect and residence time on metals removal. The reactor was loaded with 0.24 cm (1/8") alundum particles. The temperature was stabilized at 710⁰F and pretreated Hondo residuum was run through the system for 142 h. After this the temperature of the bottom thermal zone was increased to 760⁰F keeping the top zone at 710⁰F. An additional 168 h were run at these conditions. Figure 11 shows how the increase in temperature resulted in near 8% HDM difference and 10% difference in HDS.

Oriente Experiments

Run 06 (Oriente, 760-710, 5%). As indicated by the title, this run was operated at 760⁰F in the thermal zone, 710⁰F in the catalyst zone. The pretreated Oriente was

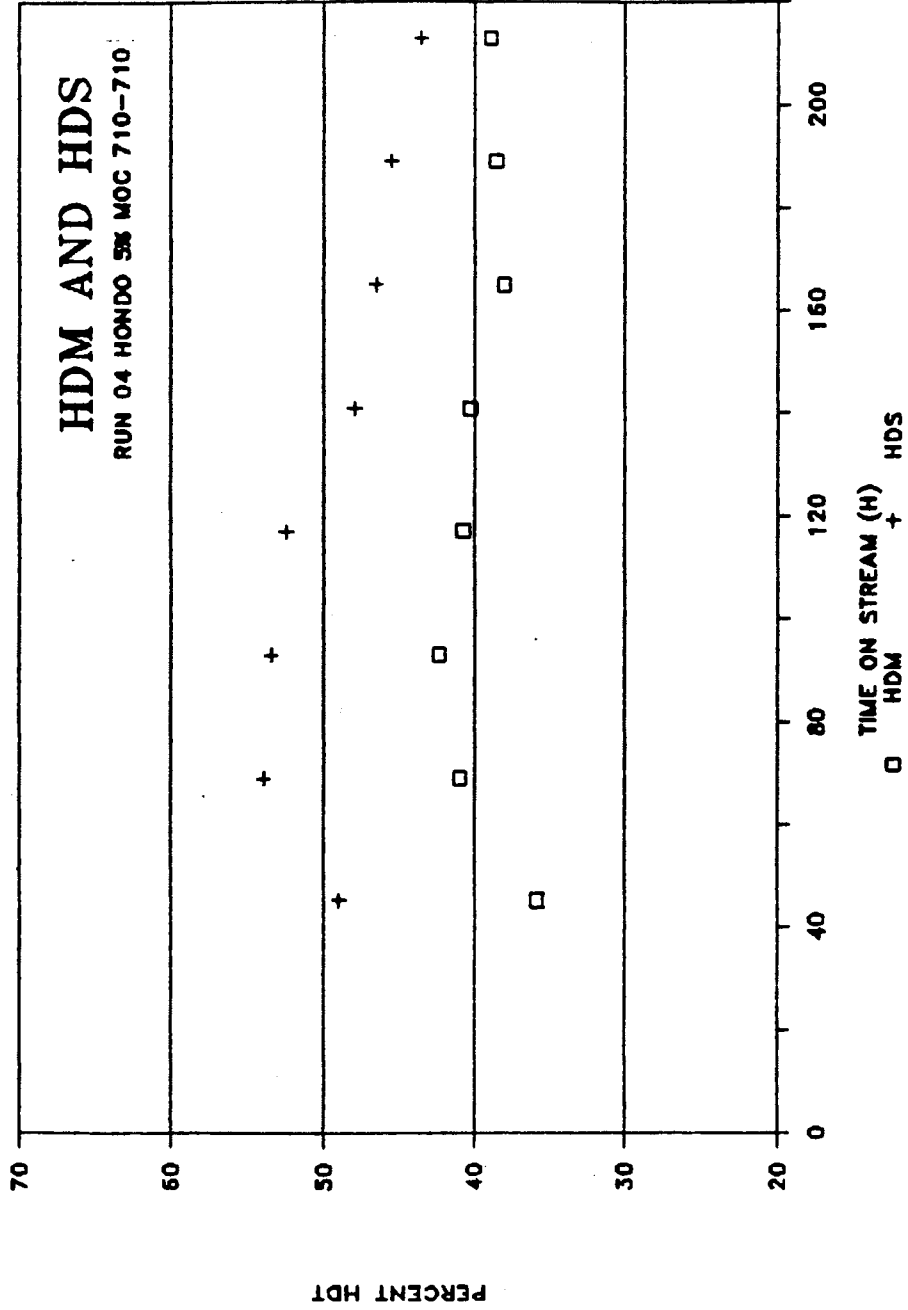


Figure 10. HDT Results for Run 04

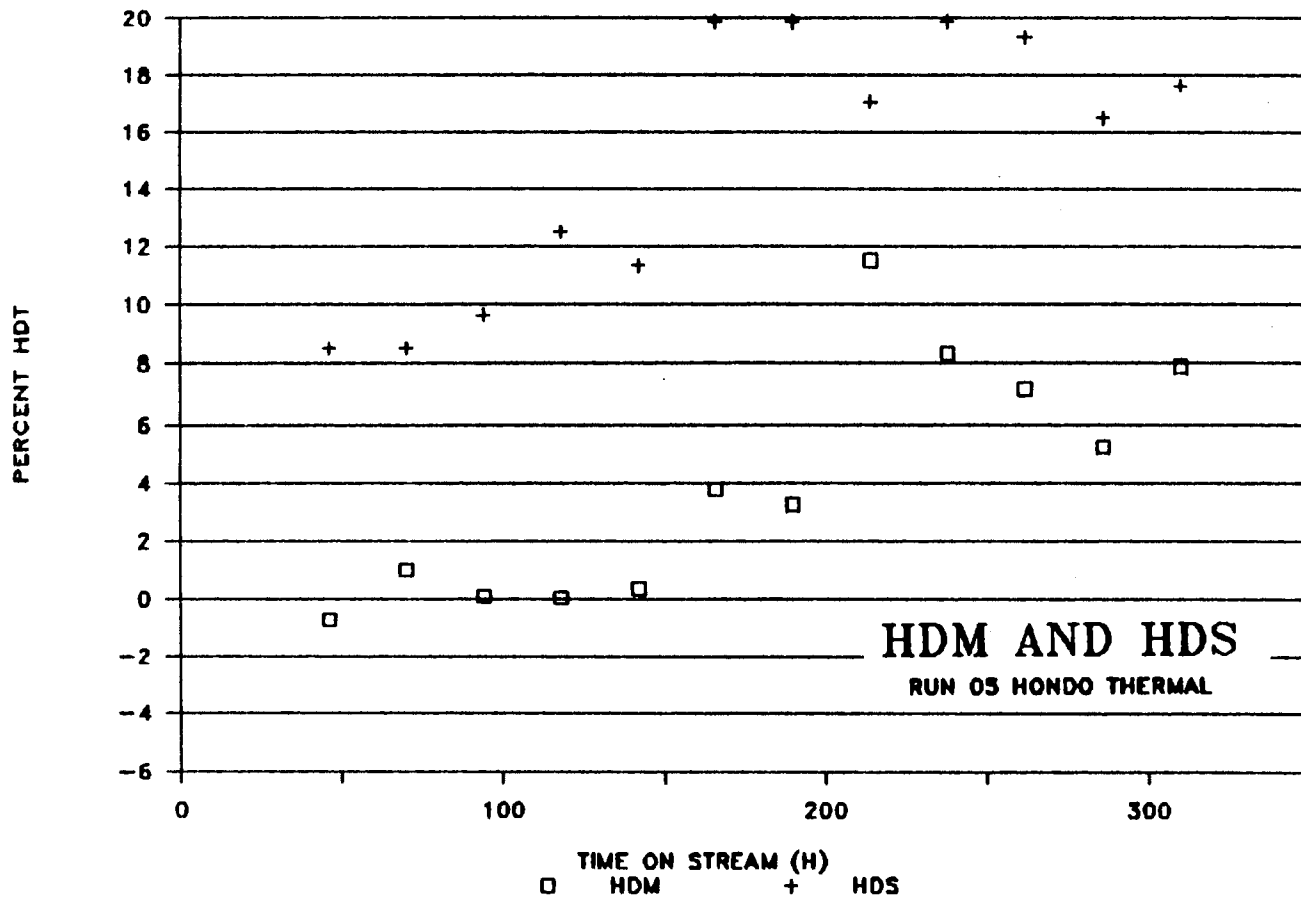


Figure 11. HDT Results for Run 05

processed for 429 h depositing 5.22 wt% metals on the catalyst. Compared to Hondo, Oriente showed a more definite deactivation trend for HDM decreasing from 19 to 13%. HDS ranged from 50 to 43% as shown in Figure 12.

Run 07 (Oriente, 710-710, 5%). In this Oriente run the temperature for both zones was 710⁰F. The duration of the run was 405 h and the metals deposited on the catalyst were 5.93%. At this condition Oriente did show higher initial activity than at the high thermal temperature. However, Figure 13 indicates that the data in this case is more scattered: HDS ranges from 53 to 39% and most of the HDM data points range from 20 to 11%. Excluding the three high HDM data points, these two runs are quite similar in performance.

Run 08 (Oriente, thermal). For this run Oriente was passed over the thermal bed at 710⁰F for 140 h and then at 760⁰F in the lower zone and 710⁰F in the top zone for another 166 h. Results from this run (Figure 14) confirm that Oriente shows no difference in HDM or HDS at the two temperature levels.

Caño Limon Experiments

Run 09 (Caño Limon, 760-710, 5%). From the three residua selected, Caño Limon has the lowest metals content, thus it required the longest time on stream to deposit the target level of metals on the catalyst. Caño Limon was run

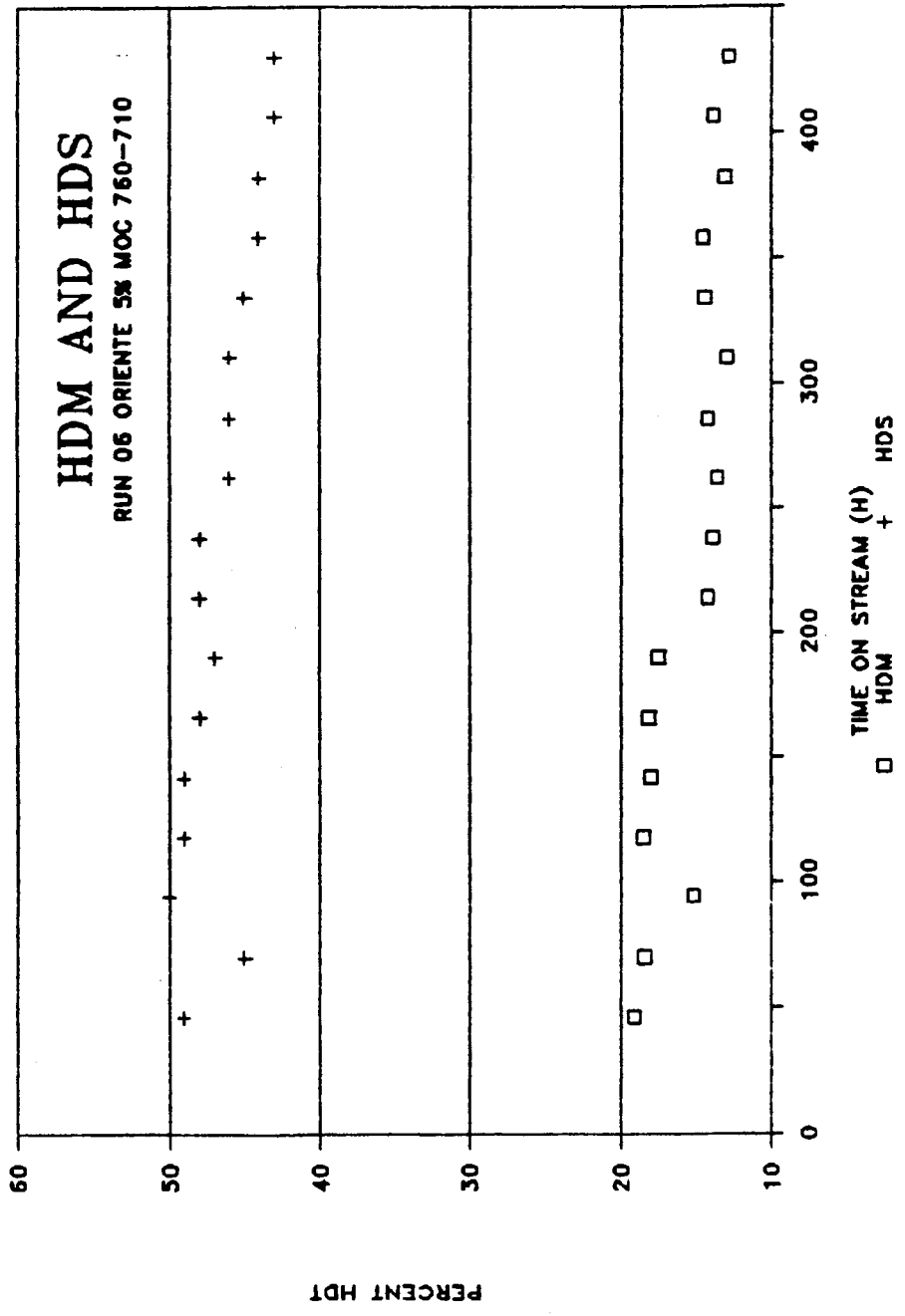


Figure 12. HDT Results for Run 06

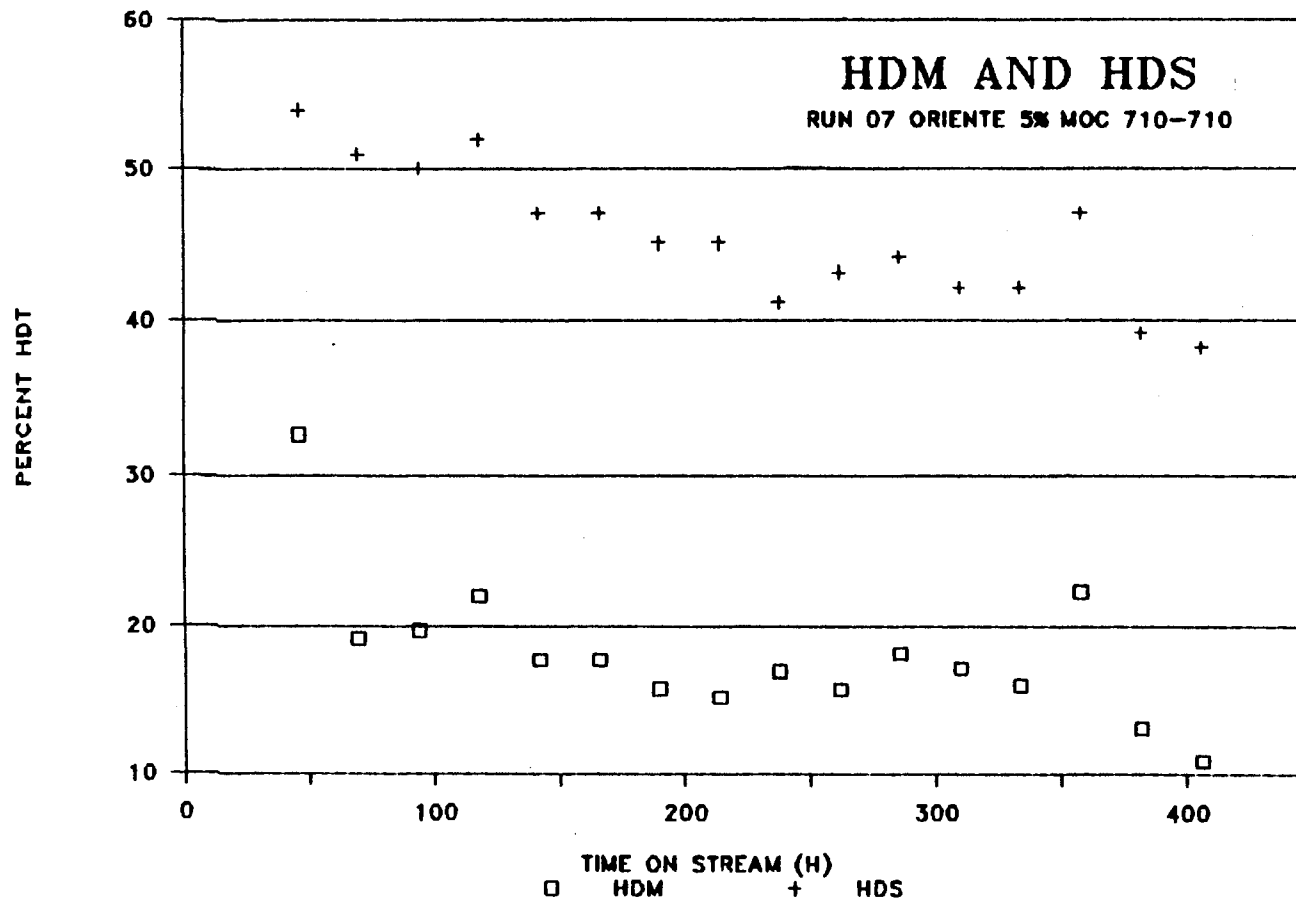


Figure 13. HDT Results for Run 07

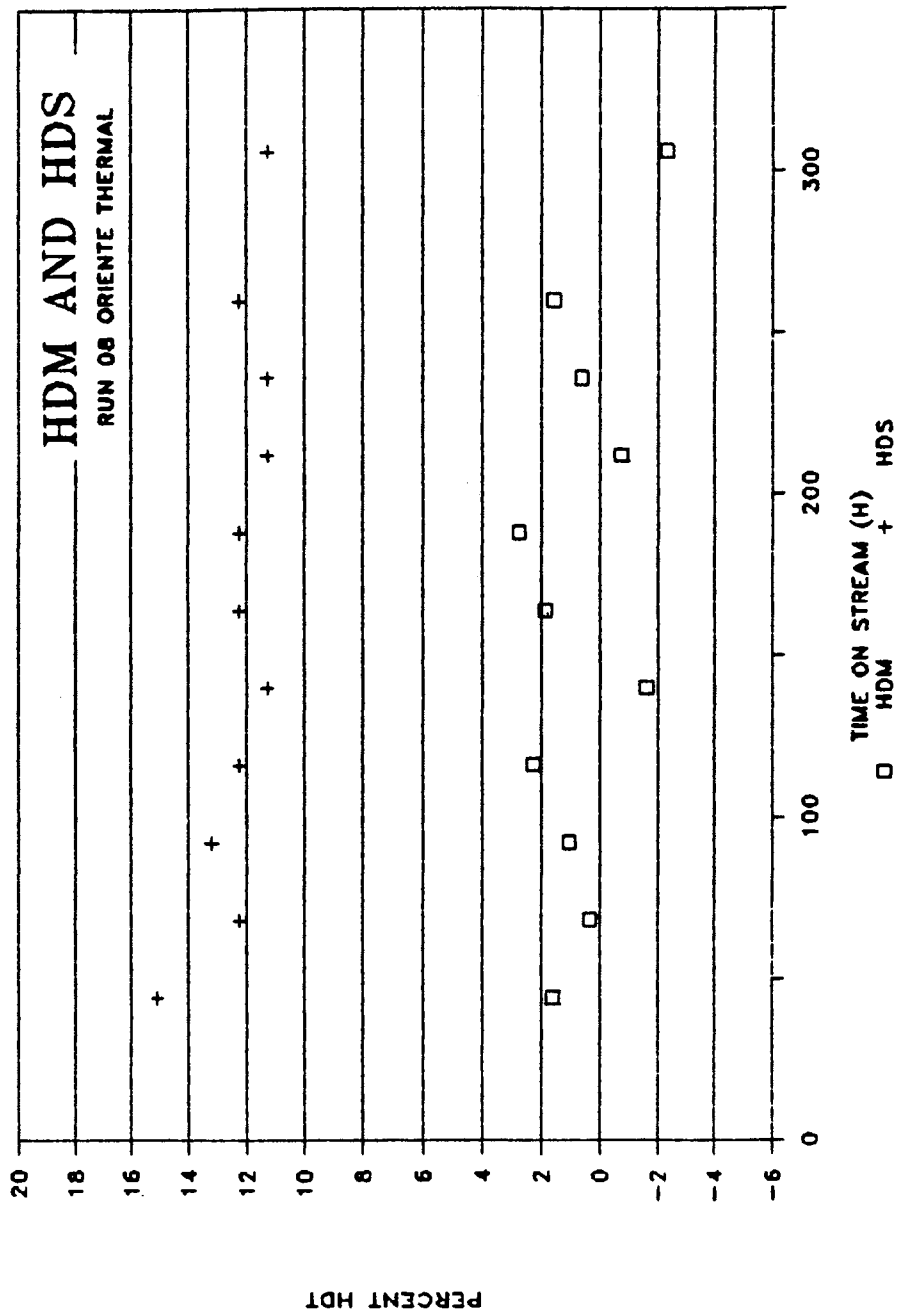


Figure 14. HDT Results for Run 08

at 760⁰F in the thermal zone and at 710⁰F in the catalytic zone. It took 659 h to deposit 4.34 wt% metals on the catalyst. The experiment was shutdown at this point due to limited feedstock. Furthermore, we considered that 4% and 5% were comparable because previous tests show no difference in the catalyst penetration factor for Hondo 10% and Hondo 5% (Runs 01, 02, 03, and 04) as shown in the section of analyses of catalyst. The low level of product metals resulted in high data scatter from plasma analysis as indicated in Figure 15. HDM was around 32% but there were values as high as 50% and as low as 12%. HDS showed a more continuous trend and ranged from 62 to 51%.

Run 10 (Caño Limon, 710-710, 5%). At 710⁰F for both thermal and catalytic zones the experiment lasted 994 h depositing 4.08 wt% metals on the catalyst. The scatter in the HDM data was lower than in Run 09. Figure 16 shows that HDM varied from 26 to 17% with an average close to 20% and HDS from 63 to 50% indicating slight catalyst deactivation for both HDS and HDM.

Run 11 (Caño Limon, thermal). This thermal test for Caño Limon was run for 141 h at 710⁰F in the whole bed. Then the temperature was increased to 760⁰F in the lower zone while keeping the catalyst zone at 710⁰F and run for additional 150 h. Figure 17 presents the HDT data. The higher temperature shows higher percent HDM but the scatter

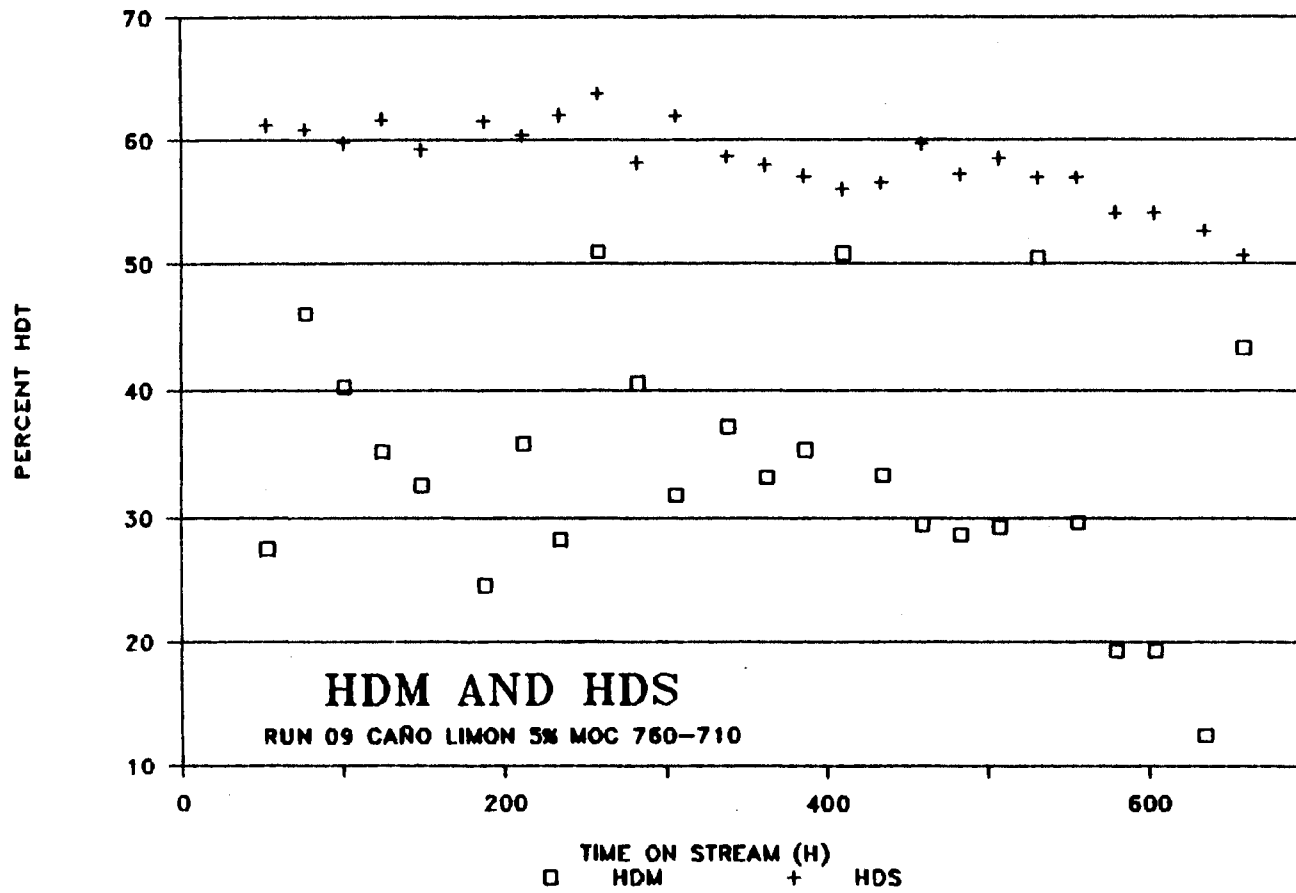


Figure 15. HDT Results for Run 09

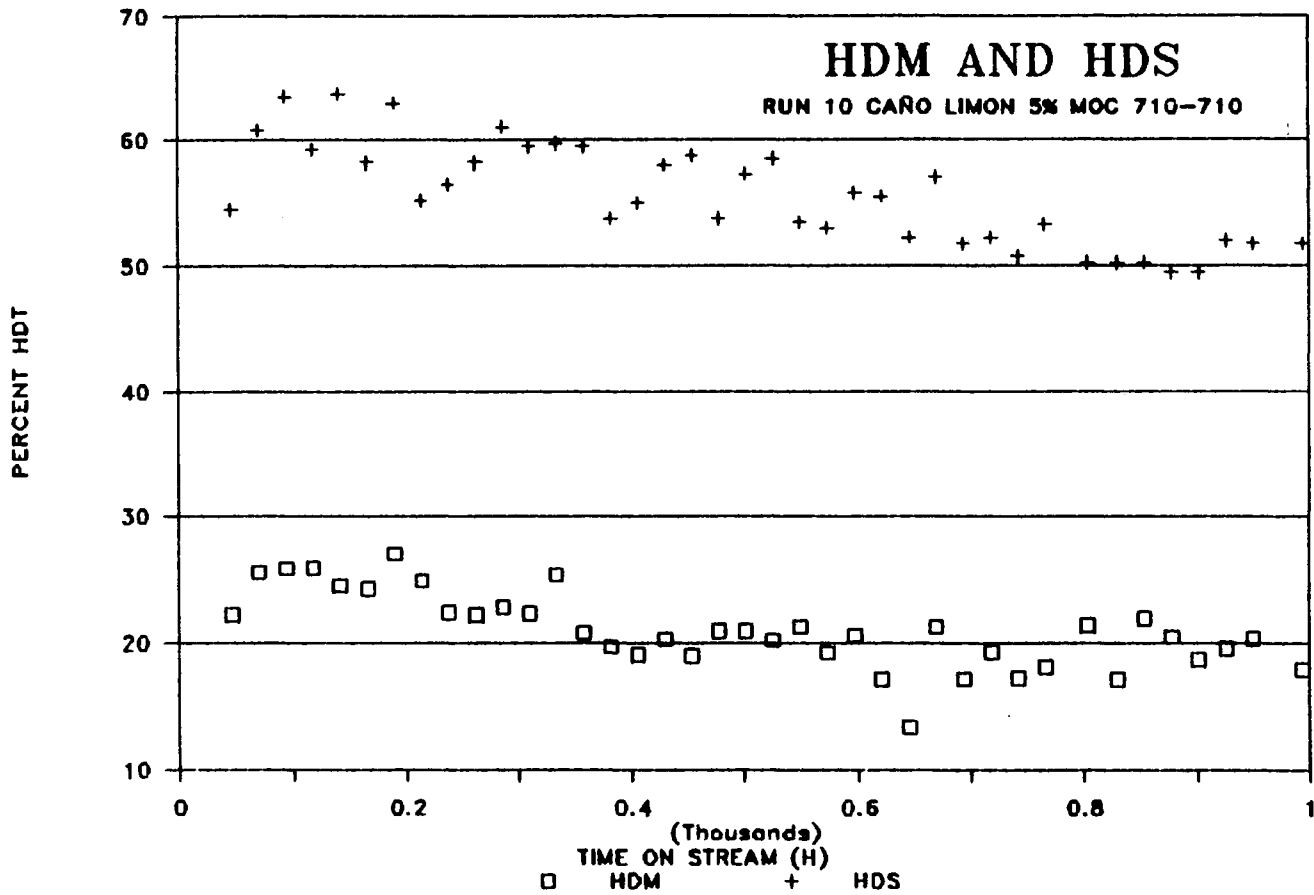


Figure 16. HDT Results for Run 10

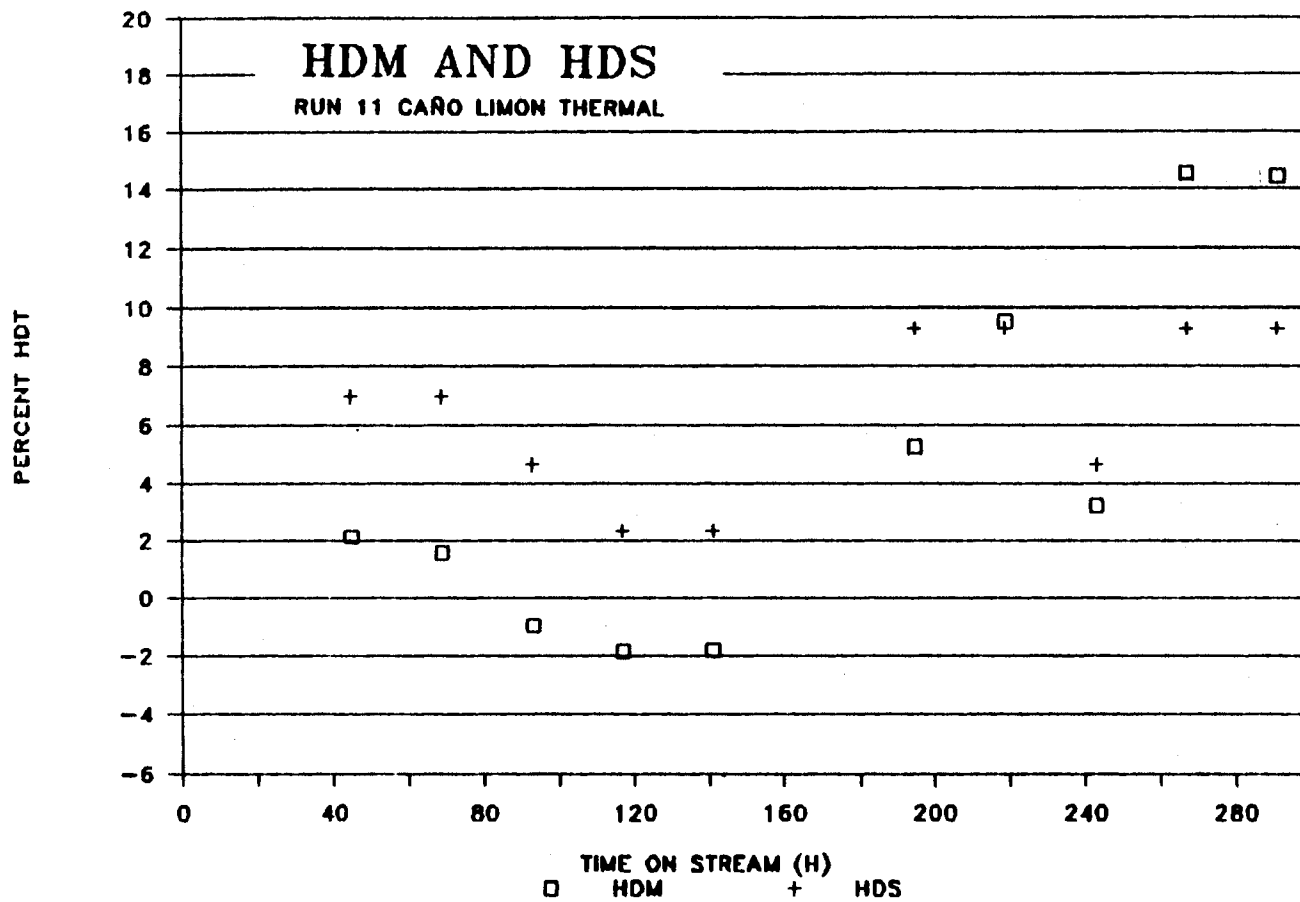


Figure 17. HDT Results for Run 11

in the data is large and it is difficult to quantify.

Asphaltenes Determination

Samples of the residua and products from each experiment were submitted to the Phillips Analytical Branch for determination of the asphaltene content and the results are presented in Table 9. Additional asphaltene precipitations were made in the Catalyst Laboratory to obtain asphaltenes for LC-ICP and Plasma analyses.

Analyses of Catalyst

Table 10 presents the bulk metal analysis for the spent catalyst from the middle section of each catalyst zone. The reported values are on a fresh catalyst basis to facilitate comparison with the material balance from reactor runs. The values for Ni and V are corrected multiplying by the factor: $Mo_{\text{fresh}} / Mo_{\text{spent}}$. Then the Ni is corrected for the Ni present in the fresh catalyst by subtracting 3.0 wt% from each value. A mass balance on metals was done over the entire reactor test to determine the proportion of metals removed that effectively gets inside the catalyst. From the bulk analysis and also from microprobe data, we calculated the ratio of metals on the catalyst to total metals removed.

TABLE 9
ASPHALTENE CONTENT (WT%) AS FUNCTION OF
REACTION CONDITIONS

CONDITIONS	HONDO	ORIENTE	CAÑO LIMON
PRETREATED RESIDUE	10	11.1	7.5
<u>CATALYTIC</u>			
710-710 PRODUCT	7	10.5	5.7
760-710 PRODUCT	5	10.0	4.5
<u>THERMAL</u>			
710-710 PRODUCT	7.5	11.1	6.0
760-710 PRODUCT	5.0	11.1	5.0

TABLE 10
ANALYTICAL RESULTS OF MIDDLE ZONE CATALYSTS

SAMPLE	V wt%	Ni wt%	MREM ^a wt%	MCAT/MREM	
				Bulk	Microprobe
HON 10% 760	3.48	2.22	10.13	0.56	----
HON 10% 710	6.72	3.27	11.24	0.89	----
HON 5% 760	2.83	1.00	5.99	0.64	0.82
HON 5% 710	3.33	1.58	5.33	0.92	0.98
ORIENTE 760	3.19	1.49	5.22	0.90	1.00
ORIENTE 710	3.57	1.57	5.93	0.87	0.90
CAÑO LI 760	0.48	2.00	4.34	0.57	0.94
CAÑO LI 710	1.16	4.21	4.08	1.31	1.50

^a MREM: Metals removed calculated by reactor mass balance

MCAT: Metals deposited on the catalyst

The results from the bulk analysis indicate that for the 710-710 experiments 90% or more of the metals that were removed for all the pretreated residua deposited onto the catalysts. When the temperature in the thermal zone was increased to 760⁰F still 90% of the metals removed for Oriente went onto the catalyst, but a lower proportion, 55 to 65% of the metals removed, went inside the catalyst for the Hondo and Caño Limon experiments. The calculations from the microprobe data show higher values but the same degree

of difference in the lower proportion of metals that went inside the catalyst for Hondo and Caño Limon at high thermal temperature. Also, when we opened the reactor for the Hondo and Caño Limon experiments at high temperature in the thermal zone, we observed a large amount of coke deposited on the walls at the top of the reactor and interstitially all over the catalyst and inert packing. In fact, for Caño Limon the interstitial coke was so high that unpacking the reactor became very difficult.

Distribution Factors

The microprobe analysis gives the radial profile for Ni, V, Mo and other selected elements. From the microprobe data we calculated a vanadium penetration factor Q_v which is the ratio of the average vanadium concentration to the maximum radial vanadium concentration. The calculation procedure is presented in Appendix B. The values found were consistent with data for other small pore catalysts (Aldag, 1989).

We used the catalysts from Runs 01 and 02 to check if there are any differences in distribution factor with different levels of metals removed from the oil and deposited in the catalyst. Table 11 shows the average penetration factors and the corresponding standard deviations. These average values are calculated as follows: For each experiment three pellets are analyzed from the top section and three from the bottom section. For each pellet

four traverses or radii are analyzed in the microprobe and four values of Q_v calculated. Appendix B shows a sample calculation and a listing of the microprobe data. We averaged the four Q_v values for each pellet, so we obtain six values of Q_v per experiment. The average of these six values is the result reported.

TABLE 11
 Q_v AT DIFFERENT METALS LOADING

CONDITIONS	HONDO 5%	HONDO 10%	T TEST
<div style="border: 1px solid black; display: inline-block; padding: 2px;">710 710</div>	0.090 ± 0.003	0.092 ± 0.009	$\mu_{\text{HON5}} = \mu_{\text{HON10}}^a$ $\mu_{\text{HON5}}^{710} \neq \mu_{\text{HON10}}^{760}$
<div style="border: 1px solid black; display: inline-block; padding: 2px;">710 760</div>	0.10 ± 0.01	0.11 ± 0.01	$\mu_{\text{HON5}} = \mu_{\text{HON10}}$

^a HON5 = HONDO AT 5%, HOND10 = HONDO AT 10%
 710 = 710-710 CASE, 760 = 760-710 CASE

With the data from all the experiments we calculated 90% confidence intervals to find out if the differences among the averages were statistically significant. Most of the intervals overlapped, so an additional test was necessary. A statistical test for significant differences

between two means when the standard deviations are known is the T test (Walpole and Myers, 1978). The main assumption in the T test is that the populations are approximately normal with equal variances. The null hypothesis is that two means are equal and the alternative hypothesis is that they are different.

The T test was applied to the Hondo experiments and the results, presented in Table 11, indicate that there are no differences between the average penetration factors for 5 and 10% metals loading. However, at higher temperature the average penetration factor increases for both 5% and 10% metals removed and the difference is statistically significant. This is a good indication of the reproducibility of the results.

Table 12 shows the average penetration factors and the corresponding standard deviation for Hondo, Oriente, and Caño Limon for 5 wt% metals removed. The T statistic test was applied to these data to see if there were differences for the different residua. From the results of this analysis, which is presented in Table 13, and the values from Table 12 we conclude with 90% confidence that the following is happening: For the 710-710 runs the average penetration factors for Hondo and Oriente are equal and smaller than the average penetration factor for Caño Limon. For the 710-760 experiments the average penetration factor for Hondo and Caño Limon are equal and greater than the average penetration factor for Oriente. We can also say

TABLE 12
AVERAGE PENETRATION FACTORS

CONDITIONS	HONDO	ORIENTE	CAÑO LIMON
710 710	0.090 ± 0.003	0.087 ± 0.005	0.11 ± 0.01
710 760	0.10 ± 0.01	0.075 ± 0.004	0.11 ± 0.01

TABLE 13
RESULTS FROM STATISTIC ANALYSIS

710 710	$\mu_{\text{HON}} = \mu_{\text{ORI}}$	$\mu_{\text{HON}} \neq \mu_{\text{CNL}}$	$\mu_{\text{ORI}} \neq \mu_{\text{CNL}}$
710 760	$\mu_{\text{HON}} \neq \mu_{\text{ORI}}$	$\mu_{\text{HON}} = \mu_{\text{CNL}}$	$\mu_{\text{ORI}} \neq \mu_{\text{CNL}}$
	$\mu_{\text{HON1}} \neq \mu_{\text{HON6}}^a$	$\mu_{\text{ORI1}} \neq \mu_{\text{ORI6}}$	$\mu_{\text{CNL1}} = \mu_{\text{CNL6}}$

^a HON = HONDO, ORI = ORIENTE, CNL = CAÑO LIMON
1 = 710-710 CASE, 6 = 760-710 CASE.

that when we increase the temperature in the thermal zone to 760 the average penetration factor increases for Hondo, decreases for Oriente, and stays the same for Caño Limon.

Results from Hg Porosimetry Analysis

The fresh and spent catalyst from the middle section of the catalyst bed were examined for mercury penetration analysis by the Phillips Analytical Branch. Table 14 lists the pore volume, surface area, and mean pore diameter for the spent catalysts. The values for the fresh catalyst are: 0.5 cm³/g pore volume, 270 m²/g surface area, and 78 Å average pore diameter.

TABLE 14
SPENT CATALYST PROPERTIES^a

CONDITIONS	HONDO 10%	HONDO 5%	ORIENTE	CAÑO LIMON
710	0.20	0.26	0.28	0.25
	126	192	176	175
	70	56	66	60
760	0.16	0.16	0.20	0.27
	112	112	132	209
	62	62	64	54

- ^a Data calculated using Hg Porosimeter
^b First number is pore volume in cm³/g
 second number is surface area in m²/g
 third number is average pore diameter in angstrom

The porosimetry data suggests higher reduction in surface and pore volume for Hondo than for Caño Limon and Oriente. However, two sets of catalysts, Hondo 5% 710-710 and Caño Limon 760-710, show much higher surface areas and smaller pore diameters than the other catalysts. There was not enough sample to duplicate these results.

LC-ICP Results

An LC-ICP chromatogram for Hondo asphaltene is shown in Figure 18. The chromatogram shows the concentration of the element, in this case vanadium, versus the retention time. Retention time is inversely proportional to the size of the molecules. The large molecules are eluted at short retention times and the small molecules at longer retention times. The asphaltene fraction for the Hondo residuum shows a broad distribution of the vanadium molecules distributed over the whole size range.

Figure 19 shows the size distribution for vanadium in the asphaltenes from the LC-ICP analysis for Hondo experiments. The top curve is the distribution for the asphaltenes from Hondo that was shown before in Figure 18. From high to low concentration the other curves are: the product from the down-flow reactor, then the product from the up-flow reactor at 710⁰F, and finally the product from the up-flow reactor when the temperature of the thermal zone was increased to 760⁰F. Essentially this figure shows that in the pretreatment step a good proportion of the

ASPHALTENE HONDO RESIDUE

MOLECULAR SIZE DISTRIBUTION

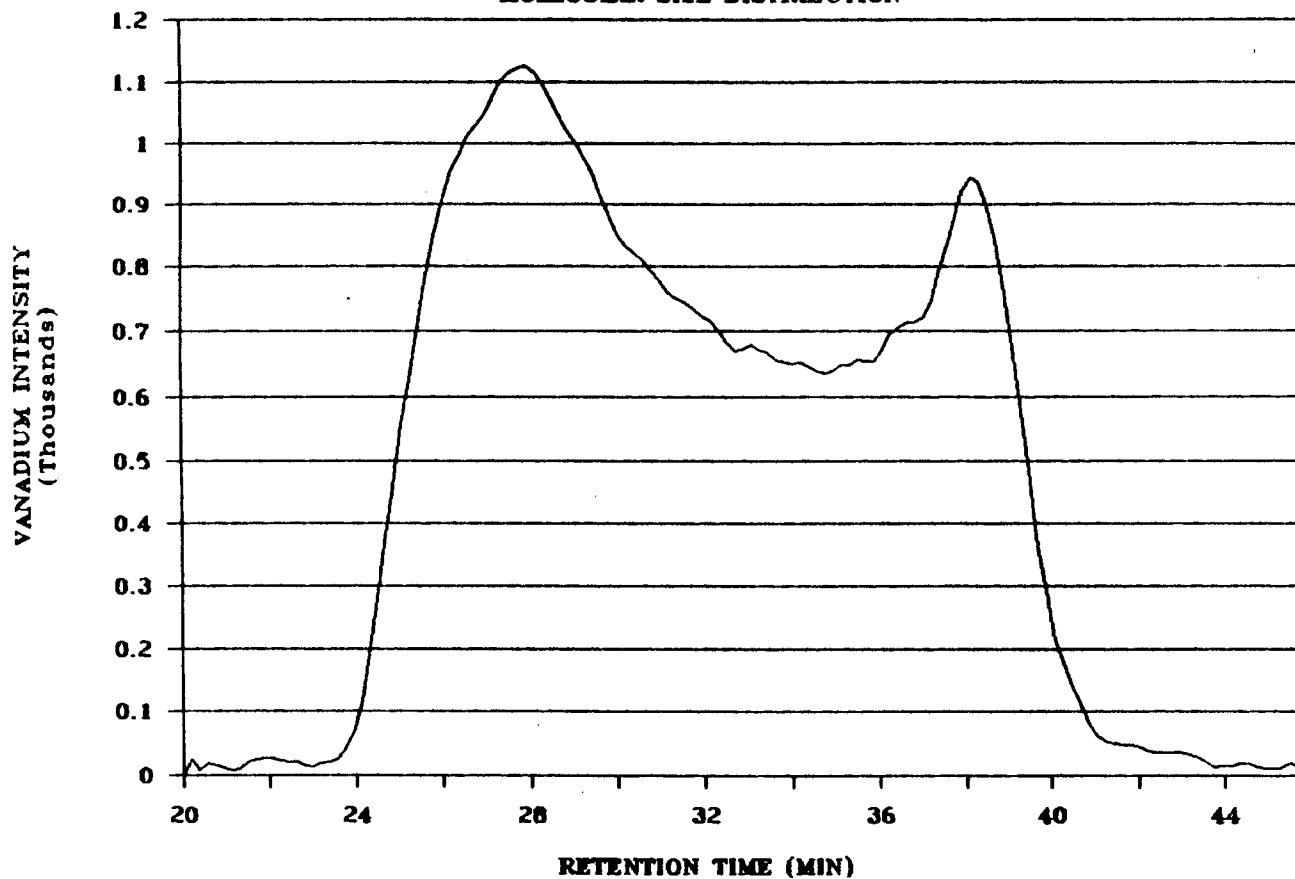
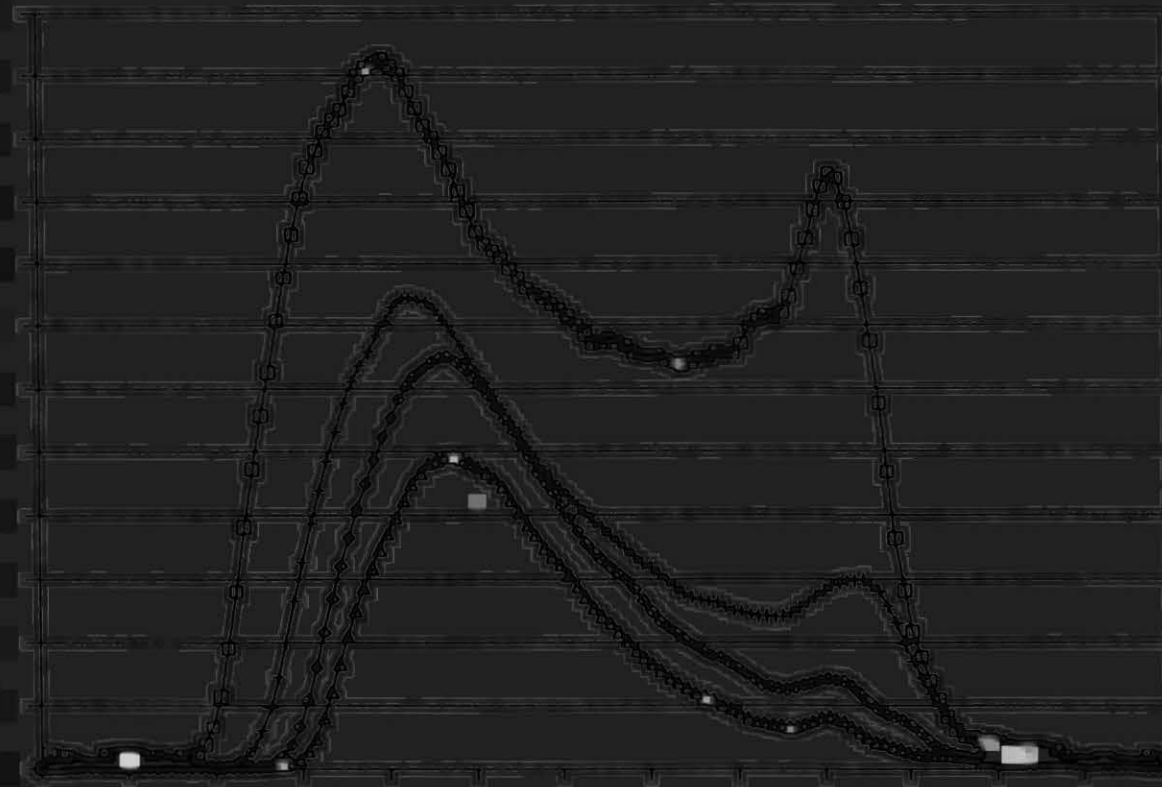


Figure 18. LC-ICP Molecular Size Distribution for Vanadium in a Hondo Residue



small molecules in the asphaltenes are removed and there is some conversion of the large molecules. The additional contact time in the up-flow reactor results in additional removal of the small molecules plus some conversion of the large molecules. The higher temperature in the thermal zone of the second reactor (Run 03) showed additional conversion over the whole molecular size range. As the conversion increased the size of the large molecules decreased as evidenced by a shift in the distribution towards smaller molecular size. This supports the hypothesis of breakdown or dealkylation of the asphaltenes into smaller molecules. Dealkylation of the asphaltenes helps to uncover vanadium molecules that are originally buried in the aromatic core of the asphaltene molecule.

Figure 20 is the molecular size distribution for Oriente asphaltenes. The curve with the higher intensity peak in the low molecular range is the asphaltene from Oriente residuum, the next curve is the product from the down-flow reactor or pretreated Oriente, and the last curve is the product from the up-flow reactor at 710⁰F. With respect to Hondo, there is a lower proportion of small to large molecules for Oriente, and the large molecules are not affected by the process conditions used. The conversion is low and restricted to small molecules. The curve for the high temperature in the thermal zone of the first reactor is not shown because it overlaps with the curve for the low temperature level. This strongly suggests that Oriente is a

ASPHALTENE ORIENTE SIZE DISTRIBUTION

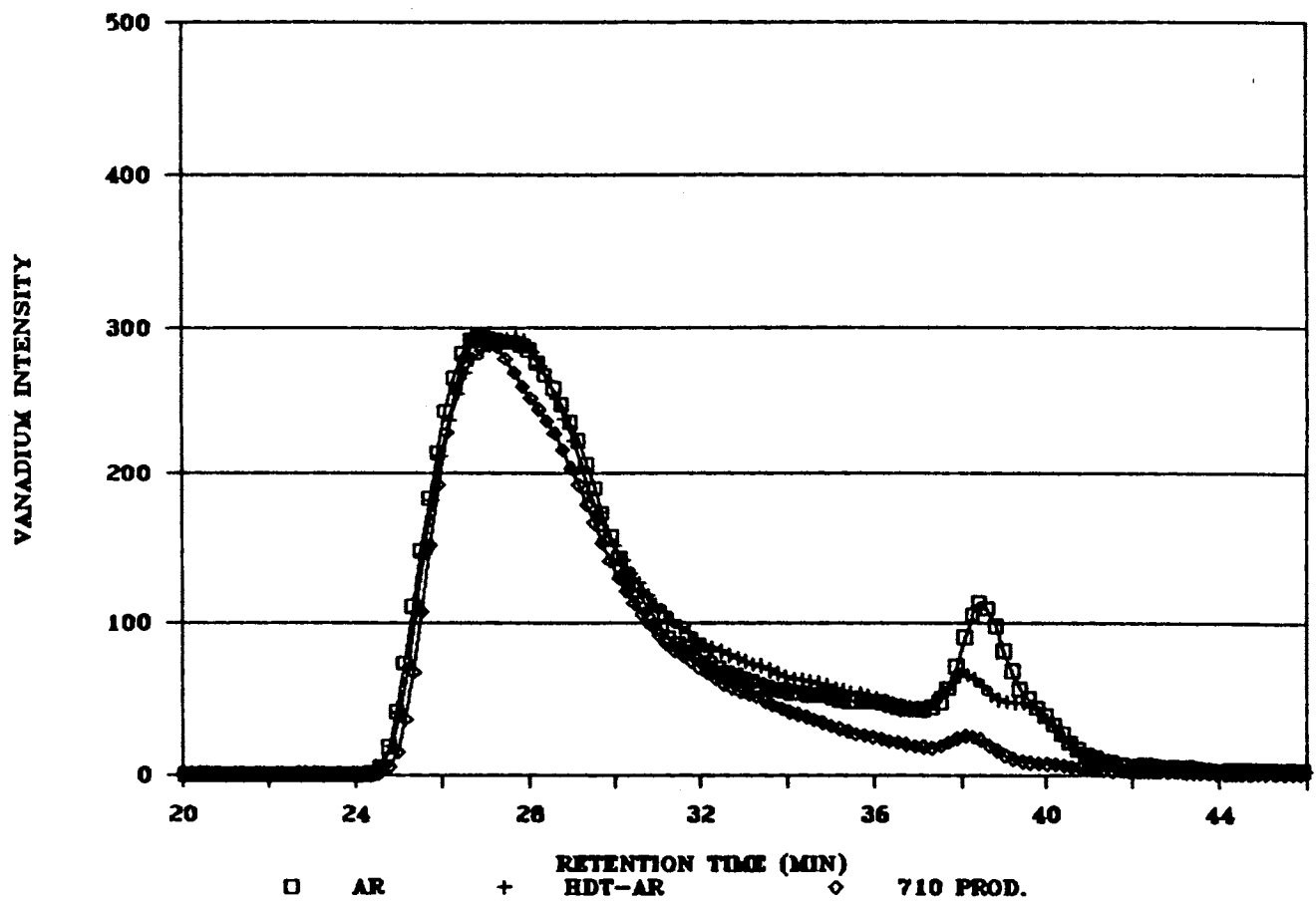


Figure 20. Molecular Size Distribution of V for Oriente as Function of Reaction Conditions

more refractory residue to process. The thermal severity used was not sufficient to crack the large Oriente molecules.

Results from Hondo and Oriente indicate that the catalyst activity is mainly in the small molecular range as expected with this catalyst. Therefore, the large molecules have to be broken thermally before they can enter the catalyst pores where vanadium is removed.

Figure 21 presents the distribution of molecular size for the Caño Limon asphaltenes. The distributions can be differentiated by looking at the intensity of the low molecular weight range peak at retention times larger than 34 minutes. The product from the down-flow reactor or hydrotreated Caño Limon is very slightly reduced in the intensity of the small size peak. On the other hand the removal of small molecules continue in the up-flow reactor at 710⁰F. When the temperature in the thermal zone is increased to 760⁰F the conversion of small molecules increases shifting the small molecular size peak towards slightly bigger size molecules. The profile for Caño Limon resembles the profile for Oriente except that Caño Limon has a somewhat larger proportion of smaller molecules. The LC-ICP profiles for Caño Limon suggest that most of the activity for the removal of the vanadium is also in the small molecules. However, at the high temperatures in the thermal zone for the up-flow reactor there is some conversion of large molecules indicated by the shift of the

ASPHALTENE CAÑO LIMON SIZE DISTRIBUTION

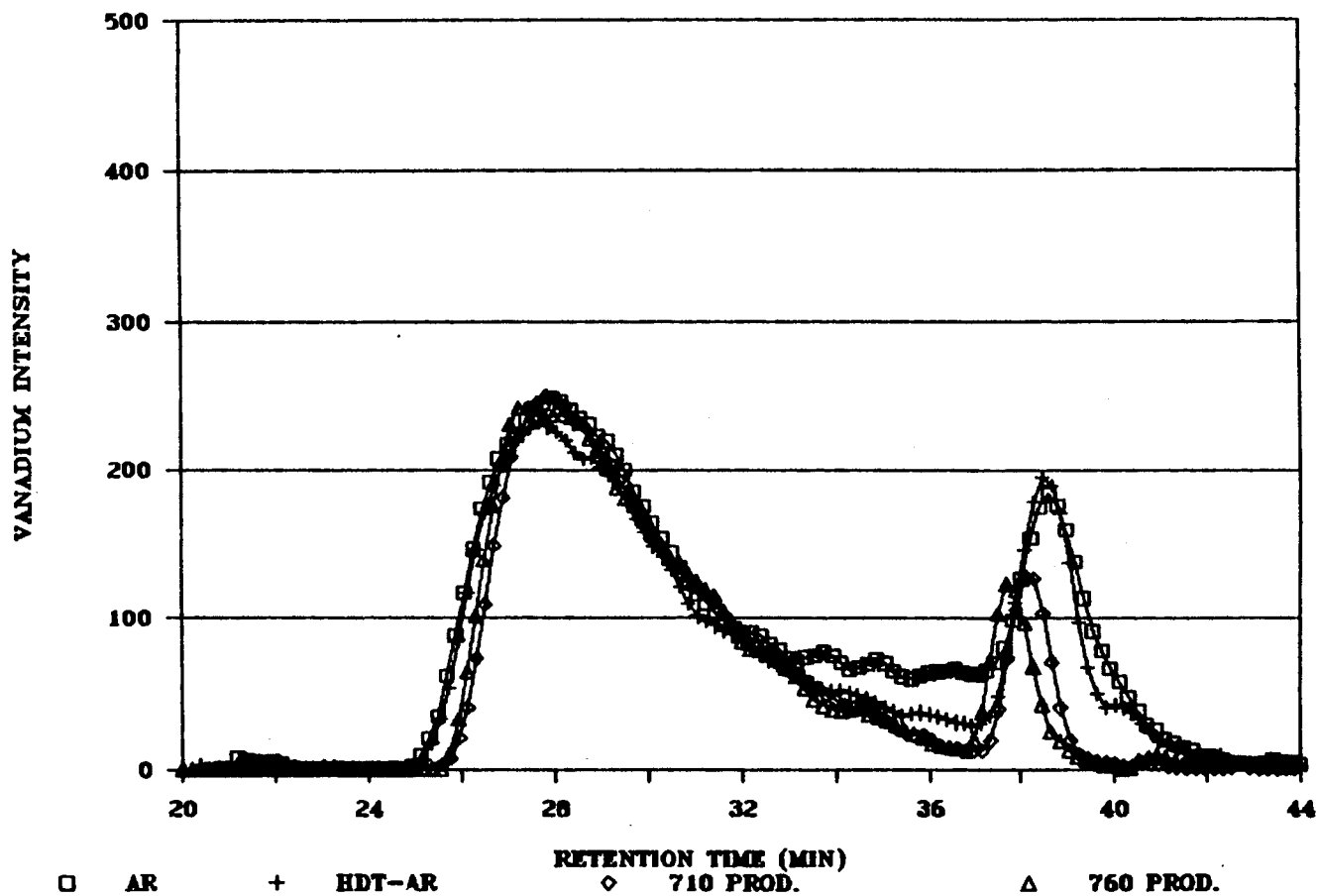


Figure 21. Molecular Size Distribution of V for Caño Limon as Function of Reaction Conditions

large molecules towards smaller molecular size. This correlates with the high levels of coke observed for this experiment as is the case of Hondo. The Caño Limon experiments support the idea that conversion of large molecules is mainly a thermal process and results in the formation of interstitial coke. The small molecules from Caño Limon asphaltenes are not as catalytically reactive as the small molecules from Hondo asphaltenes. It almost appears that some of the small molecules in Caño Limon are very unreactive and this may explain the higher penetration factor observed for Caño Limon with the microprobe data.

CHAPTER IV

DISCUSSION OF RESULTS

Asphaltenes Conversion and HDM

Table 15 presents average percent HDM results for the catalytic and thermal up-flow experiments. The conversion shown in this Table is based on the pretreated feeds and it summarizes the results presented in Figures 7 through 17. As previously found for the pretreatment, the data show that for catalytic HDM, Hondo is the most active followed by Caño Limon and then Oriente. In the catalytic experiments, as the temperature in the thermal zone is raised from 710 to 760⁰F, the conversion increases by 10%, from 39 to 49%, for Hondo, by 13%, from 20 to 33%, for Caño Limon, and remains the same for Oriente at 15%. Meanwhile, the thermal results show that at 710⁰F there is no additional metals removal. However, increasing the lower portion of the bed thermally to 760⁰F results in approximately 10% increase in metals removal for Hondo and Caño Limon and no increase for Oriente. Thus, the additional conversion that we have seen for Hondo and Caño Limon can be attributed to an increase not in catalyst activity but in thermal removal activity. Coupling of these

TABLE 15
 AVERAGE PERCENT HDM CONVERSION AS FUNCTION OF
 REACTION CONDITIONS

CONDITIONS	HONDO	ORIENTE	CAÑO LIMON
<u>CATALYTIC</u>			
710-710 PRODUCT	39	15	20
760-710 PRODUCT	49	15	33
DIFFERENCE	10	0	13
<u>THERMAL</u>			
710-710 PRODUCT	0	1	0
760-710 PRODUCT	8	1	11
DIFFERENCE	8	0	11

results with LC-ICP molecular size distribution of the V-containing asphaltenes shows how the differences in activity for the three residua correlate well with the proportion of small molecules present in the asphaltenes.

Table 16 presents the percent asphaltene conversion for the up-flow tests. Essentially, for both Hondo and Caño Limon we see considerable asphaltene conversion when the catalyst was present. At 760⁰F in the thermal zone, asphaltene conversion is 20% higher for Hondo and 16% higher for Caño Limon for the catalytic tests. Oriente shows an increase of near 5% which can be within analytical error. For the thermal results, increasing the temperature of the lower portion of the thermal bed to 760⁰F also increases conversion of the asphaltenes by 20% for Hondo and 13% for Caño Limon. In our thermal studies we see no asphaltene conversion for Oriente and the asphaltene conversions for Hondo and Caño Limon are very similar to the catalytic results. This is summarized in Figure 22 which shows that in the thermal zone asphaltene conversion is obtained with low HDM. Most of the demetallization of the converted asphaltenes occurs in the presence of the catalyst loaded in the catalyst zone. At high temperatures demetallization occurs thermally but mainly due to coking reactions.

The fact that asphaltenes are converted thermally without substantial metals removal is somewhat surprising. Consistent with the work of Savage et al. (1988), one

TABLE 16
 PERCENT ASPHALTENE CONVERSION AS FUNCTION OF
 REACTION CONDITIONS

CONDITIONS	HONDO	ORIENTE	CAÑO LIMON
<u>CATALYTIC</u>			
710-710 PRODUCT	30	5.4	24
760-710 PRODUCT	50	9.9	40
DIFFERENCE	20	4.5	16
<u>THERMAL</u>			
710-710 PRODUCT	25	0	20
760-710 PRODUCT	50	0	33
DIFFERENCE	25	0	13

HDM vs. ASPHALTENE CONVERSION

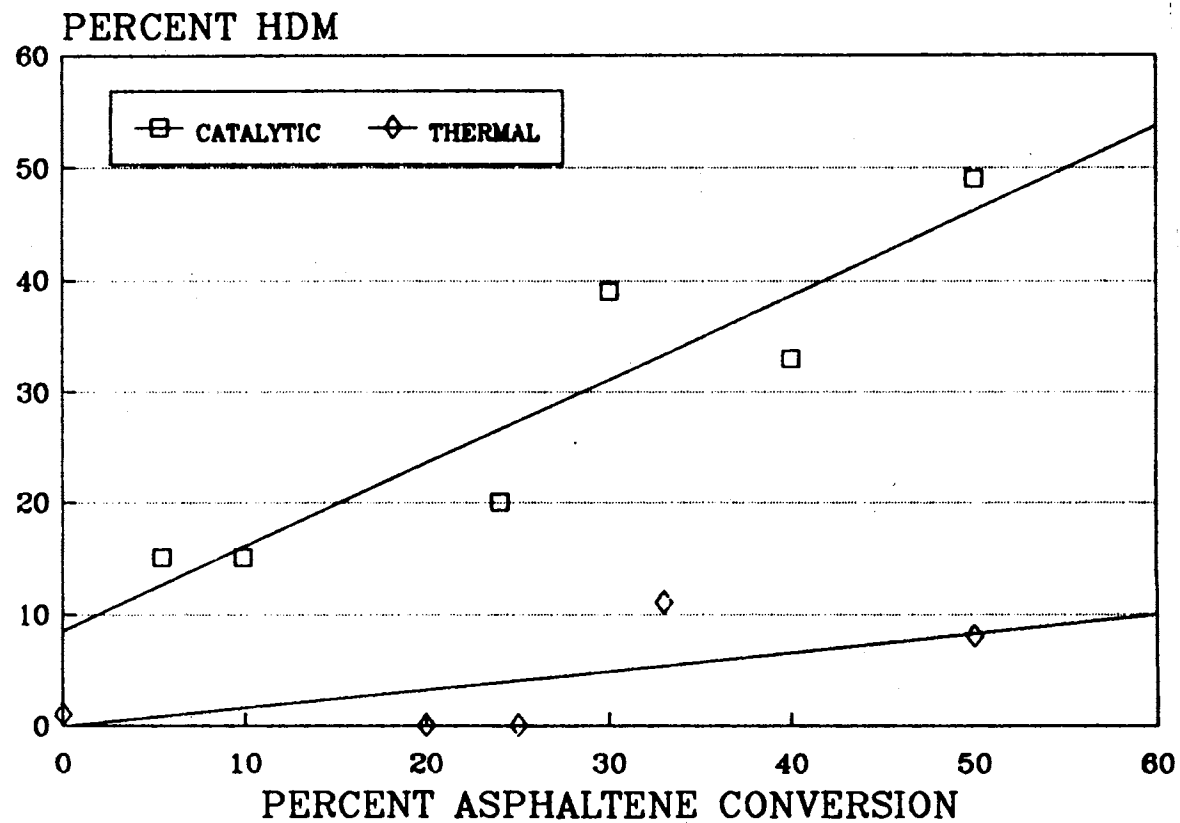


Figure 22. HDM vs Asphaltene Conversion for Catalytic and Thermal Tests

possible explanation is that at low temperature asphaltenes dealkylate or break into modified asphaltenes which contain the metals, and other metal free fractions such as maltenes and/or gases. On the other hand, at high temperature additional conversion of the asphaltenes is accompanied by some demetallization involving coke formation. Table 17 shows the vanadium concentration in the asphaltenes for the thermal and catalytic tests. At each temperature level, the concentration of vanadium is consistently higher for the thermal than for the catalytic experiments. Proportionally, the greatest increase is for Hondo, followed by Caño Limon and then Oriente. These results, obviously support the hypothesis of thermal asphaltenes conversion without substantial demetallization.

Interaction of Thermal and Catalytic Metals Removal

Results indicate that the first step in decomposition of asphaltenes from residual oils is a thermal conversion at low temperatures without metals removal. At higher temperatures there is additional thermal conversion which involves some demetallization. For Hondo asphaltenes there is a decrease in hydrogen in the reaction products. This indicates that some hydrogen rich constituents such as alkyl groups leave the asphaltene molecule during reaction. This is consistent with the work of Savage et al. (1988) who stated that some dealkylation takes place during

TABLE 17
VANADIUM CONCENTRATION IN ASPHALTENES

CONDITIONS	HONDO	ORIENTE	CAÑO LIMON
<u>CATALYTIC</u>			
710-710 PRODUCT	905	1080	230
760-710 PRODUCT	950	1110	220
<u>THERMAL</u>			
710-710 PRODUCT	1100	1150	280
760-710 PRODUCT	1260	1200	250

pyrolysis of Hondo asphaltenes. They observed high asphaltenes conversion in the first 20 minutes of reaction. LC-ICP and microprobe data indicate that there is high dealkylation and conversion of vanadium containing molecules during the pretreatment step for the Hondo asphaltenes. The fact that Hondo is highly alkylated allows its asphaltenes to undergo additional thermal conversion. Caño Limon shows lower reactivity than Hondo and Oriente is the most refractory of the three residua.

The LC-ICP molecular distribution for the thermal conversion of the asphaltenes is presented in Figure 23 for Hondo. In this Figure the distribution of vanadium-bearing molecules from the thermal experiments are compared to the distribution from the hydrotreated residue. The Hondo profiles indicate that there is some conversion of large and formation of small molecules. The formation of smaller molecules is indicated by the increase in concentration and the shift of the maximum to larger retention times. These results indicate that at least for Hondo, the thermal reaction affects the molecular size distribution by converting large into smaller molecules. This is what was expected for all the residues, but we saw it only for Hondo. Moreover, the conversion of asphaltenes into smaller fragments remains small compared to the number of small molecules initially present in the asphaltenes. Also, we observed that when severity is increased coking reactions become important and the asphaltenes are converted into

ASPHALTENES HONDO SIZE DISTRIBUTION

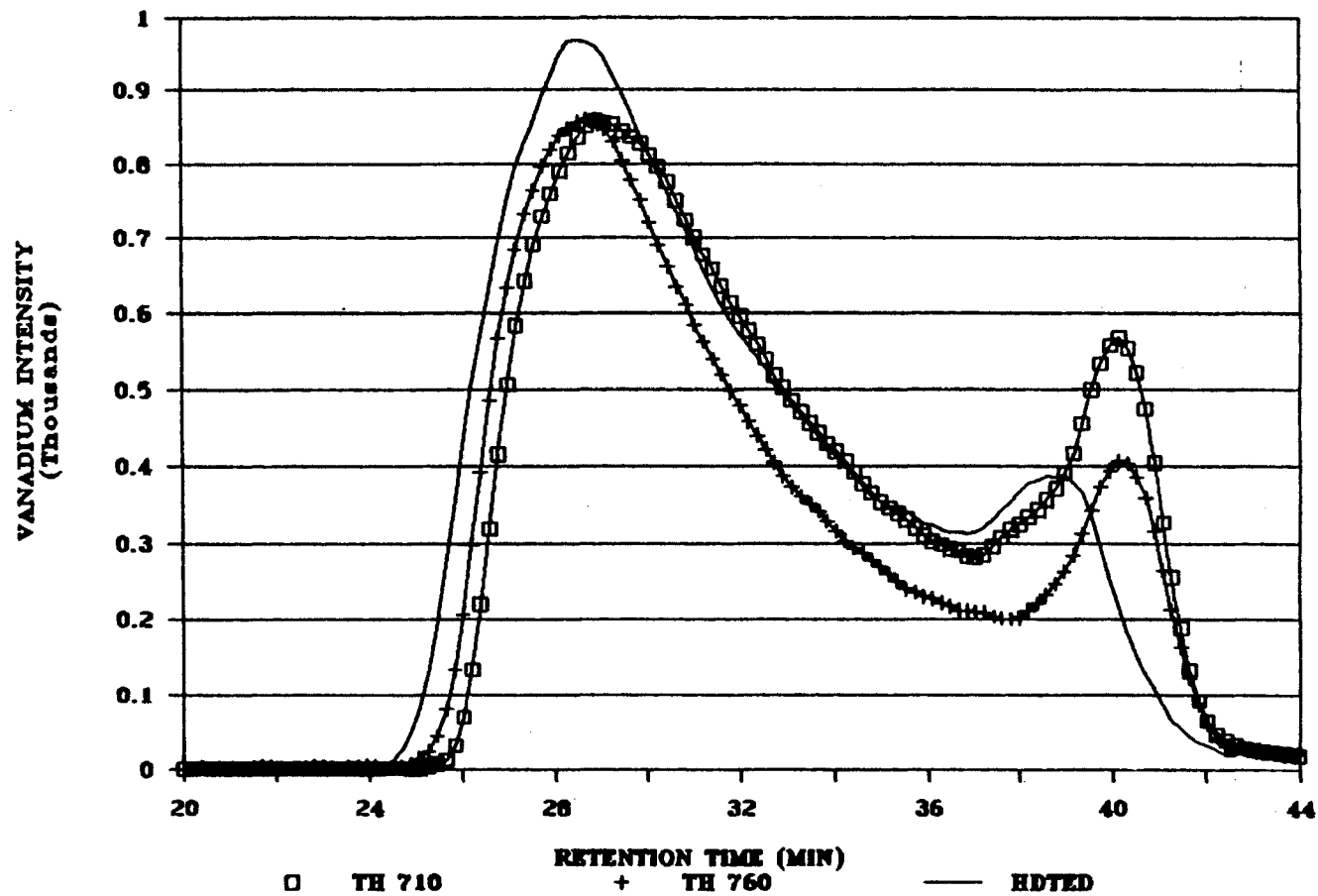


Figure 23. Molecular Size Distribution of V for Hondo at Thermal Conditions

coke instead of splitting to lower molecular weight fragments. The distribution of vanadium molecules for Oriente asphaltenes did not change by thermal treatment. For Caño Limon comparison of the profiles did not show the decomposition of the large into smaller fragments. Consequently, results indicate that metals removal at the back end of graded hydrotreaters is controlled by size distribution. For Hondo there is some additional thermal conversion but for Caño Limon and especially for Oriente, there is none. As the temperature in the thermal zone is increased, Oriente remains stable whereas Hondo and Caño Limon show added demetallization by coking. At the higher thermal temperature none of the three feeds produce extremely high metals penetration levels.

A general mechanism that we propose to represent asphaltene decomposition and demetallization is presented in Figure 24. It is a modification of the model presented by Savage and coworkers(1988). At low temperatures, asphaltenes (A) react thermally to form intermediates that are not demetallized (A^*), maltenes (M) and gases (G). The intermediate or converted asphaltenes undergo a diffusion process into the catalyst were they are partially demetallized (A^{**}) producing more maltenes and gases, and depositing metals in the catalyst surface. At higher temperatures, the partially demetallized asphaltene can undergo further thermal dehydrogenation and demetallization by coking. Therefore, at these conditions coking becomes an

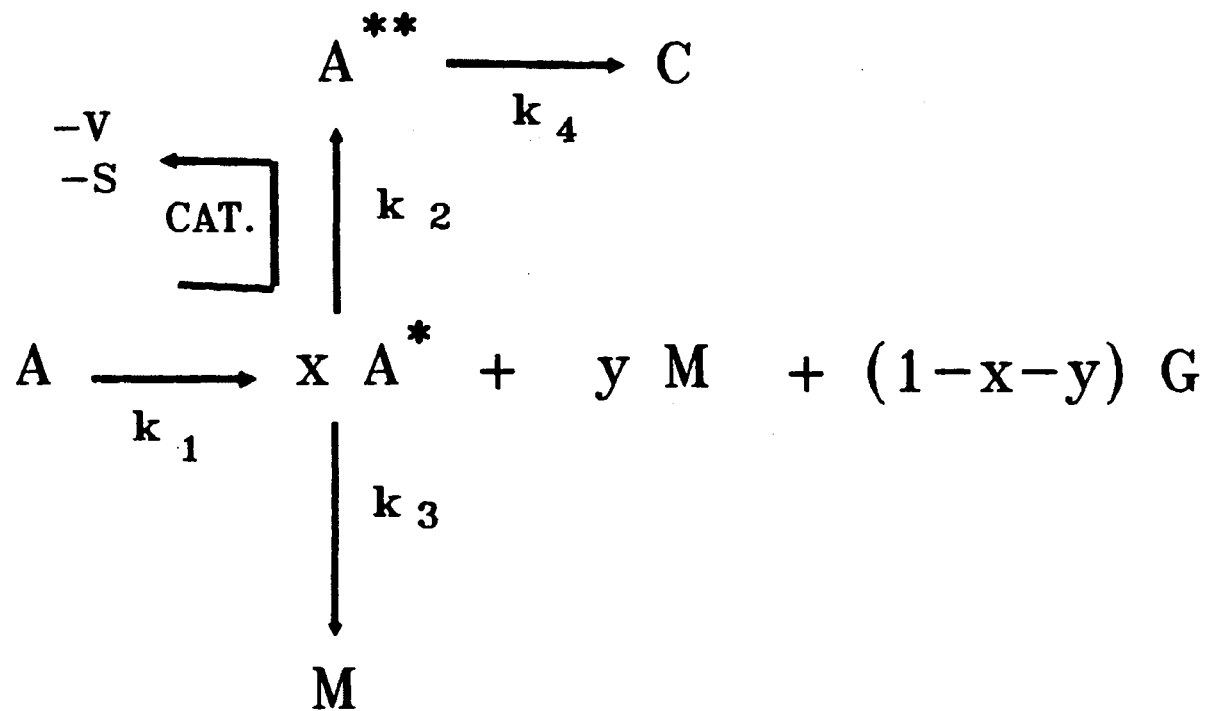


Figure 24. Mechanism for Asphaltene Decomposition

important HDM mechanism and also plays a role in asphaltene conversion. These observations are consistent with the analytical and microprobe data that show how at higher temperatures for Hondo and Caño Limon 40% of the metals are removed thermally and deposited outside the catalyst. Results are consistent with Savage and coworkers' findings of increased coke formation at high severity during asphaltene pyrolysis. It also correlates well with the amounts of interstitial coke produced in the Hondo and Caño Limon tests. A sample from the interstitial coke analyzed by ICP showed high levels of metals supporting the contention that the coking mechanism is significant in HDM. Therefore, at long times on stream the coking propensity of the feeds has a significant impact on the performance of the highly active HDS catalyst loaded at the bottom of the graded beds and the overall performance of the reactors.

Qualitative solution of Modified Delaware Mechanism

Using the modified mechanism from Savage et al. (1988) we developed kinetic equations assuming first order reactions for each one of the conversion steps in the model. The kinetic equations are presented in Table 18. This is a set of simultaneous ordinary differential equations that were solved analytically by a substitution and sequential integrating factor technique. The solution of the kinetic model gives the concentration profiles for

TABLE 18

KINETIC EQUATIONS AND ANALYTICAL SOLUTION FOR
ASPHALTENE DECOMPOSITION MODEL

KINETIC MODEL EQUATIONS

$$\begin{aligned} d[A]/dt &= K_1 [A] & d[M]/dt &= y K_1 [A] + K_2 [A^*] \\ d[G]/dt &= (1 - x - y) K_1 [A] & d[A^{**}]/dt &= K_3 [A^*] - K_4 [A^{**}] \\ d[A^*]/dt &= x K_1 [A] - (K_2 + K_3) [A^*] & d[C]/dt &= K_4 [A^{**}] \end{aligned}$$

MODEL SOLUTION

$$\begin{aligned} [A] &= CF_1 \cdot \text{EXP}(-K_1 t) + CF_2 \cdot \text{EXP}(-(K_2 + K_3)t) \\ &\quad + CF_3 \cdot \text{EXP}(-K_4 t) \\ [M] &= (CF_4 + CF_5) \cdot \{1 - \text{EXP}(-K_1 t)\} + CF_6 \cdot (\text{EXP}(-(K_2 + K_3)t) - 1) \\ [C] &= CF_7 (1 - \text{EXP}(-K_1 t)) - CF_8 (1 - \text{EXP}(-(K_2 + K_3)t)) \\ &\quad + (CF_9 + CF_{10}) \cdot (\text{EXP}(-K_4 t) - 1) \\ [G] &= CF_{11} \cdot (\text{EXP}(-K_1 t) - 1) \end{aligned}$$

asphaltenes [A], maltenes [M], gases [G], and coke [C]. In these profiles the unconverted asphaltenes and the intermediates are considered as asphaltenes until they appear in the maltene, gas or coke fractions.

We selected values for the kinetic constants that qualitatively fit the conversion of asphaltenes from Hondo, Oriente and Caño Limon. The results are shown in Figures 25 to 27. For Hondo and Caño Limon (Figures 25 and 26) there is a rapid conversion of asphaltenes in the first hour to produce maltenes and some gases. Additional contact time increases the conversion of asphaltenes by coking reactions. The dots in this Figures indicate the asphaltene conversion obtained in this study. Oriente (Figure 27) shows the lowest conversion of asphaltenes and produces only maltenes. After 60 minutes of residence time additional conversion is negligible. The formation of coke and gases with Oriente is not significant compared to either Hondo or Caño Limon. Again, this representation is qualitative and, to obtain more quantitative results, additional tests of asphaltene conversion as a function of residence time are necessary. The significance of these results for small pore catalysts at the back of graded beds is that at high severity the asphaltenes from some residua such as Hondo and Caño Limon are converted to coke which is detrimental for the HDS activity of the small pore catalysts.

HONDO ASPHALTENE CONVERSION

QUALITATIVE SIMULATION

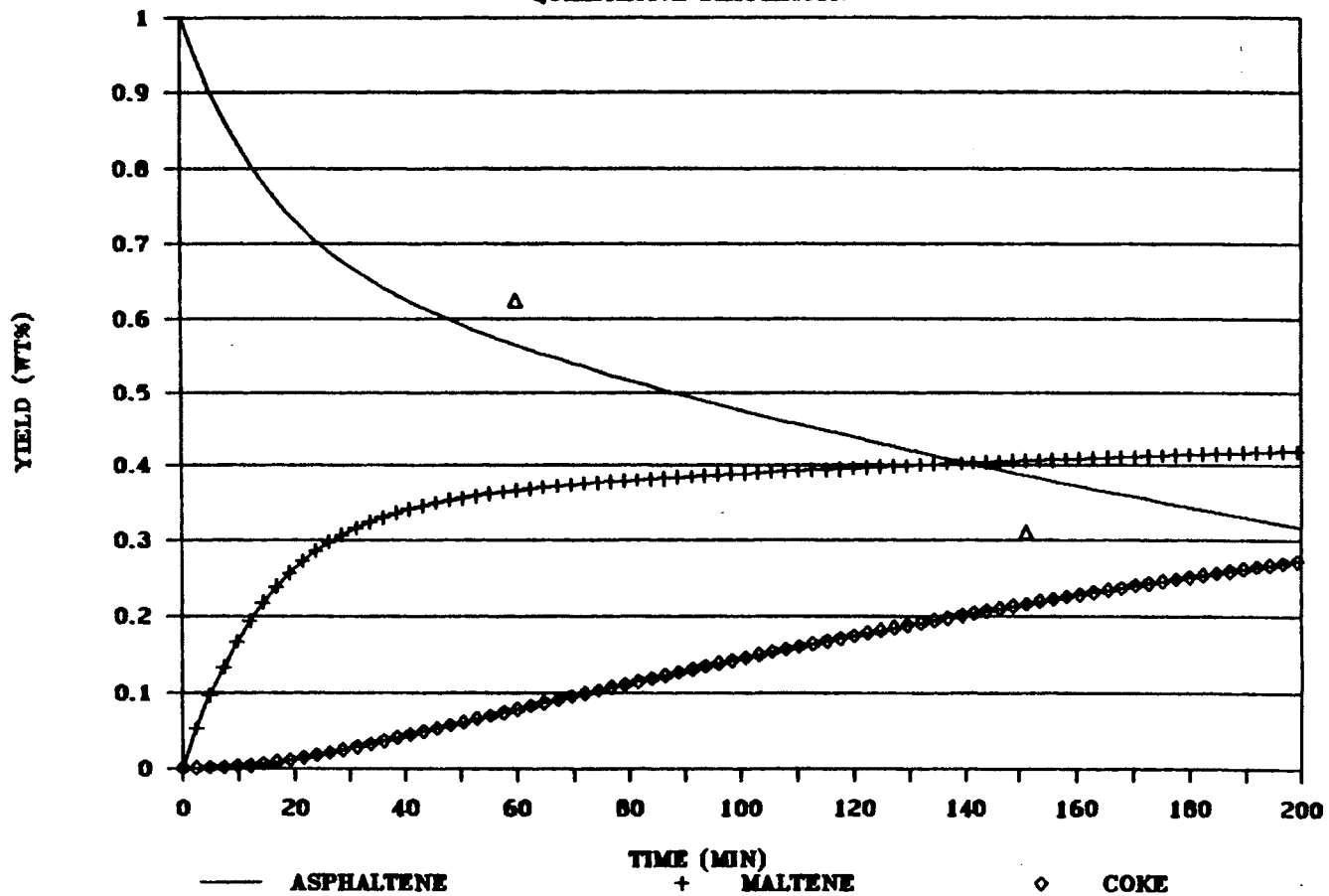


Figure 25. Asphaltene Conversion and Coking Tendency for Hondo

CAÑO LIMON ASPHALTENE CONVERSION

QUALITATIVE SIMULATION

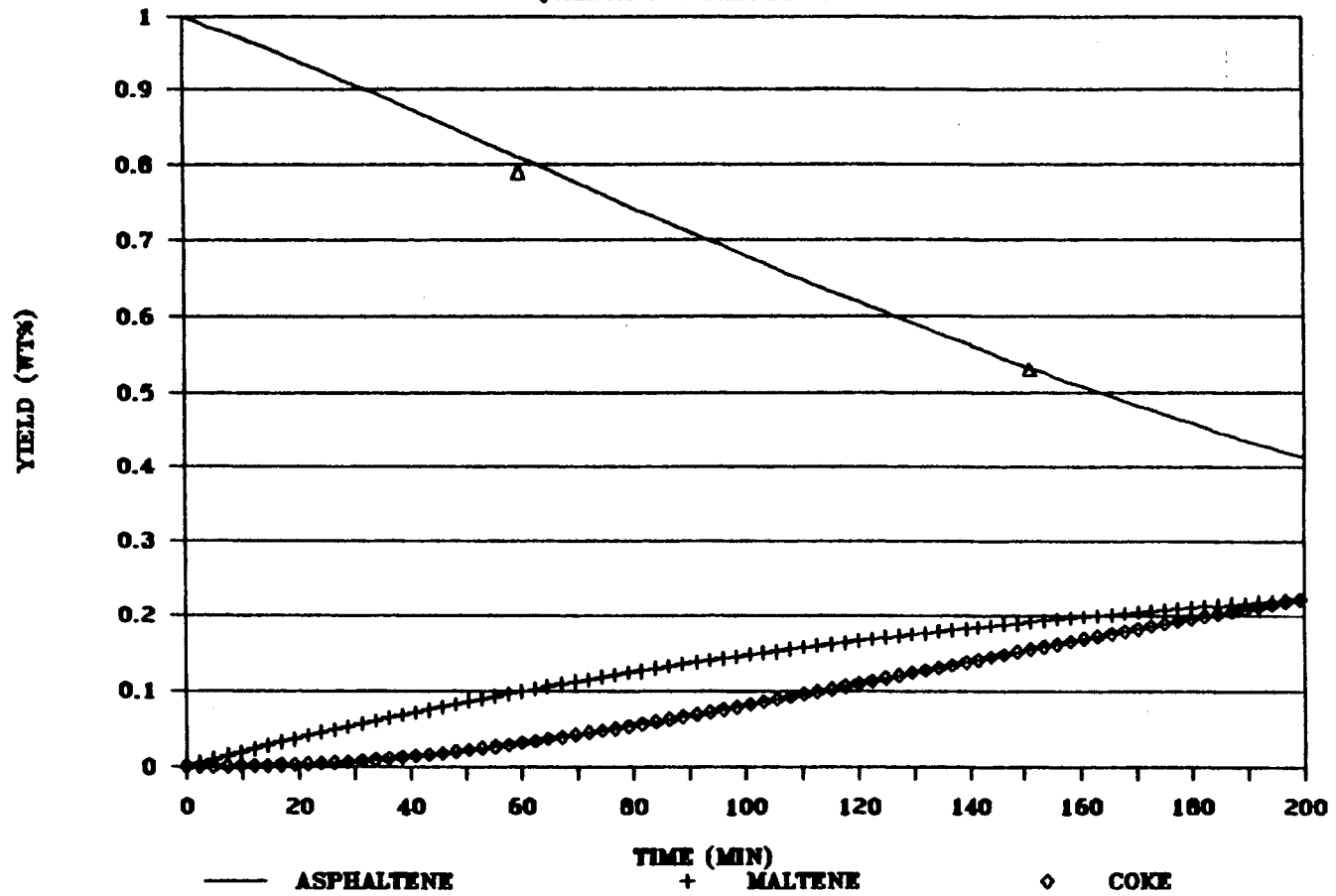


Figure 26. Asphaltene Conversion and Coking Tendency for Caño Limon

HONDO ASPHALTENE CONVERSION

QUALITATIVE SIMULATION

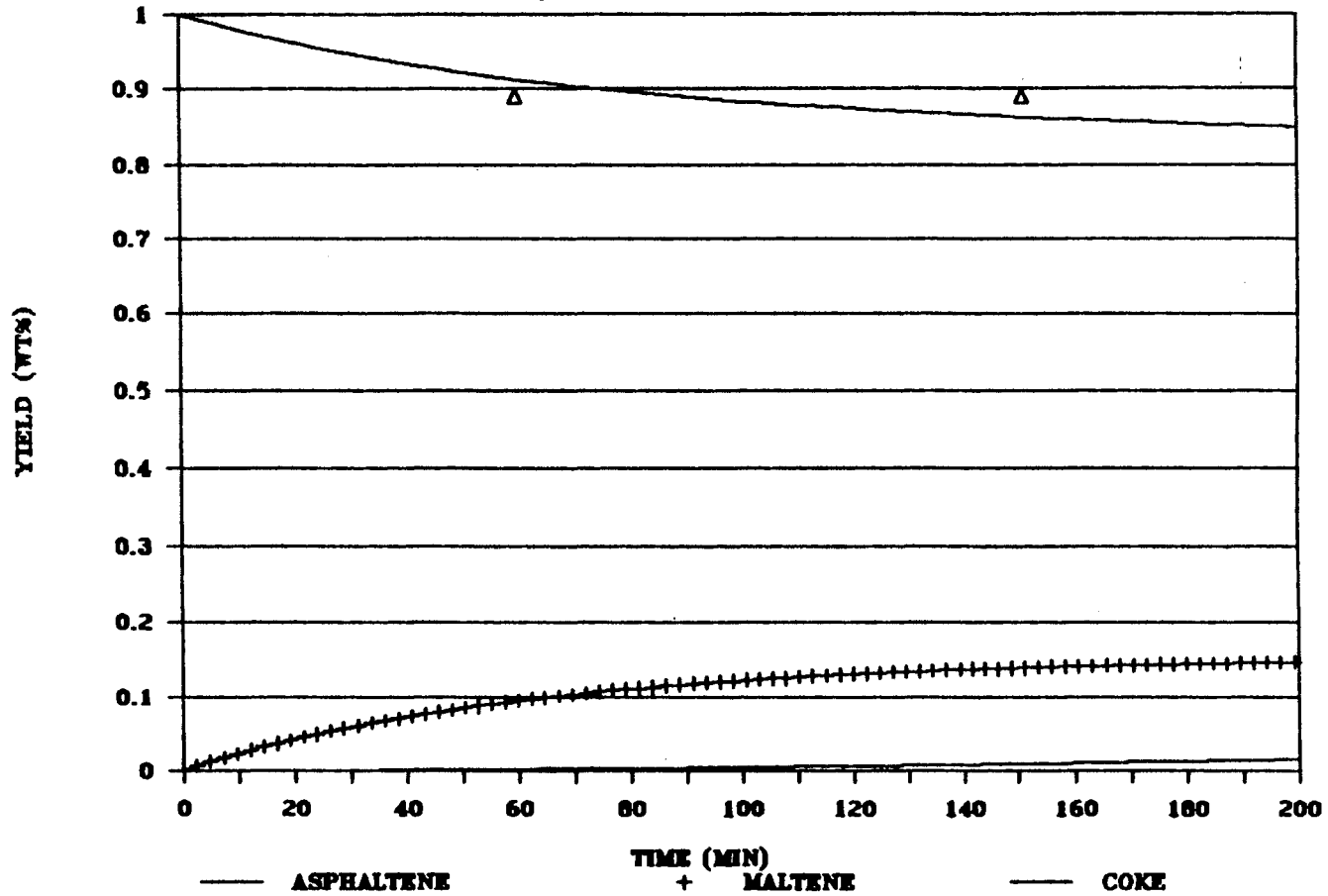


Figure 27. Asphaltene Conversion and Coking Tendency for Oriente

Catalyst Deactivation

To calculate the reaction rate constants for each one of the experiments we assumed a pseudo-first order kinetics for HDM and a second order for HDS. Many authors such as Hannerup and Jacobsen (1983) and Sughrue (1988) assume first order kinetics for HDM and second order above 50% conversion for HDS and we follow this approach. The data and sample calculations are presented in Appendix A.

To facilitate comparison among the different residues and experimental conditions, an activity factor (Levenspiel, 1972) was calculated by assuming the rate constant at 2 wt% metals removed in each run to be equal to one. The activity factor is the ratio of rate constants at other times during the run relative to the rate constant at 2 wt% metals removed. We selected metals removed as the independent variable because deactivation is strongly influenced by the amount of metals removed rather than by the time on stream.

Deactivation for Hondo Tests

760-710 Results. Runs 01 and 03 use Hondo pretreated residue to deposit 10 wt% and 5 wt% metals on the catalyst respectively. The temperature in these two runs are 760⁰F for the thermal zone and 710⁰F for the catalyst zone (See Table 8). Figure 28 shows the activity (HDM) versus the wt% metals removed for the two experiments. The calculation of

the activity factors eliminates the slight differences in properties of the two hydrotreated Hondo that we used. The activities of the two runs agree very well. Therefore any differences in rate constants for these two runs are likely to be due to feed properties and not to differences in catalyst or reactor conditions. This is true for both 710-710 and 760-710 experiments. Data from Figure 28 shows that Runs 01 and 03 have no significant deactivation for HDM. Most of the data for the activity factors vary between 0.95 and 1.1.

Figure 29 shows the activity factor (HDS) versus wt% metals removed also for runs 01 and 03. The two experiments follow the same activity profiles for HDS. The catalysts lose considerable HDS activity. The activity factors drop from 1 at 2 wt% metals removed to 0.8 at 6 wt% metals removed and subsequently to 0.6 at 10 wt% metals removed.

710-710 Results. The HDM and HDS activity for Runs 02 and 04 is shown in Figure 30 and 31. As for the 760-710 case the profiles for 5 and 10% metals removed are similar for both runs. The HDM activity factors range from 1 at 2 wt% metals removed to 0.85 at 5.5 wt% metals removed. The apparent increase in HDM activity for Run 02 after 6 wt% metals removed is due to a change in feedstock (See Appendix A) rather than to any changes in catalyst activity. From the activity profiles for these four experiments we can see that the catalyst maintained HDM

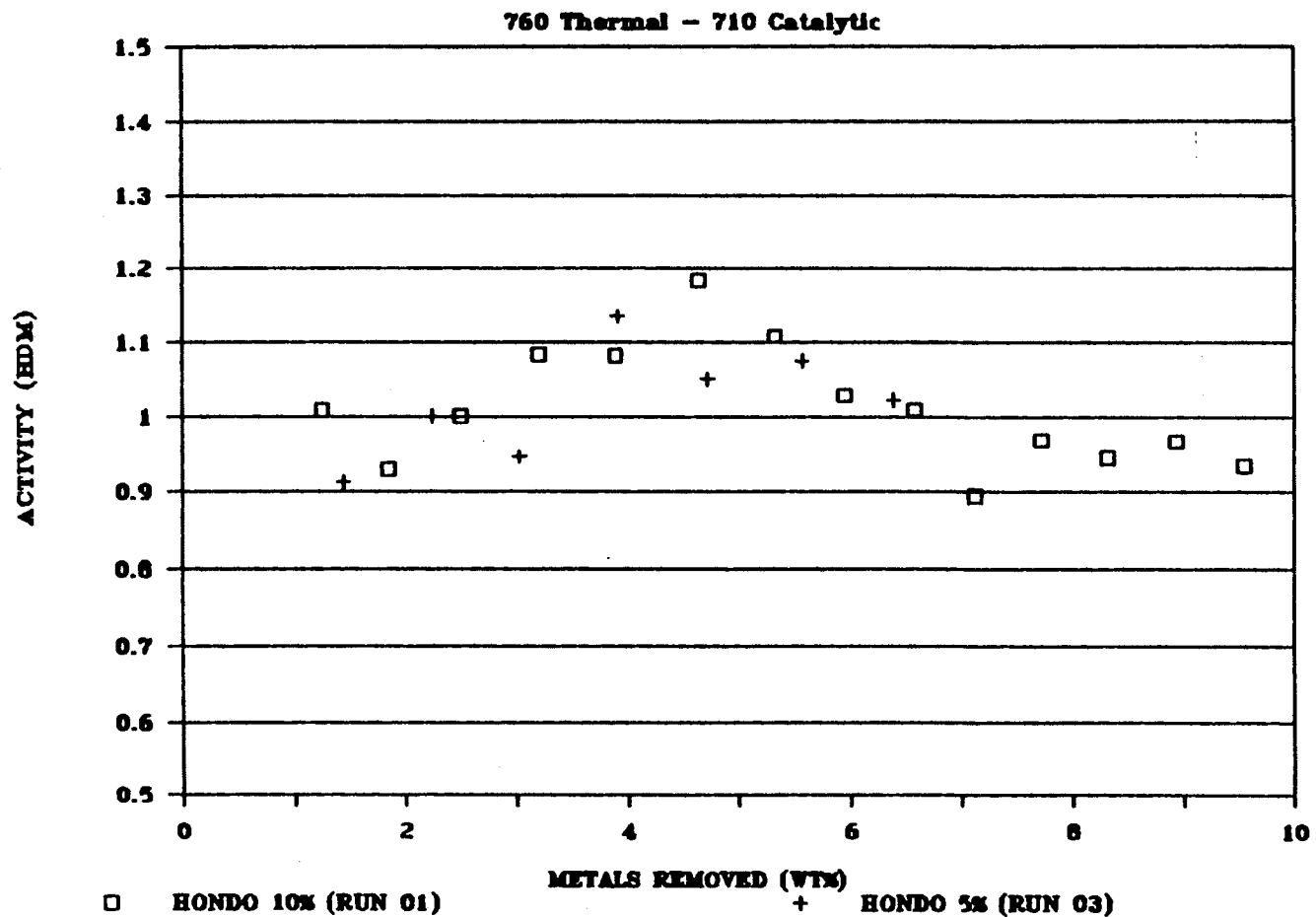


Figure 28. HDM Activity for Hondo (Runs 01 and 03)

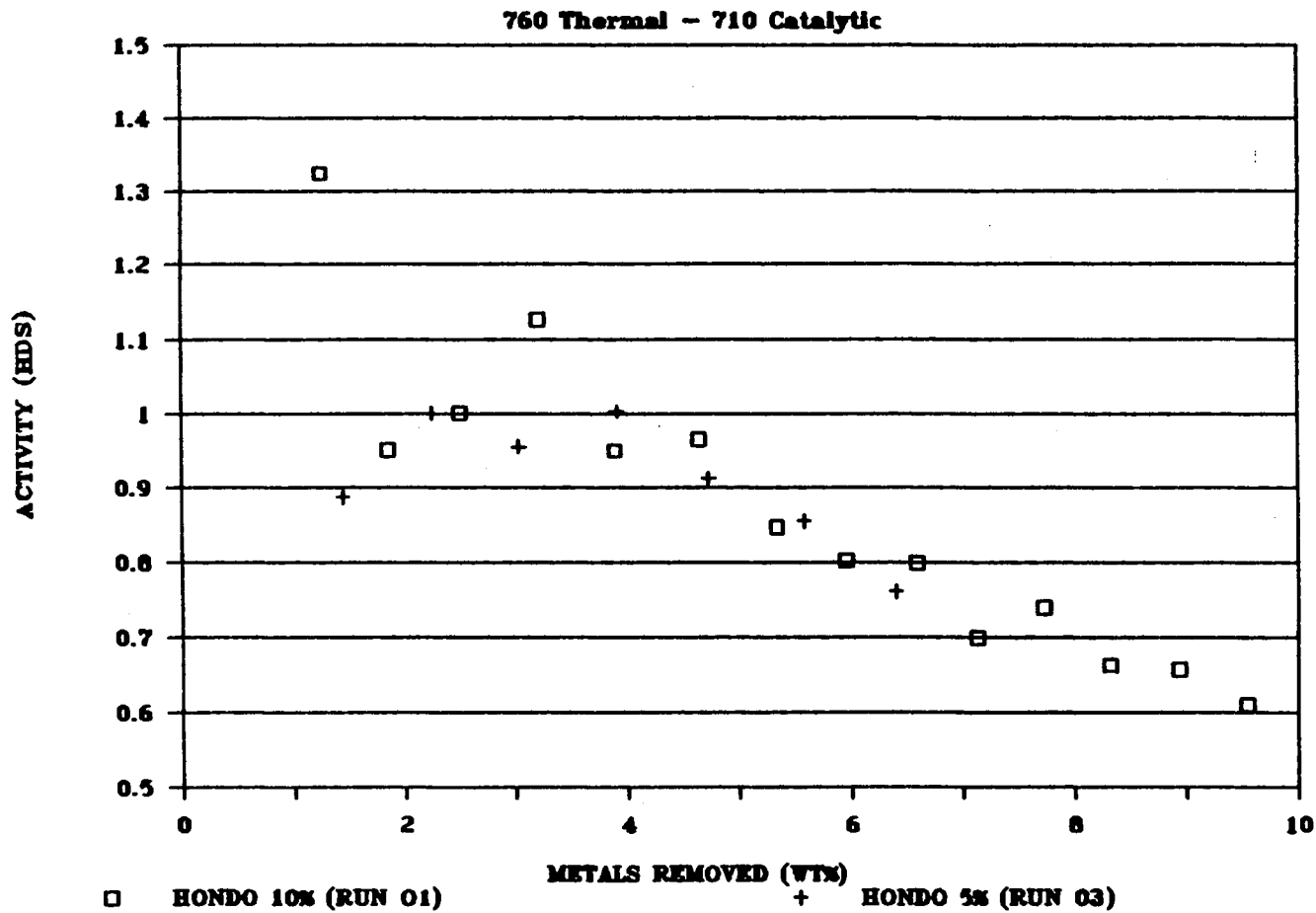


Figure 29. HDS Activity for Hondo (Runs 01 and 03)

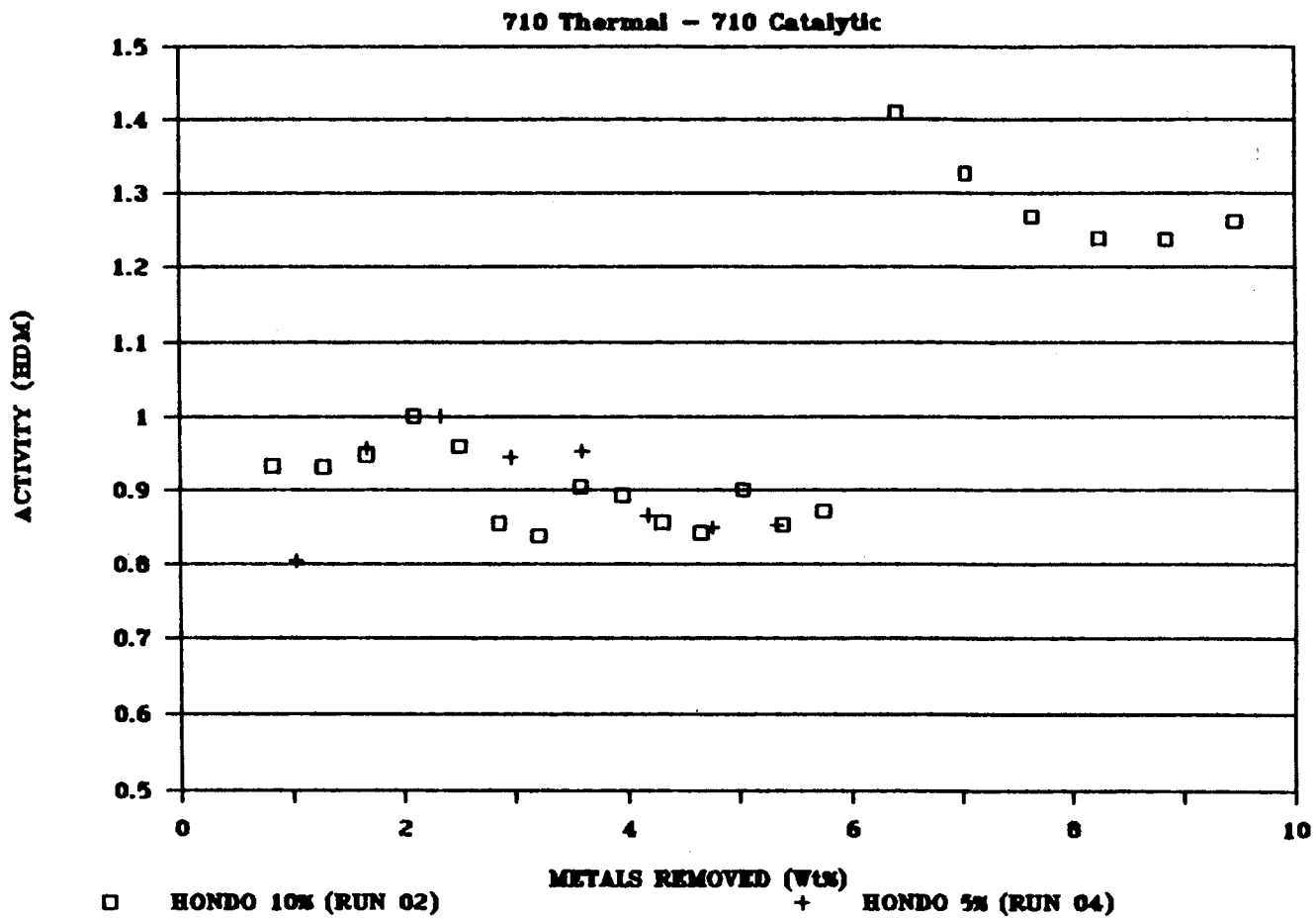


Figure 30. HDM Activity for Hondo (Runs 02 and 04)

710 Thermal - 710 Catalytic

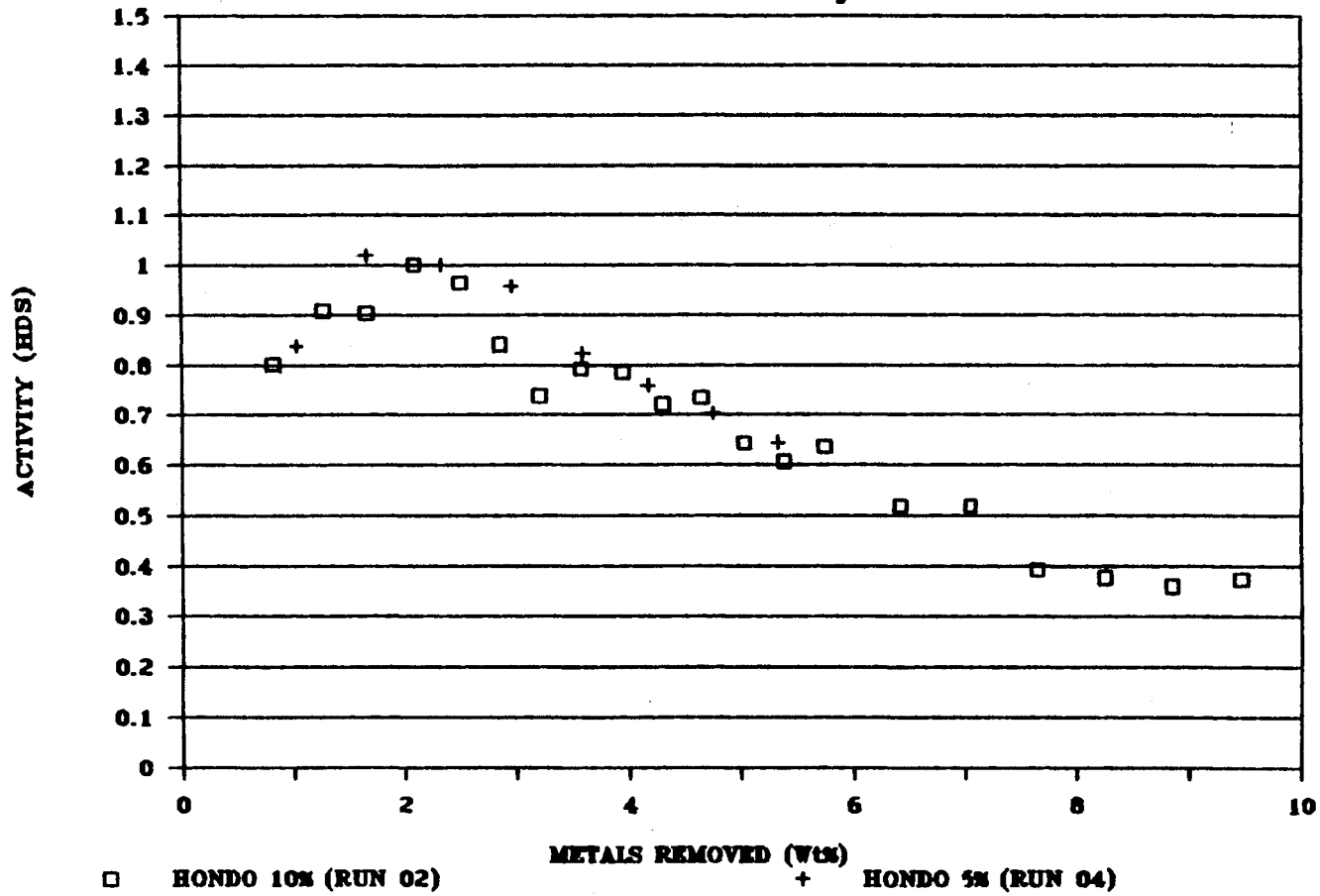


Figure 31. HDS Activity for Hondo (Runs 02 and 04)

activity much better than HDS activity. The HDS activity factors vary from 1 at 2 wt% metals removed to 0.65 at 5 wt% metals removed and to 0.35 at 10 wt%. Interestingly enough the change in feedstock after 6 wt% metals removed for Run 04 did not shift the activity profile for sulfur removal. The catalyst deactivation for HDS appear proportional to the metals removed and is higher at the lower temperature in the thermal zone.

Activity for Different Residues

The activity factors for the experiments with the different residua were plotted versus metals removed. For HDM at 710 thermal and 710 catalytic all the three residues follow the same deactivation trend (Figure 32) in spite of the spread in the data. When the thermal temperature is increased to 760⁰F Hondo shows more constant activity than either Oriente or Caño Limon (Figure 33) but the spread in the data is so large that conclusions are difficult to reach. For HDS at both 710-710 and 760-710 tests, all the residues follow the same deactivation curve despite the scatter in the data as shown in Figures 34 and 35.

Results indicate that HDS deactivation correlates better than HDM activity with the amount of metals deposited in the catalyst. While HDM is significant only in the presence of the catalyst, it is not as surface sensitive as HDS. This indicates that HDS activity is reduced by poisoning of the active sites when the metals

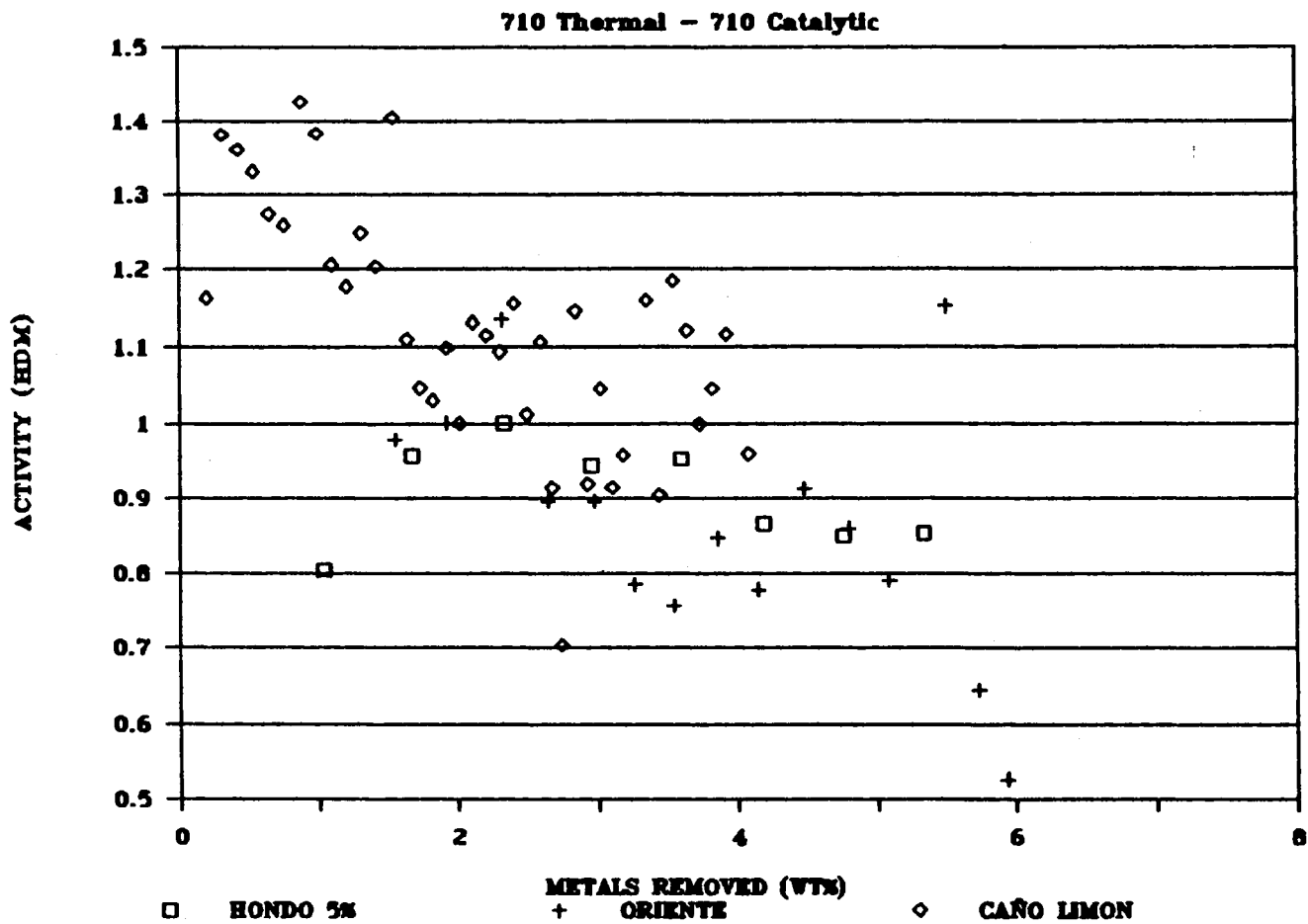


Figure 32. HDM Activity for Hondo, Oriente and Caño Limon (Runs 04, 07 and 10)

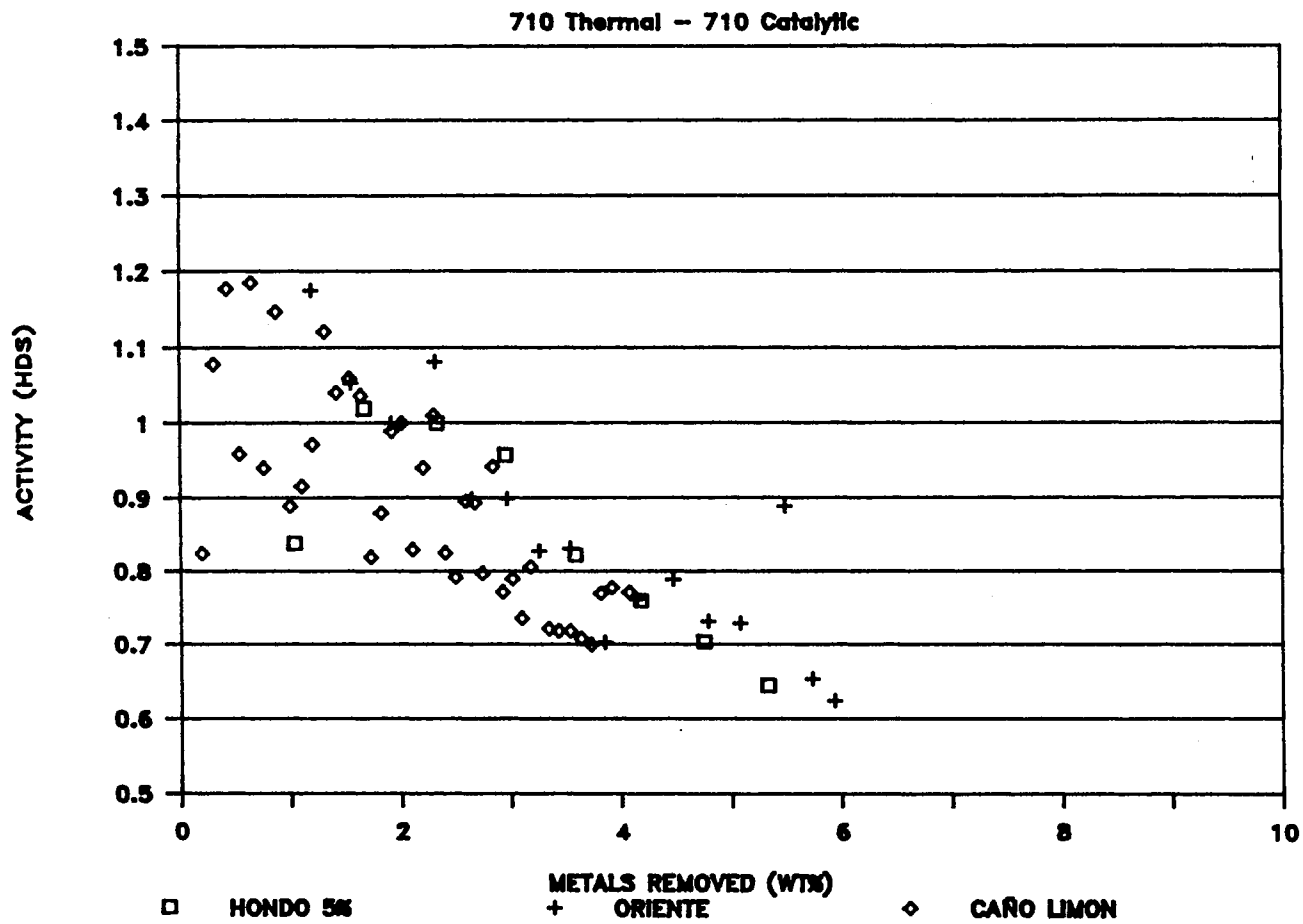


Figure 34. HDS Activity for Hondo, Oriente and Caño Limon (Runs 04, 07 and 10)

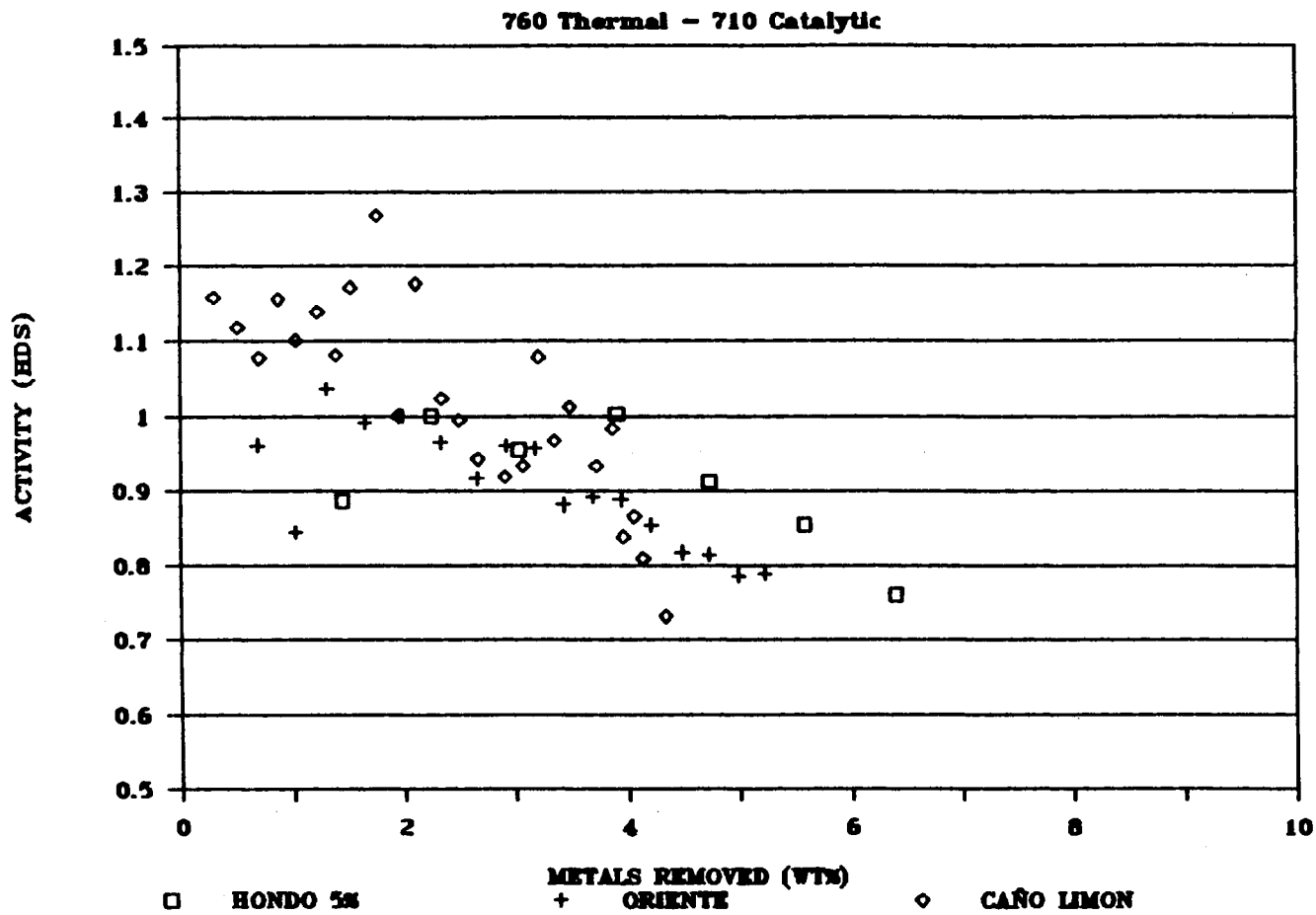


Figure 35. HDM Activity for Hondo, Oriente and Caño Limon (Runs 03, 06 and 09)

deposit on the catalyst. The activity factor at 4 wt% metals deposited in the catalyst is about 0.6 compared to 1.0 at 2 wt%. This can be tied to the penetration factor results obtained from the microprobe. The lowest average penetration factor was 0.07 for Oriente and the highest was 0.11 from Hondo or Caño Limon. This gives a difference of approximately 8% on the percent surface coverage which is not a large difference. The changes in penetration factors, even though they are statistically significant, are not large. Therefore it is difficult to see differences in catalyst activity among feeds. The fact that only 60% of the metals for Hondo and Caño Limon enter the catalyst pores at the high temperature may explain why deactivation seems more rapid for the 710-710 tests. Figures 35 and 36 show that the HDS activity for Oriente does not change significantly with temperature. For Hondo and Caño Limon the HDS activity is lower in the 710⁰F thermal - 710⁰F catalytic tests. However, if we multiplied the metals removed by 60%, that is the proportion of metals that effectively get into the catalyst, the activities are very similar. For example, at 5 wt% metal removed the activity factor at 760-710 (Figure 35) is about 0.80 for Caño Limon and 0.90 for Hondo. These values agree with the activity factors corresponding to 3 wt% metals deposited in the catalyst for the 710-710 case as shown in Figure 34. Therefore, HDS deactivation correlates well with the amount of metals that effectively deposit on the catalyst. These

results show that the primary deactivation mechanism at the end of graded beds is poisoning of the active surface of the small pores by metals deposition.

Discussion of Microprobe Results

The microprobe results can be related to aromaticity and reactivity of the residua. Hondo is a more aliphatic residuum and has more alkyl side chains bounded to the aromatic rings (NMR data, Table 7) and has a higher proportion of small molecules in the asphaltenes (LC-ICP data, Figures 19 to 21) than either Oriente or Caño Limon. Therefore increasing temperature in the thermal zone promotes dealkylation and conversion of the asphaltenes to small metal-containing fragments that can enter the catalyst pores and penetrate deeper into the catalyst. The increase in penetration of the metals deposited at higher temperatures indicates that diffusion is increased relative to metals deposition reactions. This is believed to be typical of configurational limited processes.

Oriente and Caño Limon are more aromatic than Hondo, therefore dealkylation of the asphaltene molecules is not as important. For Oriente, the increase in temperature in the thermal zone increases the reactivity of the metal-bearing molecules but with no significant decrease in molecular size. Therefore the Oriente molecules react preferentially near the pore mouth which gives lower penetration. In the Caño Limon experiments, the reactivity

of the metal-bearing molecules is not very temperature dependent. The fact that the molecules removed penetrate slightly more than the other two feeds at the low temperature level suggests that the reactivity of the very aromatic Caño Limon is lower than for Hondo and Oriente at these conditions.

The fact that the average Q_v values are close for all the residua studied indicates that the type of molecules that get inside the catalyst are essentially similar. Additionally, the differences in reactivity and diffusivity of the molecules are not large enough to cause extreme changes in the penetration factors. Therefore, for the bottom part of graded beds for residua HDT, the majority of HDM results from diffusion of existing small asphaltenes into the catalyst pores where they react without large differences in penetration. Differences in penetration factor are significantly greater at the top of the graded beds, where large pore catalysts are used for HDM and the large pores facilitate diffusion of the molecules into the catalyst.

LC-ICP Results Modelling

Combining the ideas from Savage et al. (1988) and other authors with similar hypotheses for asphaltenes decomposition and demetallization with our experimental observations we developed a model to fit LC-ICP results. Figure 36 shows the equations representing the model.

FITTING LC-ICP DATA

BREAKDOWN (Thermal)

$$V_1 = V_0 * \text{EXP}(-\underline{\text{KBD}} / \text{LHSV})$$

SIZE REDUCTION (Thermal)

$$\text{SIZE}_1 = \text{SIZE}_0 * \text{EXP}(-\underline{\text{KSR}} / \text{LHSV})$$

DIFFUSION - REACTION (Catalytic)

$$V_2 = V_1 * \text{EXP}(-\text{KRX} / \text{LHSV})$$

$$\text{KRX} \rightarrow (1 - \text{MD/PD})^2 \underline{\text{K}}^{1/2}$$

Figure 36. Equations Representing the Asphaltene Decomposition Model

First, we assume that the asphaltene molecules are converted thermally. Also we assume that if they break the vanadium is removed as it is exposed to the catalytic surface. Therefore the new concentration of vanadium is calculated based on a thermal conversion rate (K_{TC}) assuming first order reaction. However, with this approach for thermal conversion we can not differentiate between the molecules that break and are demetallized inside the catalyst quickly and the molecules that form coke. At this stage we do not predict the size of the converted molecules but assume that they are quite small. The next step in the model is to consider a thermal size reduction of the molecules to represent the shift in the size distribution that we observed for Hondo. This size reduction does not involve demetallization of the molecules. All it does is to shift the concentration profile towards a smaller size. To shift the profile in the model we calculate new sizes for the same concentrations assuming a first order change in size with a size reduction constant (K_{SR}). We assume that this shift is due to dealkylation of the side chains of the asphaltenes. Several authors have reported the same observation and they attribute this change to either dealkylation or cracking of the molecules (Reynolds and Biggs, 1985; Savage et al., 1988). After thermal conversion and size reduction, molecules smaller than the pore size diffuse into the pores and react depositing the metals inside the catalyst. The new vanadium concentration is

calculated using first order reaction kinetics with a rate constant K_{rx} . The rate constant is proportional to the intrinsic HDM rate and to the diffusivity of the molecules. Using Spry and Sawyer's (1975) correlation for limitation of diffusion by reduction in pore size, we include the diffusivity correction factor as a function of the ratio of molecular size to pore size.

The program was developed as a LOTUS spreadsheet. The input is the size distribution as vanadium concentration versus retention time. This data is readily available from the LC-ICP analysis for each sample. The next step is to translate the time into size of the molecules. To do this we calculate the size of the molecules by a logarithmic correlation:

$$\text{Molecular Diameter} = (1/\text{Ln}(\text{time}))^2 * 5000 - 340 \quad (1)$$

The values for the exponent and for the coefficients are selected to obtain a molecular size for the asphaltenes in the range of 10 to 235 Å found in prior investigations for several residua (Parrott, 1989). Researchers have attempted calibration of molecular weight with elution volume using linear polystyrene of different molecular weight. They found that the calibration is very difficult and it is still relative because of the differences in hindrance effects between linear polystyrene and asphaltenes. The reported calibrations are fitted by semilogarithmic expressions (Baltus and Anderson, 1983,

Reerink and Lijzenga, 1975).

After this conversion of data, the next step is to provide values for the model parameters: thermal conversion constant K_{TC} , size reduction constant K_{SR} , and intrinsic rate constant K . Then, calculations are done for the variation in concentration by thermal conversion, the shift in size due to dealkylation, and catalytic reaction under diffusion limitations. The final step is to convert the size variable back into time and then plot concentration versus time and compare to the experimental distribution for the product. In this way the size distribution is offset by returning to the time domain.

The model was run to fit the LC-ICP results for Hondo Oriente, and Caño Limon. Figure 37 shows the results of the model for Hondo including only the reaction term. It shows that only the small molecular size peak is demetallized catalytically. Including the terms for thermal conversion and size reduction we can fit the product distribution as shown in Figures 38 to 40 for Hondo. The Oriente case was basically fit only by catalytic reaction as the thermal conversion was null as shown in Figures 41 and 42. The model was also used to fit Caño Limon data and the results are presented in Figures 43 to 45. The values of the parameters for all of the fitted cases are presented in Table 19. The modelling exercise shows the importance of the different rates considered. At this point, for the molecules that are converted thermally, we can not

ASPH. HONDO LC-ICP SIMULATION

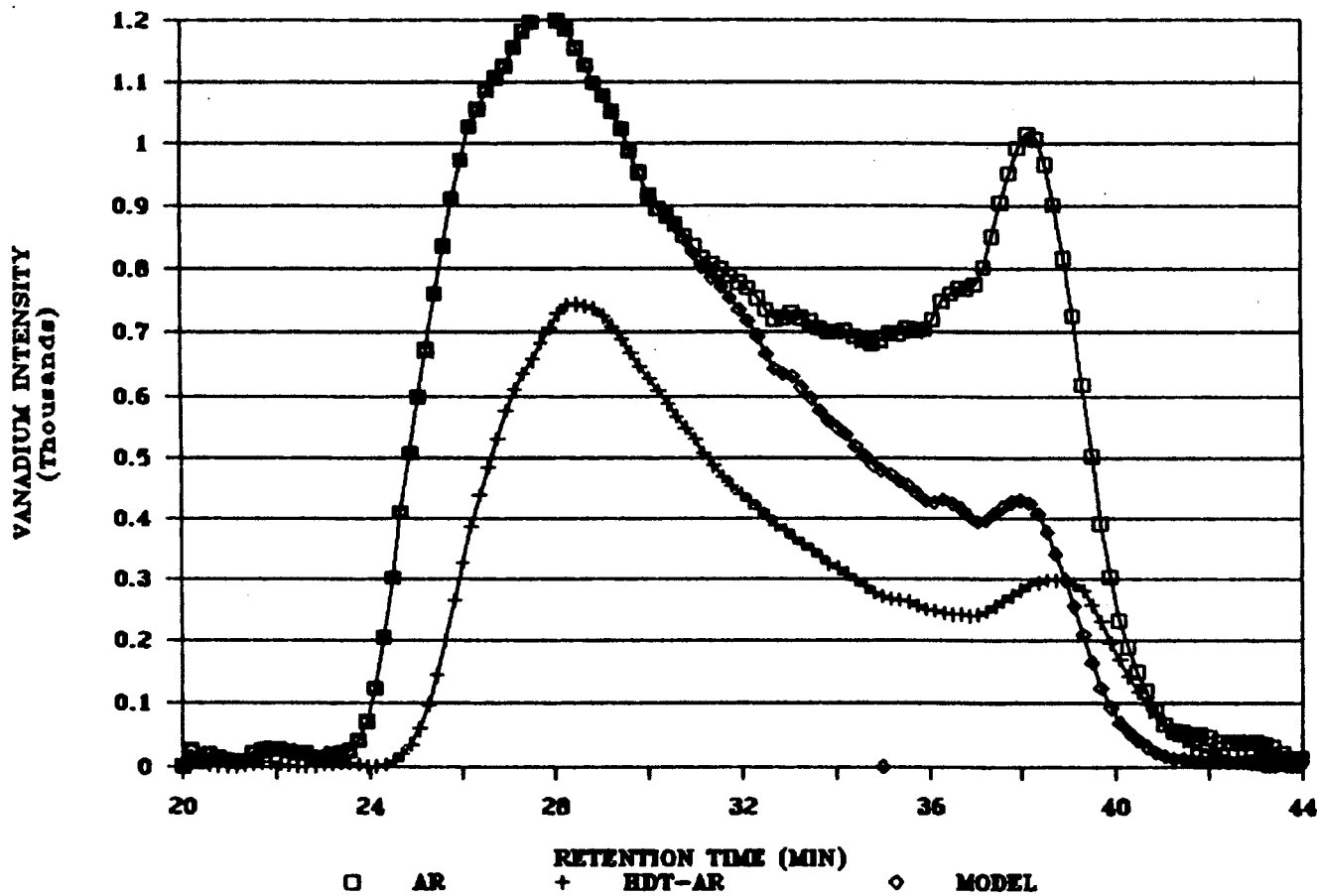


Figure 37. Model Fit of LC-ICP Data Using Diffusion-Reaction Only

ASPH. HONDO LC-ICP SIMULATION

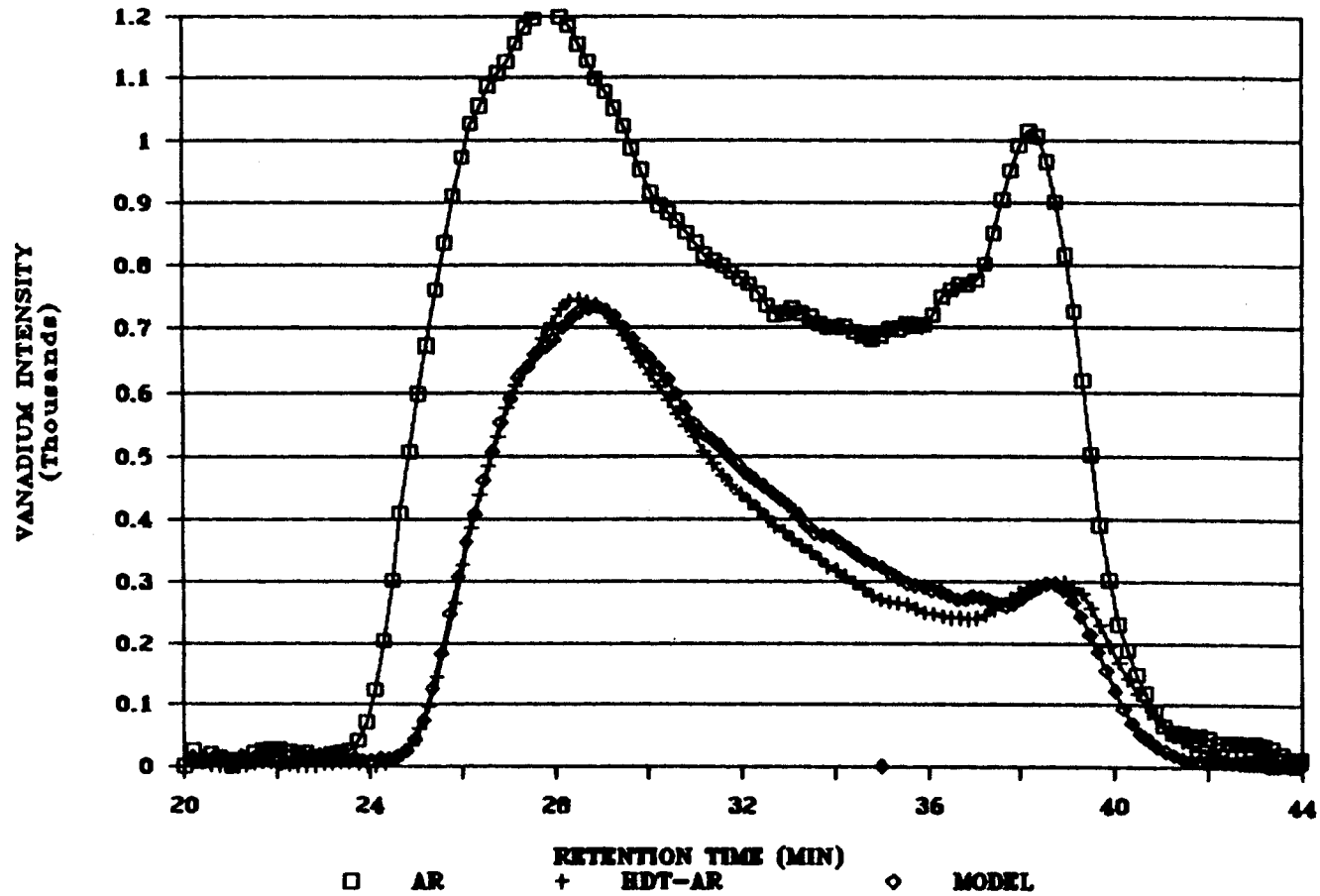


Figure 38. Model Fit of Product from Pretreatment Reactor for Hondo

ASPH. HONDO LC-ICP SIMULATION

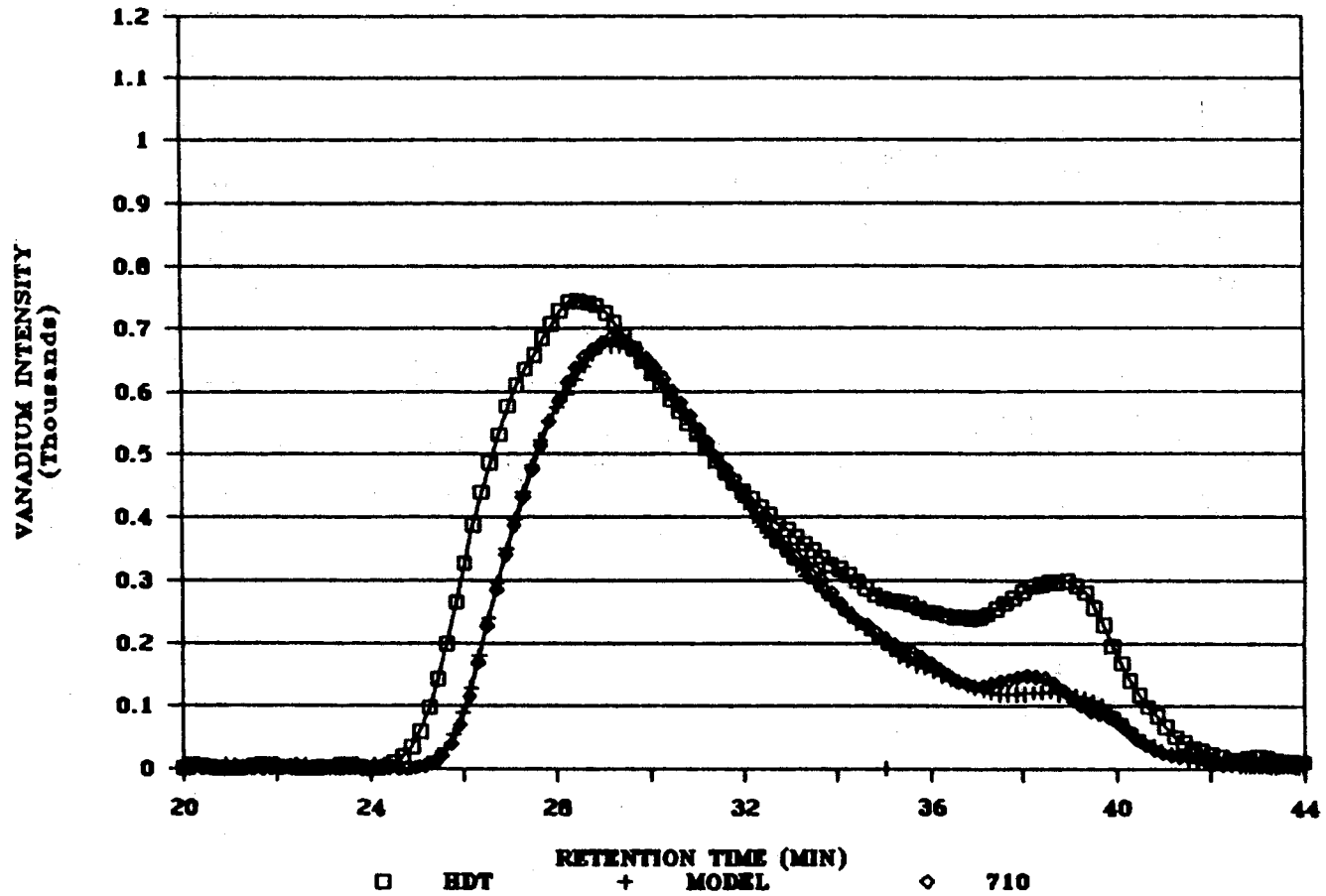


Figure 39. Model Fit of Product from Up-Flow Reactor at 710F for Hondo

ASPH. HONDO LC-ICP SIMULATION

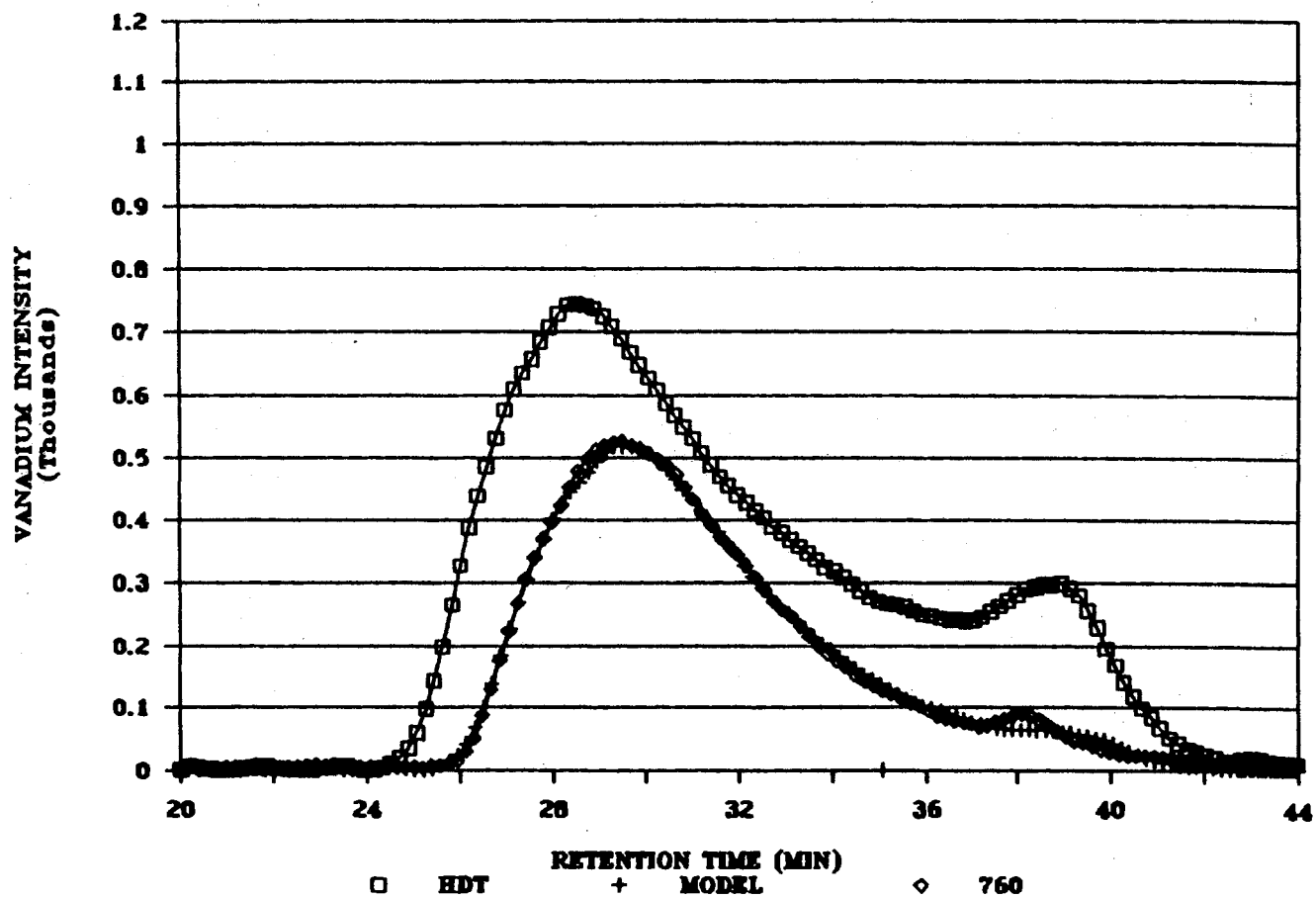


Figure 40. Model Fit of Product from Up-Flow Reactor at 760F Thermal - 710F Catalytic for Hondo

ASPH. ORIENTE LC-ICP SIMULATION

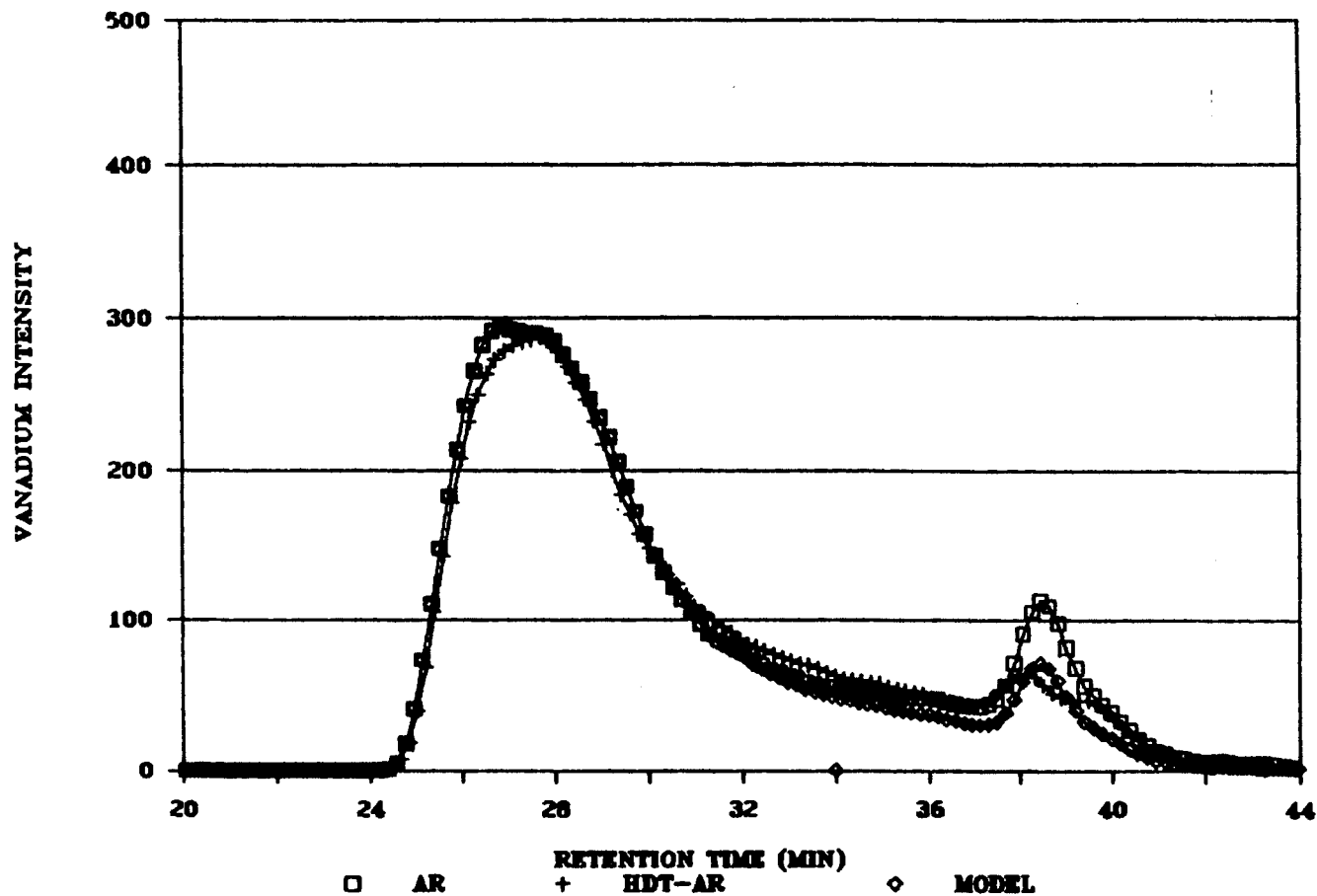


Figure 41. Model Fit of Product from Pretreatment Reactor for Oriente

ASPH. ORIENTE LC-ICP SIMULATION

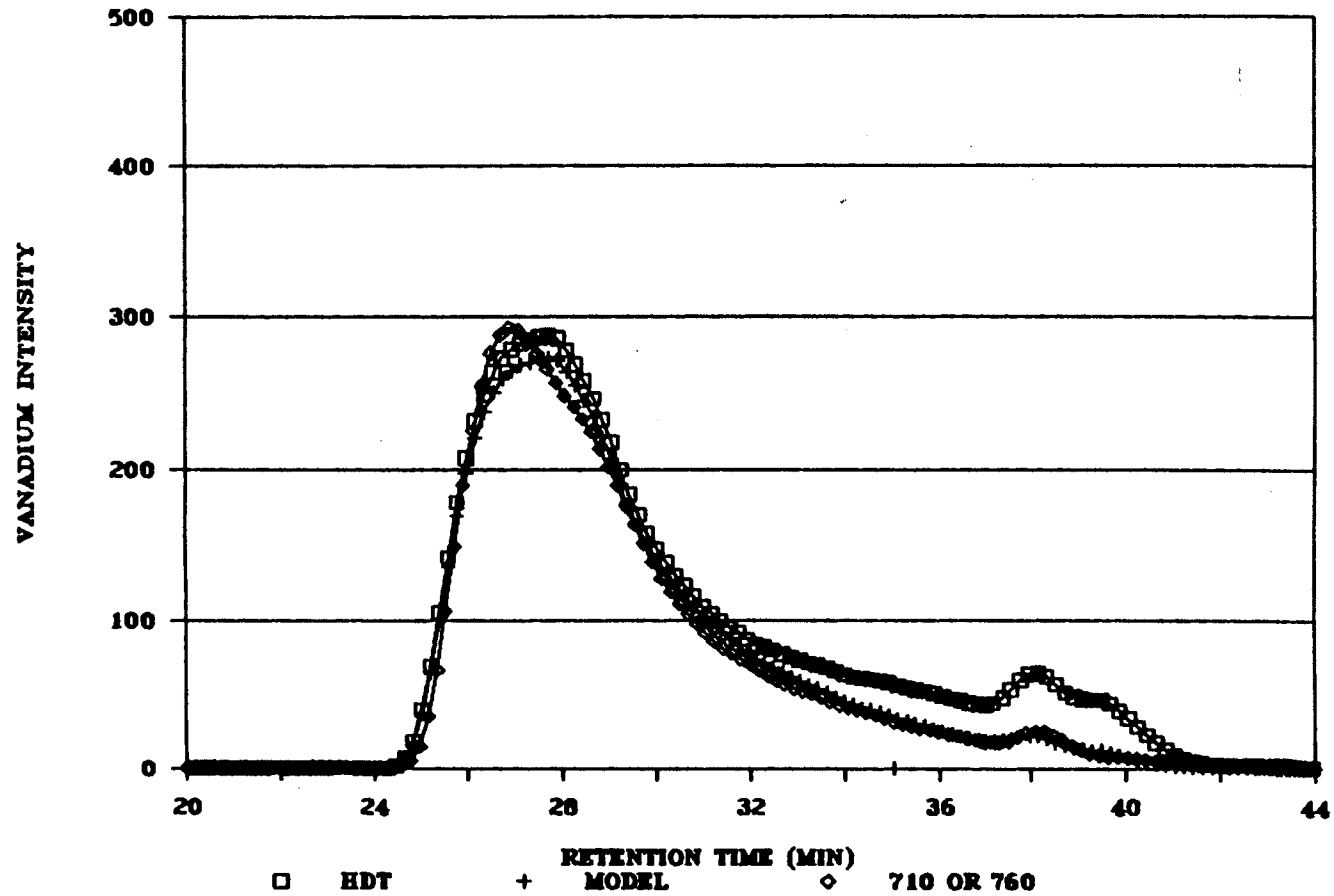


Figure 42. Model Fit of Product from Up-Flow Reactor at 710F for Oriente

ASPH. CAÑO LIMON LC-ICP SIMULATION

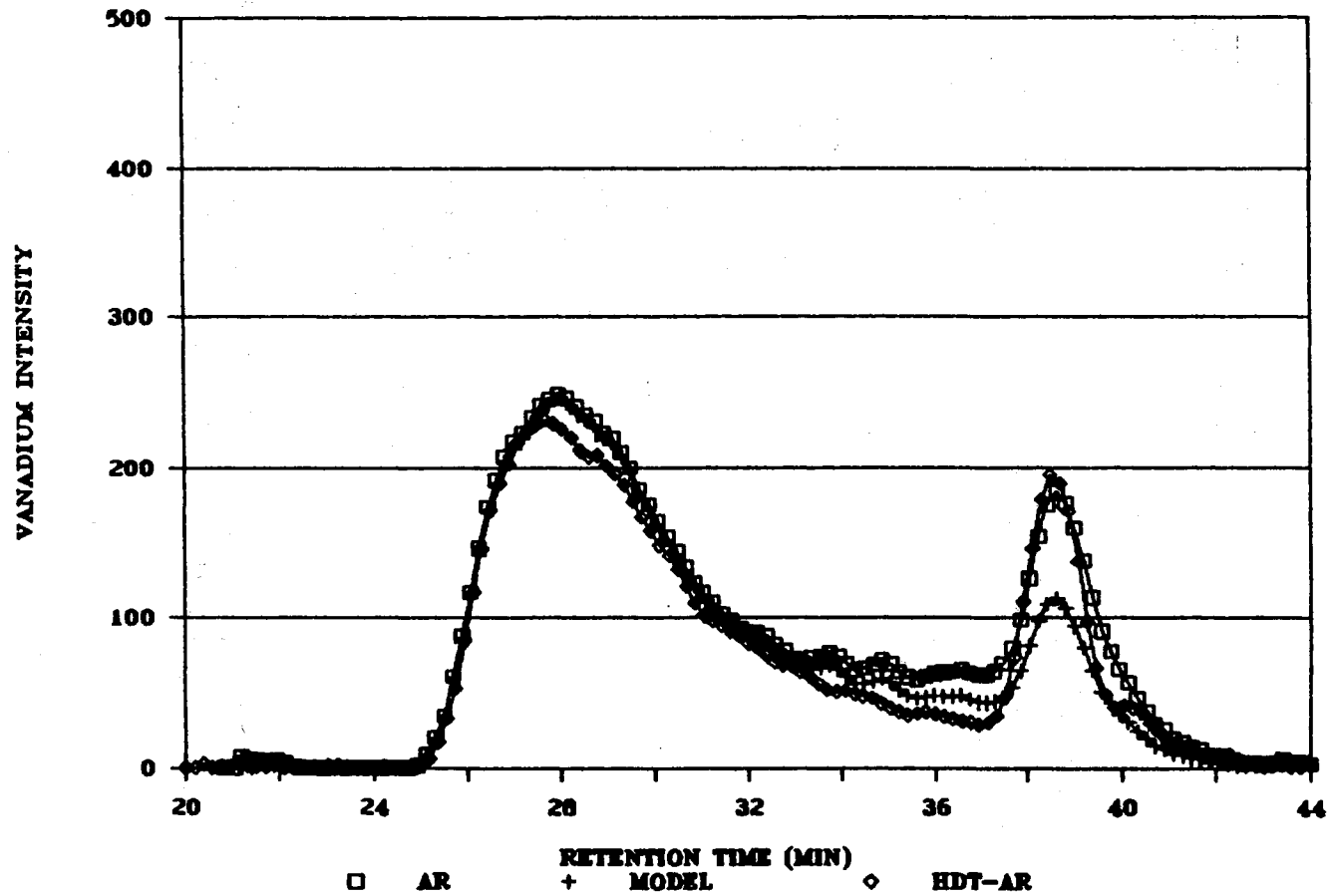


Figure 43. Model Fit of Product from Pretreatment Reactor for Caño Limon

ASPH. CAÑO LIMON LC-ICP SIMULATION

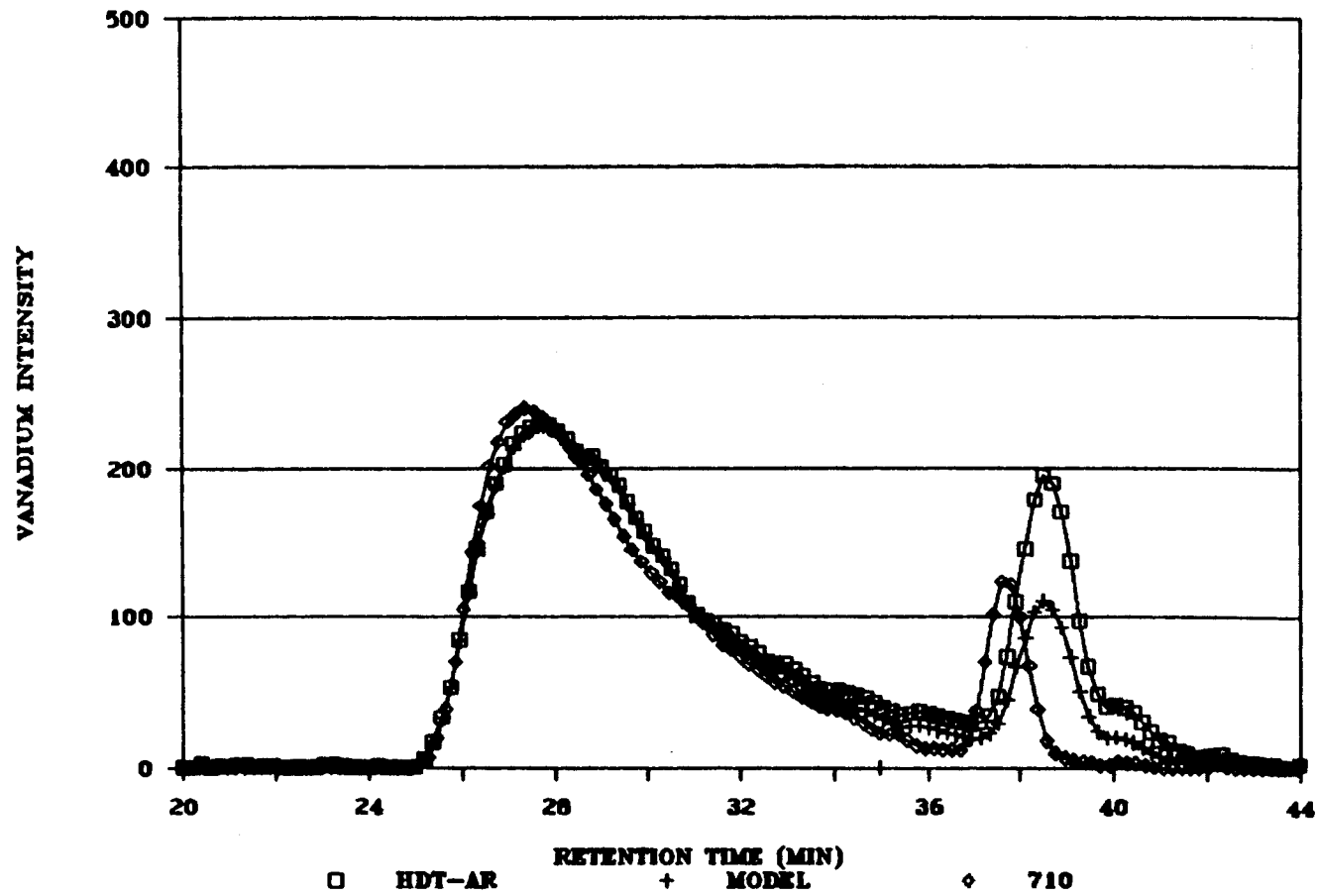


Figure 44. Model Fit of Product from Up-Flow Reactor at 710F for Caño Limon

ASPH. CAÑO LIMON LC-ICP SIMULATION

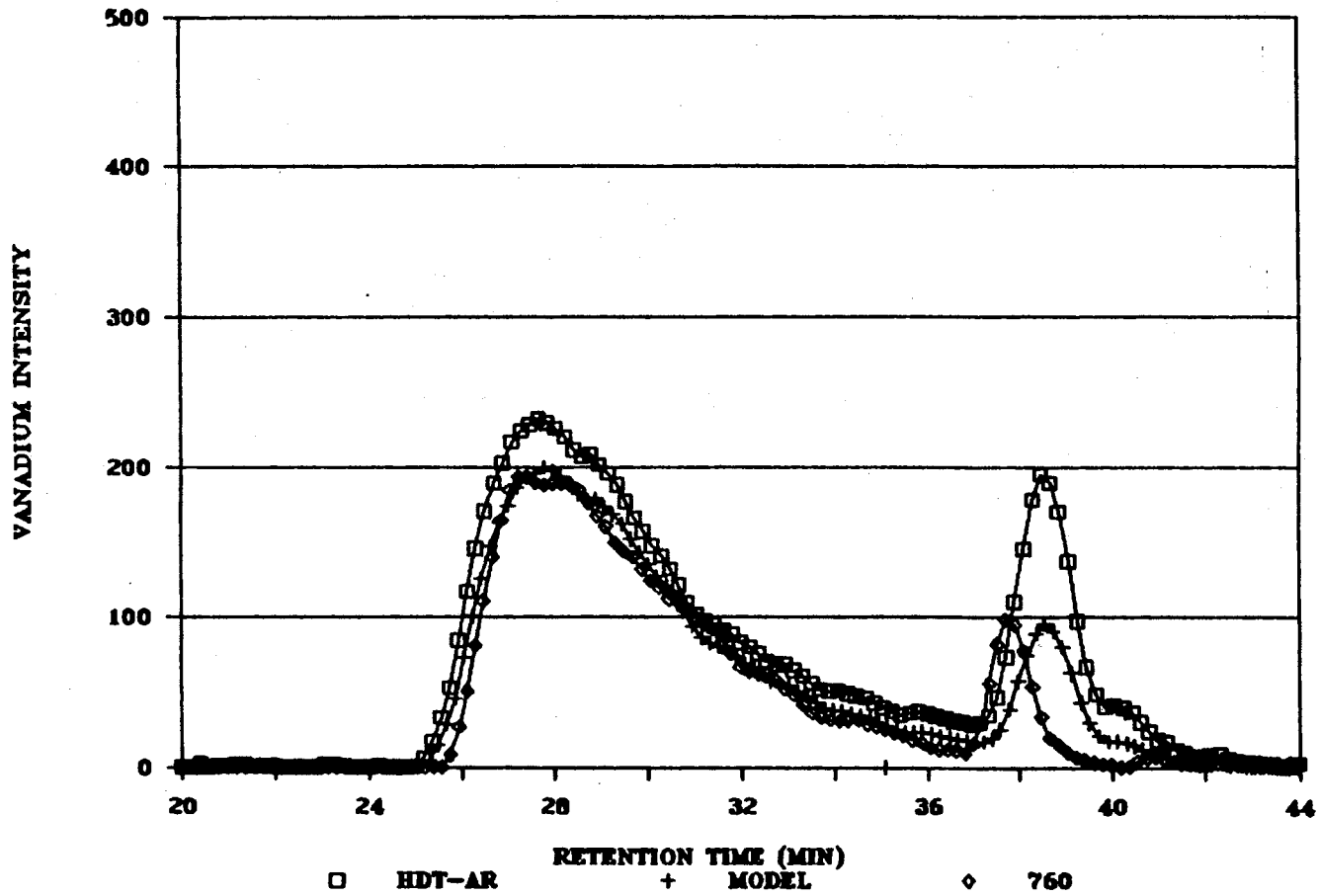


Figure 45. Model Fit of Product from Up-Flow Reactor at 760F Thermal - 710F Catalytic for Caño Limon

TABLE 19

FITTING MODEL PARAMETERS FOR HONDO, ORIENTE
AND CAÑO LIMON

PARAMETERS	CONDITIONS		
	AR HDT Trickle	HDT 710 up-flow	HDT 760 up-flow
HONDO			
K_{TC}	0.40	0.10	0.36
K_S	0.07	0.06	0.09
K_R	1.50	2.60	3.00
ORIENTE			
K_{TC}	0.00	0.05	0.05
K_S	0.00	0.0001	0.0001
K_R	1.00	3.00	3.00
CANO LIMON			
K_{TC}	0.01	0.01	0.15
K_S	0.001	0.001	0.01
K_R	1.00	1.50	1.50

differentiate between the proportion that goes to smaller molecules and are readily demetallized and the proportion that goes to coke. The results from the application of the model show how the thermal conversion (K_{TC}) is high for Hondo, low for Caño Limon and Oriente. The shift in molecular size (K_s) is high for Hondo, low for Caño Limon and virtually zero for Oriente. The reaction term (K_R) represents removal of small molecules and is high for Hondo and Oriente and low for Caño Limon. This low reactivity of the Caño Limon small molecules is consistent with the larger penetration factors observed. The easiest to fit in the small molecular size was Hondo. Caño Limon showed a shift for the small size peak towards larger molecular size that was difficult to fit with the model. This indicates that there are some small molecules in Caño Limon that are less reactive. Apparently the vanadium in small Caño Limon molecules is buried deeply into the aromatic core of the asphaltene molecule.

From the model results tied with the LC-ICP and microprobe data we conclude that Hondo hydrotreats better than Caño Limon and Oriente. The reason is because they are chemically and physically different. Hondo, which is more aliphatic and has a larger proportion of smaller molecules, has a higher thermal conversion rate. However, Hondo also has a high coking tendency. Even though Oriente did not coke at the conditions we used, some speculation from our part is that we did not reach the severity required for

coking of Oriente.

We also concluded that the LC-ICP data can be fitted using thermal conversion plus diffusion of small molecules and demetallization inside the pores. One big assumption in this model is that if the molecules break into small fragments they are immediately demetallized. Results indicate that for graded bed hydrotreaters coking may be an important HDM and deactivation mechanism at the back end of the bed. This has important implications in the operation of the unit, particularly due to the fact that if the high activity catalyst at the bottom of the unit is severely affected by coking the useful life of the unit will be reduced significantly.

CHAPTER V

CONCLUSIONS AND RECOMMENDATIONS

Conclusions

1. For the bottom part of graded beds for residua HDT, size exclusion chromatography with inductively coupled plasma shows that the majority of HDM is done by diffusion of existing small asphaltenes into the catalyst pores where they react. This explains the difference in activity noted for Hondo, Oriente and Caño Limon. Hondo, which is more aliphatic, is more active for HDM because it has the highest proportion of metals in the small molecular range. Also, Hondo shows some production of low molecular weight asphaltenes during processing. However, the increase in the production of these low molecular weight asphaltenes was found not to be significant compared to the amount of small molecular weight already existent. Caño Limon has a medium proportion of small molecules and shows medium HDM activity. Oriente has the lowest fraction of low molecular weight asphaltenes and shows the lowest HDM activity.
2. The thermal conversion of asphaltenes at the bottom of graded beds is not as significant for HDM as the molecular size distribution of the metals in the asphaltenes entering

the catalyst zone. Thermal conversion is most likely for the more paraffinic or aliphatic residua such as Hondo. At low temperature there is some conversion of high molecular weight molecules to low molecular weight molecules for Hondo. For Caño Limon and specially for Oriente this conversion is almost negligible. Results indicate that demetallization is primarily a catalytic process. At high temperatures, thermal conversion leads to additional demetallization but primarily by coking.

3. In no case did increased thermal severity result in a drastic increase in metals penetration. Thus, the bottom part of graded beds should not suffer from extremely rapid deactivation due to penetration of metals inside the catalyst pores. Instead it appears that increasing thermal severity for various feeds promotes interstitial coke formation in the voids between catalyst particles. The results show that there is a critical temperature for coke formation, dependent on the crude source, where coking increases extensively and becomes very detrimental for the overall performance of the unit. However, catalyst deactivation studies did show loss in HDS activity to correlate very well with metals deposition. This indicates that the primary deactivation mechanism is poisoning of the active surface by metals deposition.

4. Results indicate that asphaltene molecules break and, by the time they reach the back end of graded beds, thermal dealkylation of the asphaltenes is nearly complete. The

small molecules diffuse into the catalyst pores where they are demetallized by catalytic reactions and metals are deposited as metal sulfides. By coupling existing mechanisms and kinetic models with the results obtained in this study we were able to fit the LC-ICP distribution of vanadium in the asphaltenes with a simple first order rate equation for asphaltene thermal conversion combined with a diffusion reaction mechanism for loss of metals within the catalyst.

Recommendations

1. Perhaps the most important recommendation is that the experimental procedure and tests that are the basis of this study would be readily adapted to screen candidate feedstocks for commercial ARDS processes. Certainly, the evidence and insight obtained closely parallel previous long term experiments used for feedstock selection.
2. In further studies a different system with inter-stage sampling may be helpful to provide a better differentiation between thermal and catalytic effects by sampling after the thermal and the catalyst zones. For the configuration of reactors at the Phillips Catalyst Laboratory, the simplest way to do this is to employ two units, one for the thermal and the other for the catalytic zone, with interstage sampling between them.
3. Results obtained in this work should encourage additional work with the LC-ICP equipment to predict the

change in molecular size that occur with larger pore catalyst to develop a better HDM model. This should include experiments at several liquid hourly space velocities to study the kinetics of the system.

BIBLIOGRAPHY

1. Agrawal, R. and Wei, J., *Ind. Eng. Chem. Process Des. Dev.*, 1984, 23, 505-514.
2. Agrawal, R. and Wei, J., *Ind. Eng. Chem. Process Des. Dev.*, 1984, 23, 515-522.
3. Ahn, B. and Smith, J. M., *AIChE Journal*, September, 1984, 30 (5), pp 739-746.
4. Aldag, A. W., *Personal Communication*, Phillips Research and Development Center, Bartlesville, OK, 1989.
5. Asaoka, S. et al., *Ind. Eng. Chem. Process Des. Dev.*, 1983, 22, 242-248.
6. Asaoka, S. et al., *Characteristics of Vanadium Complexes in Petroleum Before and After Hydrotreating*, *ACS Symp. Ser.*, 1987; 275-289.
7. Baltus, R. E. and Anderson, J. L., *Chem. Eng. Sci.*, 1983, 38 (12), 1959-1969.
8. Beuther, H. et al., *The Mechanism of Coke Formation on Catalysts*, *Catalyst Deactivation*, 1980; Delmon, B. and Froment, G. F., ; Elsevier: Amsterdam, 1980; 271-282.
9. Billon, A. et al., *Oil Gas J.*, January 24, 1977, 43-47.
10. Boduszynski, M. M., *Characterization of Heavy Crude Components*, *Prepr. - Am. Chem. Soc., Div. Pet. Chem.*, Chicago, September 8-13; 626-635.
11. Bridge, A. J. and Green, D. C., *Prepr. - Am. Chem. Soc., Div. Pet. Chem.*, 1979; 791.
12. Brunn, L. W. et al., *Prepr. - Am. Chem. Soc., Div. Pet. Chem.*, Chicago, August 24-29, 1975.
13. Carbognani, L. et al., *Correlation Between Physical Chemical Properties and Reactivities in Hydroprocessing of Venezuelan Heavy Ends*, *Prepr. - Am. Chem. Soc., Div. Pet. Chem.*, Denver, April 5-10, 1987; 406-412.

14. Christman, R. D. et al., Prepr. - Am. Chem. Soc., Div. Pet. Chem., Miami Beach, April 28 - May 3, 1985.
15. Dickie, J. P. and Yen, T. F., Anal. Chem., 1967, 39, 435.
16. Dolbear, G. E., Fuel, February, 1987, 66, 267-270.
17. Drushel, H. V., Prepr. - Am. Chem. Soc., Div. Pet. Chem., New York, August 27 - September 1, 1972.
18. Ebel, R. H., Prepr. - Am. Chem. Soc., Div. Pet. Chem., New York, August 27 - September 1, 1972.
19. Galiasso, R. et al., Reaction of Porphyrinic and non Porphyrinic Molecules during the Hydrodemetallization of Heavy Crude Oils, Prepr. - Am. Chem. Soc., Div. Pet. Chem., Miami, Fl, April, 1985.
20. Gibson, K. R. et al., Chem. Eng. Prog., 1983, 79, 93.
21. Gonzales, C. and Galiasso, R. E., Rev. Tec. Intevap, January, 1983, 3 (1), 3-9.
22. Hannerup, P. N. and Jacobsen, A. C., A Model for the Deactivation of Residue Hydrodesulfurization Catalyst, Am. Chem. Soc., Div. Pet. Chem., 185th National Meeting, Seattle, Washington, March 20-25, 1983;
23. Hausler, D. W. and Carlson, R. S., Online SEC-ICP: A New Element Specific, Molecular Sizing Tool for the Petroleum Industry, Symposium on Developments in Hydrodemetallization Catalysts and Processes, Am. Chem. Soc., Div. Pet. Chem., Miami, April 28-May 3, 1985.
24. Higashi, H. et al., Prepr. - Am. Chem. Soc., Div. Pet. Chem., 1985; 111.
25. Hohnholt, J. F. and Fausto, C. Y., CEP, June 1985, 47-53.
26. Howell, R. L. et al., Oil Gas J., July 29, 1985, 83, 121-128.
27. Hung, C. et al., Chem. Eng. Prog., March 1986, 57-61.
28. Hydrocarbon Processing Publication, Hydrocarbon Processing, September, 1984, 62, 69-146.
29. Inoguchi, M. et al., Bull. Jpn. Petrol. Inst., 1971, 13, 153.

30. Jacobsen, A. C., Selection of Catalysts for Residue Hydrodesulfurization, AIChE Spring National Meeting, Houston, TX, March 27-31, 1983;
31. Jewell, D. M. et al., Prepr. - Am. Chem. Soc., Div. Pet. Chem., New York, August 27 - September 1, 1972.
32. Johnston, H. D. et al., An Integrated Testing Facility for Bench Scale Catalyst Research, Prepr. - Am. Chem. Soc., Div. Pet. Chem., Washington, D. C., August 28 - September 2, 1983; 960-972.
33. Kodama, S. et al., J. Japan Petrol. Inst., 1980, 23 (5), 310-320.
34. Koots, J. A. and Speight, J. G., Fuel, 1975, 54, 179.
35. Kwant, P. B. et al., The Development of Shell's RESidue Hydroconversion Process, Petroleum Refining Conference of the Japan Petroleum Institute, Tokyo, October 24-25, 1984.
36. Le Page, J. F. et al., Thermal Cracking under Hydrogen Pressure: Preliminary Step to the Conversion of Heavy Oils and Residues, Prepr. - Am. Chem. Soc., Div. Pet. Chem., Denver, April 5-10, 1987; 470-476.
37. Leung, K. and Haynes, H. W., Jr., Chem. Eng. Commun., 1984, 31, 1-20.
38. Levenspiel, O., Chemical Reaction Engineering; John Wiley & Sons, Inc.: New York, 1972.
39. McKay, J. F. and Latham, D. R., Prepr. - Am. Chem. Soc., Div. Pet. Chem., 1981; 831.
40. Murphy, J. R. et al., Hydrocarbon Processing, September, 1979, 119-122.
41. Newson, E., Ind. Eng. Chem. Process Des. Dev., 1975, 14 (1), 27-33.
42. Nielsen, A. et al., Prepr. - Am. Chem. Soc., Div. Pet. Chem., Atlanta, March 29 - April 3, 1981; 440.
43. Nitta, H. et al., Deactivation Model for Residual Hydrodesulfurization Catalysts, 86th National AIChE Meeting, Houston, TX, April 1979.
44. Parrott, S. L., Personal Communication, Phillips Research and Development Center, Bartlesville, OK,

1989.

45. Pazos, J. M., Ind. Eng. Chem. Process Des. Dev., 1983, 22, 653-659.
46. Rajagopalan, K. and Luss, D., Ind. Eng. Chem. Process Des. Dev., 1979, 18 (3), 459-465.
47. Reerink, H. and Lijzenga, J., Anal. Chem., November 1975, 47 (13), 2160-2167.
48. Reyes, S. and Jensen, K. F., Chem. Eng. Sci., 1985, 40 (9), 1723-1734.
49. Reynolds, J. G. et al., Liquids Fuels Technology, 1985, 3 (4), 423-448.
50. Reynolds, J. G. et al., Reaction Sequence of Metallopetroporphyrins During Heavy Residuum Upgrading, ACS Symp. Ser., ACS: 1987; 205-219.
51. Reynolds, J. G. and Biggs, W. R., Analysis of Residuum Demetallization by Size Exclusion Chromatography with Element Specific Detection, Prepr. - Am. Chem. Soc., Div. Pet. Chem., Chicago, September, 8-13, 1985; 679-687.
52. Reynolds, J. G. and Biggs, W. R., Analysis of Residuum Desulfurization by Size Exclusion Chromatography with Element Specific Detection, Prepr. - Am. Chem. Soc., Div. Pet. Chem., Denver, April 5-10, 1987; 398-405.
53. Richardson, R. L. and Alley, S. K., Consideration of Catalyst Pore Structure and Asphaltenic Sulfur in the Desulfurization of Resids, Prepr. - Am. Chem. Soc., Div. Pet. Chem., Philadelphia, April 6-11, 1975; 554-563.
54. Sakabe, T. and Yagi, T., Hydrocarbon Processing, December, 1979, 103-107.
55. Savage, P. E. et al., Energy & Fuels, 1988, 2, 619-628.
56. Shah, G. N. et al., Hydrocarbon Processing, May, 1979, 103-106.
57. Shaw, J. W., Personal Communication, Phillips Research and Development Center, Bartlesville, OK, 1989.
58. Shiroto, Y., Ind. Eng. Chem. Process Des. Dev., 1983, 22, 248-257.
59. Sie, S. T., Catalyst Deactivation by Poisoning and Pore

Plugging in Petroleum Processing, Catalyst Deactivation, Delmon, B.; Froment, G. F.; Elsevier: Amsterdam, 1980; 545-569.

60. Sikonia, J. G., Hydrocarbon Processing, June, 1980, 60, 73-79.
61. Speight, J. G. et al., On the Definition of Asphaltenes, Prepr. - Am. Chem. Soc., Div. Fuel Chem., Houston, March 23, 1980; 268-275.
62. Speight, J. G., Fuel, May, 1984, 63, 616-620.
63. Speight, J. G., Initial Reactions in the Coking of Residua, Prepr. - Am. Chem. Soc., Div. Pet. Chem., Denver, April 5-10, 1987; 413-418.
64. Speight, J. G., Latest Thoughts on the Molecular Nature of Petroleum Asphaltenes, Prepr. - Am. Chem. Soc., Div. Pet. Chem., Dallas, April 9-14, 1989; 321-328.
65. Spry, J. C. Jr. and Sawyer, W. H., Configurational Diffusion Effects in Catalytic Demetallization of Petroleum Feedstocks, Sixty-Eight Annual AIChE Meeting, Los Angeles, CA, November 16-20, 1975.
66. Sughrue, E. L. et al., Ind. Eng. Chem. Res., 1988, 27, 397-401.
67. Sughrue, E. L., Personal Communication, Phillips Research and Development Center, Bartlesville, OK, 1989.
68. Tamm, P. W. et al., Ind. Eng. Chem. Process Des. Dev., 1981, 20, 262-273.
69. Toulhoat, H., Modelling RDM Catalyst Deactivation by Metal Sulfides Deposits: An Original Approach supported by HREM Investigations and Pilot Tests Results, Prepr. - Am. Chem. Soc., Div. Pet. Chem., Denver, April 5-10, 1987.
70. Tsakalis, K. S. et al., Journal of Catalysis, 1984, 88, 188-202.
71. Van Driesen, R. P. and Fornoff, L. L., Hydrocarbon Processing, September 1985, 91-95.
72. Walpole, R. E. and Myers, R. H., 2nd; MacMillan Publishing Co., Inc.: New York, 1978; 249-256.
73. Ware, R. A. and Wei, J., J. Catal., 1985, 93, 100-121.

74. Yan, T. Y., Coke Formation in Visbreaking Process, Prepr. - Am. Chem. Soc., Div. Pet. Chem., Denver, April 5-10, 1987; 490-495.
75. Yen, T. F. and Pollack, S. S., Anal. Chem., 1961, 33, 1587.
76. Yen, T. F., Present Status of the Structure of Petroleum Heavy Ends and its Significance to Various Technical Applications, Prepr. - Am. Chem. Soc., Div. Pet. Chem., New York, August 27 - September 1, 1972; F102-F114.
77. Yen, T. F., The role of Asphaltenes in Heavy Crudes and Tar Sands, First International UNITAR-AUSTRA USDA: Future of Heavy Crude Oils and Tar Sands, Edmonton, June 4-12, 1979; 174-179.
78. Yen, T. F. et al., Energy Sources, 1984, 7, 203.
79. Yortsos, Y. C. and Tsotsis, T. T., Chem. Eng. Commun., 1984, 30, 331-342.

APPENDIXES

APPENDIX A

REACTOR EXPERIMENTAL DATA

This Appendix presents the data obtained from the eleven experimental runs. A sample calculation for the kinetic rate constants and the metals deposited on the catalyst follows:

Hydrodemetallization Rate Constant

This rate was calculated assuming first order kinetics on a fixed bed reactor without volume change. The units are h^{-1} and is calculated using equation A1:

$$K_{1st\ HDM} = LHSV \times \ln(Met._{feed} / Met._{product}) \quad (A1)$$

where LHSV in h^{-1} is defined as the oil flow rate divided by the catalyst volume, Met is metals in ppm, and \ln is natural logarithm.

Hydrodesulfurization Rate Constant

For the HDS rate constant the assumption is second order kinetics, the units are $(time \times concentration)^{-1}$, and the equation to calculate it is A2:

$$K_{2nd\ HDS} = LHSV \times (1/S_{product} - 1/S_{feed}) \quad (A2)$$

Metals on the Catalyst

The metals deposited on the catalyst are calculated using equation A3 as weight of metals per weight of fresh catalyst:

$$\begin{aligned} \text{Metals [wt\%]} &= (\text{Met.}_{\text{feed}} - \text{Met.}_{\text{product}}) * 10^{-4} * \text{SG} && \text{(A3)} \\ \text{Removed} & * \text{Flow rate} * (\text{delta time}) / \text{catalyst wt} \\ & + \text{prior loading} \end{aligned}$$

where SG is the density of the oil calculated from API gravity, 10^{-4} is the conversion factor from ppm to wt% and from fraction to percentage.

Sample Calculations

The following sample calculation is for Run 01 at 94 h on stream:

$$\begin{aligned} K_{1\text{st HDM}} &= 28.7/10 \times \text{Ln}(136.53 / 77.2) \\ &= 1.64 \text{ h}^{-1} \end{aligned}$$

$$\begin{aligned} K_{2\text{nd HDS}} &= 28.7/10 \times (1/0.6 - 1/1.4) \\ &= 2.73 \text{ wt\%}^{-1} \text{ h}^{-1} \end{aligned}$$

$$\begin{aligned} \text{Metals Removed} &= (136.53 - 77.2) * 1\text{E-}04 * 0.92 * 28.7 \\ & * (94 - 70) / 5.8 + 1.85 \\ &= 2.5 \text{ wt\%} \end{aligned}$$

In Table 20 through 30 the second column is the average temperature measured at three locations in the reactor: the thermal zone, the middle of the catalyst zone and the top of the catalyst zone. For example when the thermal zone is at 760⁰F and the catalyst zone is at 710⁰F the reported temperature is calculated as: $(760 + 2(710))/3$ which is 726.7⁰F

TABLE 20
ACTIVITY DATA FOR RUN 01

BONDO 760-710 10% NCC

FEED PROPERTIES

CAT WT. g	5.8	NICKEL	42.03
CAT VOL. cc10		VANADIUM	94.50
		SULFUR	1.40
		H/NMR	10.78
		Ni + V	136.53
		SG	0.92

AGE HR	TEMP F	FLOW RATE cc/h	PRODUCT METALS....ppm			METALS REMOVED WT%	K 1st HDM h ⁻¹	SULFUR WT%	K 2nd HDS (hWT%) ⁻¹	HDS %	HDM %
			Ni	V	Ni + V						
0					0.00						
46	727.0	24.8	23.90	46.30	70.20	1.25	1.65	0.46	3.62	67.14	48.58
70	727.0	26.5	25.90	51.00	76.90	1.85	1.52	0.59	2.60	57.86	43.67
94	727.0	28.7	25.30	51.90	77.20	2.50	1.64	0.60	2.73	57.14	43.45
118	727.0	31.4	26.62	51.03	77.65	3.21	1.77	0.59	3.08	57.86	43.12
142	727.0	28.9	25.76	48.22	73.98	3.89	1.77	0.62	2.60	55.71	45.81
166	726.0	31.1	24.97	48.25	73.22	4.64	1.94	0.64	2.64	54.29	46.37
190	727.0	27.3	24.10	46.19	70.29	5.33	1.81	0.64	2.32	54.29	48.52
214	727.0	23.7	23.57	43.57	67.14	5.96	1.68	0.61	2.19	56.43	50.82
238	727.0	24.3	24.58	44.62	69.20	6.58	1.65	0.62	2.18	55.71	49.31
262	726.0	21.9	24.68	45.32	70.00	7.14	1.46	0.63	1.91	55.00	48.73
286	726.0	22.5	23.23	44.25	67.48	7.73	1.59	0.62	2.02	55.71	50.57
310	727.0	24.7	25.87	47.11	72.98	8.32	1.55	0.69	1.82	50.71	46.55
334	726.0	25.2	25.77	47.09	72.86	8.94	1.58	0.70	1.80	50.00	46.63
358	726.0	26.2	26.44	49.71	76.15	9.54	1.53	0.74	1.67	47.14	44.22
382	727.0	26.3	26.43	51.12	77.55	10.13	1.49	0.78	1.49	44.29	43.20

TABLE 21

ACTIVITY DATA FOR RUN 02

HONDO 710-710 10% NCC

FEED PROPERTIES

CAT WT. g	5.9	NICKEL	42.03
CAT VOL. cc	10	VANADIUM	94.50
		SULFUR	1.40
		H/NMR	12.11
		Ni + V	136.53
		SG	0.92

AGE HR	TEMP F	FLOW RATE cc/h	PRODUCT METALS...ppm			METALS REMOVED WT%	K 1st HDM h ⁻¹	SULFUR WT%	K 2nd HDS (h wt%) ⁻¹	HDS %	HDM %
			Ni	V	Ni + V						
0						0.00					
47	710.0	24.7	31.03	65.30	96.33	0.83	0.98	0.80	1.53	42.86	29.09
71	709.5	28.5	30.71	68.00	98.70	1.28	1.04	0.78	1.50	44.29	32.59
95	710.0	26.4	29.15	64.68	93.83	1.67	0.92	0.74	1.49	47.14	32.59
119	710.8	23.4	29.67	65.88	95.55	2.10	0.97	0.74	1.65	47.14	31.35
143	709.8	25.9	27.92	65.74	93.66	2.50	0.93	0.72	1.59	48.57	32.71
167	710.1	23.6	29.51	67.54	97.05	2.85	0.83	0.76	1.39	45.71	29.74
191	710.4	23.1	30.44	67.74	98.18	3.20	0.82	0.81	1.22	42.14	28.92
215	709.8	23.4	29.46	67.53	96.99	3.58	0.88	0.80	1.31	42.86	29.78
239	710.3	24.4	29.82	67.32	97.14	3.95	0.87	0.80	1.30	42.86	29.67
263	710.0	24.2	30.11	68.64	98.74	4.31	0.83	0.83	1.19	40.71	28.51
287	710.1	24.3	29.68	68.20	97.88	4.66	0.82	0.81	1.21	42.14	29.14
311	710.0	23.3	29.54	66.61	96.15	5.03	0.88	0.86	1.06	38.57	30.39
335	709.3	23.7	29.96	67.00	96.96	5.39	0.83	0.87	1.00	37.86	29.80
359	709.7	23.0	30.23	66.61	96.84	5.75	0.85	0.86	1.05	38.57	29.89
CHANGE FEED TO FEED FOR RUN 03											
406	710	26	33.545	68.7	102.24	7.0526	1.2920	1.22	.85663	40.196	39.160
430	710.2	26	33.89	71.939	105.82	7.6582	1.2353	1.32	.64705	35.294	39.978
454	708.9	24.2	33.86	70.176	104.03	8.2530	1.2074	1.34	.61969	34.313	39.284
478	710.2	24.2	35.28	71.409	106.68	8.8495	1.2058	1.37	.59213	32.843	38.627
502	710	24.7	35.127	71.33	106.45	9.4571	1.2290	1.36	.61519	33.333	38.716
526	710	25.1	35.11	72.07	107.18	10.057	1.2147	1.36	.60784	33.333	38.725
550	710.3	24.8	33.92	69.77	103.69	10.639	1.1825	1.42	.50510	30.392	39.412
574	710.8	23.6	35.11	73.64	108.75	11.244	1.2245	1.39	.57307	31.862	38.725

TABLE 22

ACTIVITY DATA FOR RUN 03

HONDO 760-710 5% MOC

FEED PROPERTIES

CAT WT. g	6.02	NICKEL	51.38
CAT VOL. cc	10	VANADIUM	119.56
		SULFUR	2.04
		H/NMR	12.11
		Ni + V	179.94
		SG	0.92

PRODUCT METALS..ppm

AGE HR	TEMP F	FLOW RATE cc/h	Ni	V	Ni + V	METALS REMOVED WT%	K 1st HDM h ⁻¹	SULFUR WT%	K 2nd HDS (h wt%) ⁻¹	HDS %	HDM %
0						0.00					
46	727.0	24.1	29.58	62.85	92.42	1.39	1.48	0.80	1.83	60.78	45.93
70	726.0	25.0	29.17	60.09	89.25	2.14	1.62	0.76	2.06	62.75	47.79
94	727.0	24.9	29.64	62.52	92.17	2.86	1.54	0.78	1.97	61.76	46.08
118	726.9	25.6	27.36	55.84	83.20	3.68	1.84	0.77	2.07	62.25	51.33
142	726.6	23.8	27.44	56.03	83.47	4.44	1.71	0.78	1.88	61.76	51.17
166	726.6	25.2	28.91	56.55	85.46	5.23	1.75	0.84	1.76	58.82	50.01
190	726.7	24.3	28.82	57.46	86.28	5.99	1.66	0.88	1.57	56.86	49.53

TABLE 23

ACTIVITY DATA FOR RUN 04

BONDO 710-710 5% NOC

FEED PROPERTIES

CAT WT. g 6.03
 CAT VOL. cc 10

NICKEL 51.38
 VANADIUM 119.56
 SULFUR 2.04
 H/NMR 12.11
 Ni + V 170.94
 SG 0.92

AGE HR	TEMP F	FLOW RATE cc/h	PRODUCT METALS....ppm			METALS REMOVED WT%	K 1st HDM h ⁻¹	SULFUR WT%	K 2nd HDS (h wt%) ⁻¹	HDS %	HDM %
			Ni	V	Ni + V						
0						0.00					
45	710.0	24.7	33.97	75.66	109.64	1.04	1.10	1.04	1.16	49.02	35.86
69	710.0	24.7	32.45	68.32	100.77	1.67	1.31	0.94	1.42	53.92	41.05
93	710.0	24.7	31.89	66.52	98.41	2.33	1.36	0.95	1.39	53.43	42.43
117	710.0	24.6	32.30	68.98	101.28	2.96	1.29	0.97	1.33	52.45	40.75
141	710.8	25.2	33.43	68.60	102.03	3.59	1.30	1.06	1.14	48.04	40.31
165	709.3	24.7	34.81	71.16	105.97	4.18	1.18	1.09	1.06	46.57	38.01
189	709.5	23.8	34.45	70.60	105.05	4.76	1.16	1.11	0.98	45.59	38.55
213	709.8	23.6	33.52	70.92	104.44	5.33	1.16	1.15	0.90	43.63	38.90

TABLE 24

ACTIVITY DATA FOR RUN 05

HONDO THERMAL

CAT WT. g 0.00
 CAT VOL. cc 0.00

FEED PROPERTIES

NICKEL 41.00
 VANADIUM 94.00
 SULFUR 1.76
 H/NMR 12.00
 Ni + V 135.00
 SG 0.92

AGE HR	TEMP F	FLOW RATE cc/h	PRODUCT METALS....ppm			METALS REMOVED WT%	K 1st HDM h ⁻¹	SULFUR WT%	K 2nd HDS (h wt%) ⁻¹	HDS %	HDM %
			Ni	V	Ni + V						
0											
46	710.0	26.5	42.17	93.78	135.95		1.61		8.52	-0.70	
70	710.0	26.3	39.85	93.78	133.63		1.61		8.52	1.01	
94	710.0	26.4	41.62	93.26	134.88		1.59		9.66	0.09	
118	710.0	26.5	41.46	93.47	134.93		1.54		12.50	0.05	
142	710.8	26.3	40.45	94.08	134.53		1.56		11.36	0.35	
166	727.0	26.5	40.54	89.34	129.88		1.41		19.89	3.79	
190	727.0	26.3	40.88	89.72	130.6		1.41		19.89	3.26	
214	727.0	26.2	37.59	81.83	119.42		1.46		17.05	11.54	
238	727.0	26.4	38.98	84.76	123.74		1.41		19.89	8.34	
262	727.0	26.4	39.26	86.07	125.33		1.42		19.32	7.16	
286	727.0	26.5	40.23	87.7	127.93		1.47		16.48	5.24	
310	727.0	26.1	39.54	84.77	124.31		1.45		17.61	7.92	

TABLE 25

ACTIVITY DATA FOR RUN 06

ORIENTE 760-710 5% NOC

FEED PROPERTIES

CAT WT. g 5.93
CAT VOL. cc 10NICKEL 58.63
VANADIUM 125.74
SULFUR 1.02
H/NMR 11.37
Ni + V 184.37
SG 0.95

AGE HR	TEMP F	FLOW RATE cc/h	PRODUCT METALS....ppm			METALS REMOVED WT%	K 1st HDM h ⁻¹	SULFUR WT%	K 2nd HDS (h wt%) ⁻¹	HDS %	HDM %
			Ni	V	Ni + V						
0											
45	726.7	25.3	49.78	99.29	149.07	0.69	0.54	0.52	2.38	49.02	19.15
69	726.8	26.0	49.64	100.63	150.27	1.03	0.53	0.56	2.09	45.10	18.49
93	726.6	26.2	50.32	105.98	156.29	1.31	0.43	0.51	2.57	50.00	15.23
117	726.5	26.1	48.26	101.91	150.17	1.65	0.54	0.52	2.46	49.02	18.55
141	726.4	26.3	49.45	101.59	151.03	1.99	0.52	0.52	2.48	49.02	18.08
165	726.5	26.4	48.76	102.00	150.76	2.33	0.53	0.53	2.39	48.04	18.23
189	726.8	26.1	48.97	102.99	151.97	2.66	0.50	0.54	2.27	47.06	17.57
213	726.6	26.3	50.16	107.91	158.07	2.92	0.40	0.53	2.38	48.04	14.26
237	726.7	26.2	50.69	108.02	158.71	3.18	0.39	0.53	2.37	48.04	13.92
261	726.5	26.1	50.97	108.28	159.25	3.43	0.38	0.55	2.19	46.08	13.62
285	726.5	26.4	49.36	108.68	158.04	3.70	0.41	0.55	2.21	46.08	14.28
309	726.4	26.3	50.60	109.87	160.47	3.94	0.37	0.55	2.20	46.08	12.96
333	726.7	26.3	50.40	107.23	157.63	4.21	0.41	0.56	2.12	45.10	14.50
357	726.7	26.2	50.72	106.72	157.44	4.48	0.41	0.57	2.03	44.12	14.60
381	726.5	26.1	51.80	108.37	160.17	4.73	0.37	0.57	2.02	44.12	13.13
405	726.7	26.2	51.37	107.44	158.81	4.98	0.39	0.58	1.95	43.14	13.86
429	726.7	26.3	51.92	108.77	160.69	5.22	0.36	0.58	1.96	43.14	12.84

TABLE 26

ACTIVITY DATA FOR RUN 07

ORIENTE 710-710 5 $\frac{1}{2}$ MOC

FEED PROPERTIES

CAT WT. g 5.97
CAT VOL. cc 10NICKEL 58.63
VANADIUM 125.74
SULFUR 1.02
H/NMR 11.37
Ni + V 184.37
SG 0.95

AGE HR	TEMP F	FLOW RATE cc/h	PRODUCT METALS....ppm			METALS REMOVED WT%	K 1st HDM h ⁻¹	SULFUR WT%	K 2nd HDS (h wt%) ⁻¹	HDS %	HDM %
			Ni	V	Ni + V						
0											
45	710.0	26.1	39.62	84.49	124.11	1.20	1.03	0.47	2.99	53.92	32.69
69	711.0	26.3	48.01	101.00	149.01	1.56	0.56	0.50	2.68	50.98	19.18
93	710.0	26.0	47.95	100.00	147.96	1.92	0.57	0.51	2.55	50.00	19.75
117	711.0	26.0	46.34	97.29	143.63	2.32	0.65	0.49	2.76	51.96	22.10
165	710.0	26.3	49.23	102.48	151.71	2.97	0.51	0.54	2.29	47.06	17.72
189	711.0	26.2	50.72	104.60	155.32	3.26	0.45	0.56	2.11	45.10	15.75
213	710.0	26.3	51.03	105.37	156.39	3.54	0.43	0.56	2.12	45.10	15.17
237	710.0	26.1	48.96	104.16	153.12	3.86	0.48	0.60	1.79	41.18	16.95
261	710.0	26.1	50.63	104.82	155.44	4.14	0.44	0.58	1.94	43.14	15.69
285	711.0	26.0	48.13	102.67	150.80	4.48	0.52	0.57	2.01	44.12	18.21
309	710.0	26.1	49.03	103.68	152.71	4.79	0.49	0.59	1.86	42.16	17.17
333	710.0	26.0	49.34	105.58	154.92	5.08	0.45	0.59	1.86	42.16	15.97
357	711.0	26.0	46.27	96.82	143.09	5.49	0.66	0.54	2.27	47.06	22.39
381	712.0	26.3	52.13	108.11	160.24	5.73	0.37	0.62	1.66	39.22	13.09
405	708.0	26.2	52.80	111.56	164.36	5.93	0.30	0.63	1.59	38.24	10.85

TABLE 27

ACTIVITY DATA FOR RUN 08

ORIENTE THERMAL

CAT WT. g 0.00
 CAT VOL. cc 0.00

FEED PROPERTIES

NICKEL 58.63
 VANADIUM 125.74
 SULFUR 1.06
 H/NMR 11.37
 Ni + V 184.37
 SG 0.95

AGE HR	TEMP F	FLOW RATE cc/h	PRODUCT METALS....ppm			METALS REMOVED WT%	K 1st HDM h ⁻¹	SULFUR WT%	K 2nd HDS (h wt%) ⁻¹	HDS %	HDM %
			Ni	V	Ni + V						
0											
44	709.9	26.2	57.22	124.21	181.43		0.90		15.09	1.59	
68	709.9	26.2	58.07	125.68	183.75		0.93		12.26	0.34	
92	709.7	26.2	57.53	124.91	182.44		0.92		13.21	1.05	
116	709.9	26.0	57.66	122.52	180.18		0.93		12.26	2.27	
140	709.8	26.1	59.51	127.82	187.33		0.94		11.32	-1.61	
164	726.6	26.1	57.92	123.05	180.97		0.93		12.26	1.84	
188	726.6	26.1	58.28	121.03	179.31		0.93		12.26	2.74	
212	726.4	26.2	59.28	126.44	185.72		0.94		11.32	-0.73	
236	726.8	26.3	59.62	123.58	183.20		0.94		11.32	0.63	
260	726.6	26.2	58.89	122.62	181.51		0.93		12.26	1.55	
306	727.0	26.3	59.75	128.83	188.58		0.94		11.32	-2.28	

TABLE 28

ACTIVITY DATA FOR RUN 09

CAÑO LINON 760-710 5% MOC

FEED PROPERTIES

CAT WT. g 5.99
CAT VOL. cc 10NICKEL 39.25
VANADIUM 13.61
SULFUR 0.40
H/NMR 12.53
Ni + V 52.86
SG 0.90

AGE HR	TEMP F	FLOW RATE cc/h	PRODUCT METALS....ppm			METALS REMOVED WT%	K 1st HDM h ⁻¹	SULFUR WT%	K 2nd HDS (h wt%) ⁻¹	HDS %	HDM %
			Ni	V	Ni + V						
0											
53	727.0	25.4	28.60	9.71	38.31	0.29	0.82	0.16	10.04	61.25	27.53
77	726.0	24.9	21.47	7.08	28.55	0.51	1.53	0.16	9.69	60.88	45.99
101	727.0	25.1	23.61	8.00	31.61	0.70	1.29	0.16	9.33	59.80	40.20
125	727.0	24.9	25.45	8.81	34.26	0.87	1.08	0.15	10.02	61.68	35.19
149	726.8	26.3	26.75	8.90	35.65	1.04	1.04	0.16	9.54	59.20	32.56
188	726.5	24.7	29.88	9.99	39.87	1.22	0.70	0.15	9.86	61.50	24.57
212	727.1	24.6	25.15	8.77	33.92	1.39	1.09	0.16	9.37	60.38	35.83
235	726.8	24.9	28.48	9.43	37.91	1.52	0.83	0.15	10.15	61.98	28.29
259	726.8	25.0	19.42	6.50	25.91	1.76	1.78	0.15	10.99	63.75	50.98
283	726.7	24.9	23.65	7.80	31.45	1.96	1.29	0.17	8.67	58.20	40.50
307	726.6	25.1	26.80	9.24	36.04	2.11	0.96	0.15	10.19	61.90	31.81
339	726.9	25.0	24.78	8.45	33.23	2.34	1.16	0.17	8.86	58.65	37.14
363	726.6	25.0	26.32	9.01	35.33	2.50	1.01	0.17	8.62	57.98	33.17
387	726.7	24.6	25.26	8.93	34.19	2.67	1.07	0.17	8.17	57.05	35.32
411	726.6	25.0	19.28	6.71	25.99	2.91	1.78	0.18	7.97	56.05	50.84
435	726.7	24.9	26.11	9.12	35.23	3.07	1.01	0.17	8.09	56.53	33.36
460	726.7	25.2	27.67	9.61	37.28	3.21	0.88	0.16	9.34	59.73	29.48
484	726.8	25.1	28.13	9.59	37.72	3.35	0.85	0.17	8.39	57.20	28.64
508	726.6	24.9	27.28	10.10	37.38	3.49	0.86	0.17	8.78	58.50	29.29
532	726.7	24.5	19.18	6.98	26.16	3.73	1.72	0.17	8.09	56.93	50.52
556	728.2	25.8	27.20	10.00	37.20	3.87	0.91	0.17	8.52	56.93	29.63
580	726.5	24.7	30.75	11.95	42.70	3.96	0.53	0.18	7.27	54.08	19.23
604	726.6	25.5	30.75	11.90	42.65	4.06	0.55	0.18	7.51	54.08	19.32
635	726.6	25.3	34.11	12.18	46.29	4.13	0.34	0.19	7.02	52.60	12.43
659	726.6	24.7	22.35	7.64	29.99	4.34	1.40	0.20	6.34	50.68	43.27

TABLE 29

ACTIVITY DATA FOR RUN 10

CAÑO LIMÓN 710-710 5% NCC

FEED PROPERTIES

CAT WT. g 6.00
CAT VOL. cc 10NICKEL 39.25
VANADIUM 13.61
SULFUR 0.40
H/NMR 12.53
Ni + V 52.86
SG 0.90

AGE HR	TEMP F	FLOW RATE cc/h	PRODUCT METALS....ppm			METALS REMOVED WT%	K 1st HDM h ⁻¹	SULFUR WT%	K 2nd HDS (h wt%) ⁻¹	HDS %	HDM %
			Ni	V	Ni + V						
0											
45	711.7	24.1	29.93	11.22	41.15	0.19	0.60	0.18	7.22	54.50	22.15
69	710.4	24.4	29.08	10.32	39.40	0.31	0.72	0.16	9.44	60.75	25.46
93	710.2	23.7	29.23	10.01	39.24	0.43	0.71	0.15	10.31	63.50	25.77
117	709.9	23.1	28.84	10.35	39.20	0.54	0.69	0.16	8.40	59.25	25.85
141	710.3	23.6	29.86	10.08	39.95	0.65	0.66	0.15	10.38	63.75	24.43
165	710.1	23.6	29.90	10.18	40.08	0.76	0.65	0.17	8.23	58.25	24.18
189	710.4	23.6	28.73	9.90	38.63	0.88	0.74	0.15	10.05	63.00	26.93
213	709.6	25.2	28.88	10.88	39.76	1.00	0.72	0.18	7.78	55.25	24.78
237	709.3	24.7	30.19	10.84	41.03	1.11	0.63	0.17	8.02	56.50	22.38
261	711.0	24.4	30.52	10.63	41.15	1.21	0.61	0.17	8.51	58.25	22.16
285	710.2	25.1	30.30	10.53	40.84	1.32	0.65	0.16	9.81	61.00	22.75
309	709.9	24.8	30.24	10.85	41.09	1.42	0.62	0.16	9.11	59.50	22.27
333	709.9	25.0	29.23	10.25	39.48	1.54	0.73	0.16	9.28	59.75	25.31
357	710.1	24.7	30.93	10.94	41.87	1.64	0.58	0.16	9.07	59.50	20.79
381	710.2	24.7	31.00	11.43	42.43	1.73	0.54	0.19	7.18	53.75	19.74
405	710.0	25.2	31.52	11.24	42.75	1.83	0.53	0.18	7.70	55.00	19.12
429	709.9	25.1	31.13	11.00	42.12	1.92	0.57	0.17	8.67	58.00	20.32
453	710.6	24.6	31.74	11.07	42.81	2.01	0.52	0.17	8.76	58.75	19.02
477	710.2	25.0	30.76	11.04	41.80	2.11	0.59	0.19	7.26	53.75	20.92
501	709.9	24.6	31.01	10.77	41.78	2.21	0.58	0.17	8.24	57.25	20.96
525	710.0	25.1	31.17	11.00	42.17	2.31	0.57	0.17	8.85	58.50	20.23
549	709.8	25.1	30.92	10.70	41.62	2.41	0.60	0.19	7.22	53.50	21.27
573	710.0	24.6	31.64	11.06	42.70	2.50	0.53	0.19	6.94	53.00	19.22
597	710.0	24.9	31.04	10.94	41.98	2.59	0.57	0.18	7.84	55.75	20.59
621	710.0	25.1	32.13	11.63	43.76	2.68	0.47	0.18	7.83	55.50	17.22
645	710.0	25.5	33.69	12.11	45.80	2.74	0.37	0.19	6.98	52.25	13.35
669	710.3	24.9	30.59	11.04	41.63	2.84	0.59	0.17	8.25	57.00	21.25
693	710.2	25.2	32.12	11.62	43.74	2.93	0.48	0.19	6.76	51.75	17.25

TABLE 29(Continued)

AGE HR	TEMP F	FLOW RATE cc/h	PRODUCT METALS....ppm			METALS REMOVED WT%	K 1st HDM h ⁻¹	SULFUR WT%	K 2nd HDS (h wt%) ⁻¹	HDS %	HDM %
			Ni	V	Ni + V						
717	710.1	25.3	31.21	11.45	42.66	3.02	0.54	0.19	6.92	52.25	19.30
741	709.7	25.0	31.91	11.81	43.72	3.10	0.47	0.20	6.44	50.75	17.30
765	710.7	24.8	31.71	11.55	43.26	3.19	0.50	0.19	7.06	53.25	18.17
804	709.7	25.0	30.00	11.55	41.55	3.35	0.60	0.20	6.31	50.25	21.40
830	710.1	24.9	32.23	11.55	43.78	3.44	0.47	0.20	6.29	50.25	17.19
854	710.8	24.9	30.39	10.90	41.29	3.54	0.62	0.20	6.29	50.25	21.89
878	710.0	25.3	31.07	10.94	42.01	3.64	0.58	0.20	6.20	49.50	20.53
902	710.1	25.0	31.83	11.13	42.96	3.73	0.52	0.20	6.13	49.50	18.72
926	709.3	24.9	31.18	11.32	42.51	3.82	0.54	0.19	6.74	52.00	19.59
950	710.0	25.4	30.94	11.15	42.08	3.92	0.58	0.19	6.81	51.75	20.39
994	710.0	25.2	32.02	11.35	43.38	4.08	0.50	0.19	6.76	51.75	17.94

TABLE 30

ACTIVITY DATA FOR RUN 11

CAÑO LIMON THERMAL

CAT WT. g 0.00
 CAT VOL. cc 0.00

FEED PROPERTIES

NICKEL 39.25
 VANADIUM 13.61
 SULFUR 0.40
 H/NMR 12.53
 Ni + V 52.86
 SG 0.90

AGE HR	TEMP F	FLOW RATE cc/h	PRODUCT METALS....ppm			METALS REMOVED WT%	K 1st HDM h ⁻¹	SULFUR WT%	K 2nd HDS (h wt%) ⁻¹	HDS %	HDM %
			Ni	V	Ni + V						
0											
45	709.8	26.3	38.26	15.82	54.08		0.40		6.98	2.12	
69	710.1	23.4	38.73	15.66	54.39		0.40		6.98	1.56	
93	710.0	18.2	39.19	16.58	55.77		0.41		4.65	-0.94	
117	710.0	21.4	40.02	16.25	56.27		0.42		2.33	-1.85	
141	709.9	24.8	40.86	15.39	56.25		0.42		2.33	-1.81	
195	726.9	26.2	38.13	14.21	52.34		0.39		9.30	5.27	
219	726.9	26.2	36.92	13.06	49.98		0.39		9.30	9.54	
243	726.7	26.4	38.13	15.34	53.47		0.41		4.65	3.22	
267	726.3	27.0	34.22	12.98	47.20		0.39		9.30	14.57	
291	727.7	25.9	34.17	13.10	47.27		0.39		9.30	14.44	

APPENDIX B

MICROPROBE DATA

This Appendix shows a sample calculation of the penetration factor for vanadium from the microprobe data, it shows a complete set of data for a traverse of a particle for Run 03, and then summarizes the data necessary to calculate the vanadium penetration factors for all the catalyst particles analyzed in Tables 28 to 43. The data for the other elements, namely Ni and C are not included here because the emphasis of the study was on vanadium. One of the reasons for this is that Ni does not show a good signal from the LC-ICP analysis. However, for the interested reader, the original data will be available in diskette at the Department of Chemical Engineering of Oklahoma State University and at the Catalyst Laboratory of Phillips Petroleum Company. In the main text of the thesis some reference is made to the average coke content calculated from the microprobe data.

Vanadium Penetration Factor (Q_v)

For a cylindrical catalyst, Tamm et al. (1981) defined a penetration or distribution factor as the ratio of the average to the maximum radial vanadium concentration as

given by equation B1:

$$Q_v = \frac{\int_0^r V(r) r dr}{V_{\max} \int_0^r r dr} = \frac{\text{average vanadium concentration}}{\text{concentration at maximum}} \quad (\text{B1})$$

Where r is the distance from the center of the particle. The integral are calculated numerically by summing the areas of small increments and modifying the vanadium content as the ratio of V to Al_2O_3 as shown in equation B2:

$$Q_v = \frac{\int_0^r V(r) r dr}{V_{\max} \int_0^r r dr} = \frac{\sum (V/\text{Al}_2\text{O}_3)_n r_n (r_{n+1} - r_n)}{(V/\text{Al}_2\text{O}_3)_{\max} \sum r_n (r_{n+1} - r_n)} \quad (\text{B2})$$

The subscripts $n+1$ and n indicate the position of the increments.

Sample Calculation

The following procedure uses the data for Run 03, pellet 1, traverse 1 as presented in Table 27 to calculate the penetration factor for Vanadium:

- a) Convert Al to Al_2O_3 by multiplying column C by $M(\text{Al}_2\text{O}_3)/M(\text{Al}_2) = 1.89$ and store it in Column S.
- b) Calculate the ratio $V / \text{Al}_2\text{O}_3$ as Column E/Column S and store it in column M.
- c) Calculate the summation $(V/\text{Al}_2\text{O}_3)_n r_n (r_{n+1} - r_n)$ with r_n as the particle radius (cell B34 or R1) minus the position (B5 for the first value) and $(r_{n+1} - r_n)$ as the difference in adjacent positions (B6-B5 for the first value) and store in column T.

- d) Calculate the summation $r_n (r_{n+1} - r_n)$ as indicated before and store in column Y.
- e) Calculate $(V/Al_2O_3)_{avg}$ by dividing cell T34 over cell Y34 and store in cell L1.
- f) Calculate the V penetration Factor Q_v by dividing L1 over the maximum value of (V/Al_2O_3) from column M, divide over a 100 and store it in cell F38. The same procedure was followed to calculate average values and penetration factors for other elements for all four traverses of each particle analyzed.

TABLE 31

SAMPLE OF MICROPROBE DATA FOR RUN 03

	A	B	C	D	E	F	G	H	I	J	K	L
1	21-89 Pellet One			Sample #34413-17								
2	Ni-Mo catalyst, 760F preheat, 710F bed temperature, top of bed, 5% loading Honda											
3	12 o'clock traverse											
4	Point	Position	Wt% Al	Wt% Ni	Wt% V	Wt% Mo	Wt% S	Wt% C	Wt% O	Wt% Si	Total	
5	1	0	21.81	6.94	8.43	6.46	10.80	9.13	21.76	0.22	85.55	
6	2	5	24.24	5.67	9.65	6.66	10.78	10.19	21.93	0.50	89.02	
7	3	10	24.00	5.54	10.00	5.24	9.81	10.00	16.77	0.30	78.63	
8	4	15	23.87	5.92	11.13	6.14	11.57	7.17	20.29	0.17	86.26	
9	5	20	24.61	5.30	10.78	5.86	10.44	7.49	21.09	0.35	85.92	
10	6	25	25.38	5.55	10.49	6.50	9.51	7.25	22.03	0.36	87.07	
11	7	30	27.00	4.64	9.25	6.85	8.13	7.25	23.39	0.42	86.93	
12	8	35	27.71	3.02	8.63	6.66	5.94	6.56	25.08	0.28	83.88	
13	9	40	29.69	2.62	7.34	7.43	4.47	6.98	27.32	0.40	86.25	
14	10	45	30.08	2.85	6.31	7.19	4.63	6.12	27.65	0.38	85.21	
15	11	50	30.17	3.05	5.32	7.58	4.47	6.15	27.04	0.40	84.18	
16	12	65	30.58	3.60	3.07	7.18	5.54	4.63	29.92	0.32	84.84	
17	13	80	33.47	4.30	1.58	6.74	6.03	4.64	33.96	0.44	91.16	
18	14	95	33.77	4.31	1.07	6.54	5.94	4.74	33.23	0.55	90.15	
19	15	110	34.27	4.53	0.63	6.73	6.74	5.54	34.71	0.51	93.66	
20	16	125	34.43	4.19	0.41	6.86	6.65	4.56	34.64	0.18	91.92	
21	17	140	34.93	4.29	0.24	7.17	6.87	4.65	36.30	0.44	94.89	
22	18	155	35.25	4.65	0.16	6.79	6.51	4.45	37.64	0.18	95.63	
23	19	170	35.05	4.42	0.13	6.90	6.60	3.97	36.47	0.18	93.72	
24	20	185	35.38	4.60	0.09	6.44	6.06	4.02	37.56	0.29	94.44	
25	21	200	35.16	4.26	0.08	6.75	6.32	4.28	38.06	0.30	95.21	
26	22	265	36.80	3.20	0.03	6.47	4.90	3.85	38.80	0.25	94.10	
27	23	330	36.28	2.97	0.00	6.51	5.35	3.59	41.69	0.26	96.65	
28	24	395	37.81	2.54	0.00	6.25	3.33	2.76	43.21	0.28	96.18	
29	25	460	37.52	2.14	0.02	6.43	4.89	3.31	44.53	0.37	99.21	
30	26	525	37.06	2.39	0.00	6.98	3.26	2.76	43.83	0.43	96.71	
31	27	590	37.60	2.04	0.00	6.09	4.13	2.53	44.76	0.32	97.47	
32	28	655	38.34	1.87	0.00	5.93	2.73	2.46	44.02	0.38	95.73	
33	29	720	39.04	1.77	0.00	6.09	3.61	2.24	45.25	0.26	98.26	
34	30	785	37.60	1.99	0.01	6.28	2.83	2.58	43.83	0.35	95.45	
35												
36												
37												

TABLE 31 (Continued)

	M	N	O	P	Q	R	S	T	U	V	W	X	Y	
1	V av wt%	2.96	Cavg wt%	7.06	R=	785.00	um	SUMMATIONS.....						
2	Ni av wt%	5.65	Savg wt%	9.02				V(r)rdr	Ni(r)rdr	Mo(r)rdr	C(r)rdr	S(r)rdr	rdr	
3	Mo av wt%	10.29	METAL RATIOS.....											
4	V/AI2O3	Ni/AI2O3	V/Ni	Mo/AI2O3	S/AI2O3	C/AI2O3	AI2O3							
5	0.205	0.168	1.215	0.157	0.262	0.222	41.210	80291	66099	61528	86958	102863	3925	
6	0.211	0.124	1.702	0.145	0.235	0.222	45.801	162460	114379	118238	173726	194655	7825	
7	0.221	0.122	1.805	0.116	0.216	0.221	45.348	247911	161719	163013	259176	278482	11700	
8	0.247	0.131	1.880	0.136	0.257	0.159	45.102	342918	212253	215425	320380	377245	15550	
9	0.232	0.114	2.034	0.126	0.225	0.161	46.501	431591	255849	263628	381991	463121	19375	
10	0.219	0.116	1.890	0.136	0.198	0.151	47.956	514714	299827	315134	439440	538478	23175	
11	0.181	0.091	1.994	0.134	0.159	0.142	51.017	583160	334161	365821	493086	598637	26950	
12	0.165	0.058	2.858	0.127	0.113	0.125	52.358	644970	355791	413521	540071	641181	30700	
13	0.131	0.047	2.802	0.132	0.080	0.124	56.099	693708	373188	462857	586418	670862	34425	
14	0.111	0.050	2.214	0.127	0.081	0.108	56.836	734785	391741	509663	626259	701003	38125	
15	0.093	0.054	1.744	0.133	0.078	0.108	57.006	837674	450728	656280	745200	787452	49150	
16	0.053	0.062	0.853	0.124	0.096	0.080	57.781	895056	518017	790464	831740	891002	59950	
17	0.025	0.068	0.367	0.107	0.095	0.073	63.242	921476	589920	903167	909329	991833	70525	
18	0.017	0.068	0.248	0.102	0.093	0.074	63.808	938832	659830	1009249	986214	1088183	80875	
19	0.010	0.070	0.139	0.104	0.104	0.086	64.753	948683	730662	1114481	1072839	1193572	91000	
20	0.006	0.064	0.098	0.105	0.102	0.070	65.055	954922	794425	1218875	1142232	1294770	100900	
21	0.004	0.065	0.056	0.109	0.104	0.070	66.000	958441	857312	1323981	1210396	1395477	110575	
22	0.002	0.070	0.034	0.102	0.098	0.067	66.605	960711	923287	1420318	1273533	1487842	120025	
23	0.002	0.067	0.029	0.104	0.100	0.060	66.227	962522	984855	1516431	1328833	1579776	129250	
24	0.001	0.069	0.020	0.096	0.091	0.060	66.851	963733	1046784	1603132	1382954	1661361	138250	
25	0.001	0.064	0.019	0.102	0.095	0.064	66.435	968312	1290612	1989479	1627926	2023096	176275	
26	0.000	0.046	0.009	0.093	0.070	0.055	69.534	969770	1446162	2303983	1815073	2261283	210075	
27	0.000	0.043	0.000	0.095	0.078	0.052	68.551	969770	1574297	2584844	1969957	2492098	239650	
28	0.000	0.036	0.000	0.087	0.047	0.039	71.442	969770	1664425	2806614	2067891	2610258	265000	
29	0.000	0.030	0.009	0.091	0.069	0.047	70.894	970366	1728193	2998216	2166522	2755970	286125	
30	0.000	0.034	0.000	0.100	0.047	0.039	70.025	970366	1785874	3166673	2233133	2834648	303025	
31	0.000	0.029	0.000	0.086	0.058	0.036	71.045	970366	1822269	3275323	2278270	2908330	315700	
32	0.000	0.026	0.000	0.082	0.038	0.034	72.443	970366	1844081	3344492	2306964	2940173	324150	
33	0.000	0.024	0.000	0.083	0.049	0.030	73.766	970366	1854219	3379373	2319794	2960850	328375	
34	0.000	0.028	0.005	0.088	0.040	0.036	71.045	970366	1854219	3379373	2319794	2960850	328375	
35	DISTRIBUTION PARAMETERS Xavg/Xmax (Cx)													
36	V	0.120	Mo	0.657	C	0.318								
37	Ni	0.335	S	0.344										

TABLE 32

V/AL2O3 VALUES FOR RUN 01, HONDO 10%,780-710, TOP OF BED

Point	Position	Pellet One				Pellet two				Pellet three			
		Trav. 1	Trav. 2	Trav. 3	Trav. 4	Trav. 1	Trav. 2	Trav. 3	Trav. 4	Trav. 1	Trav. 2	Trav. 3	Trav. 4
1	0	0.125	0.178	0.254	0.149	0.125	0.138	0.117	0.147	0.156	0.158	0.139	0.191
2	5	0.130	0.099	0.128	0.407	0.125	0.138	0.131	0.147	0.200	0.158	0.177	0.260
3	10	0.122	0.136	0.127	0.361	0.132	0.166	0.157	0.151	0.145	0.156	0.248	0.247
4	15	0.114	0.141	0.144	0.366	0.141	0.154	0.141	0.146	0.211	0.245	0.234	0.237
5	20	0.099	0.140	0.131	0.236	0.111	0.147	0.149	0.120	0.205	0.231	0.210	0.211
6	25	0.089	0.124	0.105	0.106	0.118	0.128	0.129	0.103	0.197	0.215	0.214	0.188
7	30	0.074	0.112	0.082	0.113	0.113	0.103	0.115	0.087	0.179	0.177	0.171	0.154
8	35	0.063	0.094	0.070	0.119	0.098	0.080	0.115	0.089	0.155	0.143	0.119	0.118
9	40	0.051	0.084	0.058	0.111	0.090	0.067	0.079	0.057	0.124	0.114	0.104	0.091
10	45	0.048	0.074	0.049	0.093	0.080	0.053	0.066	0.049	0.094	0.109	0.099	0.078
11	50	0.039	0.060	0.044	0.076	0.067	0.051	0.053	0.042	0.083	0.094	0.074	0.065
12	65	0.026	0.045	0.028	0.044	0.050	0.025	0.030	0.030	0.048	0.058	0.048	0.041
13	80	0.015	0.022	0.019	0.023	0.027	0.011	0.017	0.017	0.028	0.039	0.029	0.023
14	95	0.009	0.012	0.009	0.014	0.018	0.007	0.010	0.011	0.017	0.021	0.019	0.015
15	110	0.006	0.004	0.005	0.009	0.008	0.004	0.006	0.007	0.008	0.011	0.010	0.008
16	125	0.004	0.004	0.003	0.006	0.005	0.002	0.004	0.004	0.005	0.007	0.007	0.005
17	140	0.002	0.003	0.002	0.004	0.002	0.001	0.002	0.003	0.003	0.004	0.004	0.003
18	155	0.002	0.002	0.001	0.002	0.001	0.001	0.002	0.002	0.002	0.003	0.003	0.002
19	170	0.001	0.001	0.001	0.002	0.000	0.001	0.001	0.001	0.002	0.001	0.002	0.001
20	185	0.001	0.002	0.001	0.001	0.001	0.001	0.000	0.001	0.001	0.001	0.002	0.001
21	200	0.001	0.001	0.000	0.001	0.001	0.000	0.000	0.001	0.001	0.001	0.001	0.000
22	265	0.000	0.000	0.000	0.000	0.000	0.000	0.000	0.000	0.000	0.000	0.000	0.000
23	330	0.000	0.000	0.000	0.000	0.000	0.000	0.000	0.000	0.000	0.000	0.000	0.000
24	395	0.000	0.000	0.000	0.000	0.000	0.000	0.000	0.000	0.000	0.000	0.000	0.000
25	460	0.000	0.000	0.000	0.000	0.000	0.000	0.000	0.000	0.000	0.000	0.000	0.000
26	525	0.000	0.000	0.000	0.000	0.000	0.000	0.000	0.000	0.000	0.000	0.000	0.000
27	590	0.000	0.000	0.000	0.000	0.000	0.000	0.000	0.000	0.000	0.000	0.000	0.000
28	655	0.000	0.000	0.000	0.000	0.000	0.000	0.000	0.000	0.000	0.000	0.000	0.000
29	720	0.000	0.000	0.000	0.000	0.000	0.000	0.000	0.000	0.000	0.000	0.000	0.000
30	785	0.000	0.001	0.000	0.000	0.000	0.000	0.000	0.000	0.000	0.000	0.000	0.000

TABLE 33

V/AL2O3 VALUES FOR RUN 01, HONDO 10%, 760-710, BOTTOM OF BED

Point	Position	Pellet One				Pellet two				Pellet three			
		Trav. 1	Trav. 2	Trav. 3	Trav. 4	Trav. 1	Trav. 2	Trav. 3	Trav. 4	Trav. 1	Trav. 2	Trav. 3	Trav. 4
1	0	0.262	0.188	0.832	0.251	0.157	0.424	0.178	0.178	0.538	0.504	0.645	0.512
2	5	0.316	0.298	0.473	0.344	0.249	0.174	0.155	0.231	0.623	0.504	0.378	0.625
3	10	0.380	0.353	0.263	0.355	0.256	0.214	0.176	0.242	0.500	0.570	0.488	0.527
4	15	0.370	0.381	0.420	0.314	0.280	0.268	0.220	0.227	0.456	0.545	0.529	0.497
5	20	0.312	0.389	0.322	0.307	0.255	0.274	0.222	0.214	0.397	0.398	0.482	0.399
6	25	0.286	0.330	0.306	0.199	0.201	0.296	0.262	0.164	0.320	0.415	0.440	0.345
7	30	0.240	0.281	0.204	0.250	0.180	0.262	0.210	0.153	0.295	0.333	0.347	0.276
8	35	0.198	0.252	0.220	0.225	0.168	0.247	0.223	0.138	0.239	0.277	0.220	0.239
9	40	0.142	0.198	0.224	0.203	0.136	0.224	0.190	0.108	0.201	0.223	0.220	0.194
10	45	0.136	0.161	0.217	0.184	0.113	0.199	0.177	0.102	0.161	0.207	0.176	0.146
11	50	0.104	0.142	0.144	0.137	0.093	0.161	0.150	0.085	0.127	0.156	0.139	0.111
12	65	0.060	0.080	0.207	0.112	0.058	0.107	0.110	0.063	0.078	0.083	0.070	0.072
13	80	0.035	0.042	0.173	0.060	0.038	0.065	0.076	0.039	0.045	0.040	0.037	0.044
14	95	0.021	0.026	0.117	0.046	0.025	0.044	0.052	0.026	0.027	0.029	0.023	0.026
15	110	0.011	0.016	0.048	0.029	0.015	0.024	0.034	0.017	0.016	0.014	0.013	0.015
16	125	0.006	0.009	0.027	0.019	0.010	0.014	0.022	0.009	0.010	0.010	0.008	0.008
17	140	0.005	0.005	0.013	0.011	0.006	0.010	0.016	0.006	0.006	0.005	0.004	0.003
18	155	0.003	0.002	0.007	0.006	0.004	0.005	0.011	0.005	0.004	0.003	0.003	0.003
19	170	0.002	0.002	0.004	0.004	0.003	0.003	0.007	0.003	0.003	0.002	0.001	0.002
20	185	0.001	0.001	0.002	0.003	0.002	0.003	0.005	0.002	0.001	0.001	0.001	0.001
21	200	0.001	0.001	0.001	0.001	0.001	0.002	0.004	0.001	0.001	0.001	0.001	0.000
22	265	0.000	0.000	0.000	0.000	0.000	0.001	0.000	0.000	0.000	0.000	0.000	0.000
23	330	0.000	0.000	0.000	0.000	0.000	0.000	0.000	0.000	0.000	0.000	0.000	0.000
24	395	0.000	0.000	0.000	0.000	0.000	0.001	0.000	0.000	0.000	0.000	0.000	0.000
25	460	0.000	0.000	0.000	0.000	0.000	0.000	0.000	0.000	0.000	0.000	0.000	0.000
26	525	0.000	0.000	0.000	0.000	0.000	0.000	0.000	0.000	0.000	0.000	0.000	0.000
27	590	0.000	0.000	0.000	0.000	0.000	0.000	0.000	0.000	0.000	0.000	0.000	0.000
28	655	0.000	0.000	0.000	0.000	0.000	0.000	0.000	0.000	0.000	0.000	0.000	0.000
29	720	0.000	0.000	0.000	0.000	0.000	0.000	0.000	0.000	0.000	0.000	0.000	0.000
30	785	0.000	0.000	0.000	0.000	0.000	0.000	0.000	0.000	0.000	0.000	0.000	0.000

TABLE 34

V/AL2O3 VALUES FOR RUN 02, HONDO 10%,710-710, TOP OF BED

Point	Position	Pellet One				Pellet two				Pellet three			
		Trav. 1	Trav. 2	Trav. 3	Trav. 4	Trav. 1	Trav. 2	Trav. 3	Trav. 4	Trav. 1	Trav. 2	Trav. 3	Trav. 4
1	0	0.000	0.000	0.000	0.000	0.477	0.361	0.385	0.493	0.429	0.423	0.423	0.331
2	5	0.130	0.099	0.128	0.407	0.477	0.416	0.456	0.429	0.564	0.532	0.478	0.378
3	10	0.122	0.136	0.127	0.361	0.487	0.428	0.440	0.433	0.472	0.507	0.454	0.361
4	15	0.114	0.141	0.144	0.366	0.580	0.451	0.437	0.389	0.454	0.448	0.382	0.484
5	20	0.099	0.140	0.131	0.236	0.400	0.388	0.373	0.386	0.351	0.327	0.332	0.492
6	25	0.089	0.124	0.105	0.106	0.389	0.336	0.341	0.439	0.275	0.218	0.251	0.372
7	30	0.074	0.112	0.082	0.113	0.283	0.279	0.291	0.333	0.249	0.186	0.193	0.367
8	35	0.063	0.094	0.070	0.119	0.244	0.236	0.253	0.295	0.190	0.162	0.164	0.337
9	40	0.051	0.084	0.058	0.111	0.195	0.192	0.205	0.252	0.150	0.127	0.129	0.262
10	45	0.048	0.074	0.049	0.093	0.165	0.157	0.174	0.203	0.125	0.109	0.103	0.202
11	50	0.039	0.060	0.044	0.076	0.141	0.140	0.137	0.182	0.097	0.085	0.087	0.168
12	65	0.026	0.045	0.028	0.044	0.088	0.079	0.090	0.113	0.055	0.052	0.050	0.096
13	80	0.015	0.022	0.019	0.023	0.059	0.045	0.056	0.069	0.033	0.031	0.029	0.060
14	95	0.009	0.012	0.009	0.014	0.039	0.030	0.046	0.047	0.020	0.018	0.018	0.036
15	110	0.006	0.004	0.005	0.009	0.030	0.020	0.026	0.032	0.012	0.010	0.012	0.025
18	125	0.004	0.004	0.003	0.006	0.023	0.014	0.018	0.022	0.007	0.002	0.008	0.019
17	140	0.002	0.003	0.002	0.004	0.016	0.009	0.012	0.014	0.004	0.003	0.005	0.008
18	155	0.002	0.002	0.001	0.002	0.010	0.007	0.008	0.009	0.003	0.002	0.003	0.005
19	170	0.001	0.001	0.001	0.002	0.008	0.005	0.004	0.006	0.001	0.001	0.002	0.003
20	185	0.001	0.002	0.001	0.001	0.005	0.004	0.003	0.004	0.001	0.001	0.001	0.002
21	200	0.001	0.001	0.000	0.001	0.003	0.003	0.002	0.002	0.001	0.000	0.001	0.001
22	285	0.000	0.000	0.000	0.000	0.001	0.002	0.000	0.002	0.000	0.000	0.000	0.000
23	330	0.000	0.000	0.000	0.000	0.000	0.001	0.000	0.001	0.000	0.000	0.000	0.000
24	395	0.000	0.000	0.000	0.000	0.000	0.001	0.000	0.000	0.000	0.000	0.000	0.000
25	460	0.000	0.000	0.000	0.000	0.000	0.000	0.000	0.000	0.000	0.000	0.000	0.000
26	525	0.000	0.000	0.000	0.000	0.000	0.000	0.000	0.000	0.000	0.000	0.000	0.000
27	590	0.000	0.000	0.000	0.000	0.000	0.000	0.000	0.000	0.000	0.000	0.000	0.000
28	655	0.000	0.000	0.000	0.000	0.000	0.000	0.001	0.000	0.000	0.000	0.000	0.000
29	720	0.000	0.000	0.000	0.000	0.000	0.000	0.000	0.000	0.000	0.000	0.000	0.000
30	785	0.000	0.001	0.000	0.000	0.000	0.000	0.000	0.000	0.000	0.000	0.000	0.000

TABLE 35

WAL203 VALUES FOR RUN 02, HONDO 10%,710-710, BOTTOM OF BED

Point	Position	Pellet One				Pellet two				Pellet three			
		Trav. 1	Trav. 2	Trav. 3	Trav. 4	Trav. 1	Trav. 2	Trav. 3	Trav. 4	Trav. 1	Trav. 2	Trav. 3	Trav. 4
1	0	0.496	0.556	0.493	0.561	0.777	0.726	0.879	0.685	0.262	0.466	0.372	0.365
2	5	0.538	0.556	0.571	0.552	0.710	0.717	0.768	0.622	0.378	0.498	0.470	0.404
3	10	0.539	0.606	0.534	0.486	0.641	0.734	0.665	0.578	0.453	0.531	0.433	0.383
4	15	0.405	0.510	0.468	0.448	0.581	0.531	0.528	0.471	0.439	0.364	0.347	0.495
5	20	0.341	0.429	0.356	0.337	0.337	0.429	0.462	0.377	0.355	0.299	0.306	0.378
6	25	0.300	0.338	0.336	0.324	0.354	0.328	0.365	0.326	0.297	0.234	0.227	0.329
7	30	0.239	0.267	0.217	0.217	0.289	0.278	0.268	0.284	0.234	0.200	0.176	0.338
8	35	0.188	0.197	0.186	0.190	0.250	0.244	0.246	0.234	0.190	0.169	0.149	0.271
9	40	0.168	0.149	0.147	0.120	0.211	0.216	0.194	0.185	0.187	0.137	0.125	0.271
10	45	0.137	0.108	0.137	0.120	0.165	0.176	0.160	0.170	0.135	0.119	0.105	0.306
11	50	0.109	0.109	0.100	0.095	0.128	0.148	0.116	0.140	0.105	0.084	0.078	0.278
12	65	0.064	0.061	0.063	0.057	0.078	0.086	0.071	0.082	0.066	0.055	0.049	0.207
13	80	0.041	0.036	0.036	0.037	0.045	0.052	0.045	0.047	0.039	0.032	0.029	0.128
14	95	0.028	0.021	0.023	0.022	0.029	0.028	0.026	0.029	0.026	0.020	0.017	0.080
15	110	0.019	0.012	0.013	0.015	0.016	0.016	0.018	0.017	0.015	0.010	0.006	0.047
16	125	0.012	0.007	0.007	0.010	0.011	0.009	0.010	0.010	0.009	0.003	0.006	0.028
17	140	0.008	0.005	0.004	0.006	0.005	0.005	0.005	0.007	0.005	0.003	0.004	0.014
18	155	0.005	0.002	0.003	0.004	0.003	0.003	0.003	0.005	0.003	0.002	0.002	0.009
19	170	0.004	0.002	0.000	0.003	0.002	0.002	0.002	0.003	0.002	0.001	0.001	0.006
20	185	0.003	0.001	0.001	0.002	0.001	0.001	0.001	0.002	0.001	0.001	0.001	0.004
21	200	0.000	0.001	0.000	0.001	0.001	0.001	0.001	0.002	0.000	0.000	0.001	0.002
22	265	0.000	0.000	0.001	0.001	0.000	0.000	0.000	0.001	0.000	0.000	0.001	0.000
23	330	0.000	0.000	0.000	0.001	0.000	0.000	0.000	0.000	0.000	0.000	0.000	0.000
24	395	0.000	0.000	0.000	0.000	0.000	0.000	0.000	0.000	0.000	0.000	0.000	0.000
25	460	0.000	0.000	0.000	0.000	0.000	0.000	0.000	0.000	0.000	0.000	0.000	0.000
26	525	0.000	0.000	0.000	0.000	0.000	0.000	0.000	0.000	0.000	0.000	0.000	0.000
27	590	0.000	0.000	0.000	0.000	0.001	0.000	0.000	0.000	0.000	0.000	0.000	0.000
28	655	0.000	0.000	0.000	0.000	0.001	0.000	0.000	0.000	0.000	0.000	0.000	0.000
29	720	0.000	0.000	0.000	0.000	0.000	0.000	0.000	0.000	0.000	0.000	0.000	0.000
30	785	0.000	0.000	0.000	0.000	0.000	0.000	0.000	0.001	0.000	0.000	0.000	0.000

TABLE 36

V/AL2O3 VALUES FOR RUN 03, HONDO 5%, 780-710, TOP OF BED

Point	Position	Pellet One				Pellet two				Pellet three			
		Trav. 1	Trav. 2	Trav. 3	Trav. 4	Trav. 1	Trav. 2	Trav. 3	Trav. 4	Trav. 1	Trav. 2	Trav. 3	Trav. 4
1	0	0.205	0.169	0.217	0.184	0.103	0.150	0.128	0.161	0.166	0.192	0.225	0.151
2	5	0.211	0.172	0.230	0.205	0.128	0.184	0.150	0.154	0.190	0.188	0.213	0.176
3	10	0.221	0.192	0.243	0.218	0.141	0.141	0.156	0.219	0.215	0.208	0.207	0.200
4	15	0.247	0.212	0.243	0.212	0.136	0.135	0.170	0.165	0.221	0.226	0.199	0.174
5	20	0.232	0.183	0.235	0.203	0.127	0.114	0.139	0.143	0.193	0.198	0.154	0.149
6	25	0.219	0.160	0.217	0.167	0.126	0.113	0.120	0.133	0.197	0.160	0.132	0.130
7	30	0.181	0.147	0.151	0.147	0.108	0.099	0.113	0.125	0.120	0.112	0.098	0.095
8	35	0.165	0.138	0.157	0.125	0.107	0.084	0.109	0.109	0.103	0.091	0.080	0.081
9	40	0.131	0.109	0.105	0.096	0.125	0.076	0.077	0.102	0.069	0.072	0.058	0.053
10	45	0.111	0.098	0.109	0.087	0.070	0.056	0.057	0.095	0.056	0.056	0.051	0.047
11	50	0.093	0.076	0.085	0.064	0.051	0.052	0.046	0.069	0.045	0.040	0.038	0.039
12	65	0.053	0.049	0.051	0.032	0.022	0.028	0.025	0.034	0.022	0.023	0.023	0.016
13	80	0.025	0.031	0.026	0.016	0.010	0.014	0.014	0.012	0.011	0.009	0.010	0.008
14	95	0.017	0.021	0.015	0.009	0.006	0.008	0.007	0.008	0.006	0.006	0.006	0.005
15	110	0.010	0.014	0.009	0.006	0.004	0.006	0.005	0.005	0.003	0.004	0.003	0.003
16	125	0.006	0.010	0.006	0.004	0.003	0.004	0.004	0.003	0.002	0.002	0.003	0.002
17	140	0.004	0.007	0.004	0.003	0.002	0.003	0.003	0.002	0.001	0.002	0.001	0.001
18	155	0.002	0.005	0.003	0.002	0.001	0.002	0.002	0.002	0.001	0.001	0.001	0.001
19	170	0.002	0.004	0.002	0.002	0.001	0.002	0.002	0.001	0.001	0.001	0.001	0.000
20	185	0.001	0.003	0.002	0.001	0.001	0.001	0.001	0.001	0.001	0.001	0.001	0.001
21	200	0.001	0.002	0.001	0.001	0.000	0.001	0.001	0.001	0.000	0.001	0.000	0.000
22	265	0.000	0.001	0.000	0.001	0.000	0.001	0.001	0.001	0.000	0.000	0.000	0.000
23	330	0.000	0.000	0.000	0.001	0.000	0.001	0.000	0.001	0.000	0.000	0.000	0.000
24	395	0.000	0.000	0.000	0.000	0.000	0.001	0.000	0.001	0.000	0.000	0.000	0.000
25	460	0.000	0.000	0.000	0.000	0.000	0.001	0.000	0.000	0.000	0.000	0.000	0.000
26	525	0.000	0.000	0.000	0.000	0.000	0.001	0.000	0.000	0.000	0.000	0.000	0.000
27	590	0.000	0.000	0.000	0.001	0.000	0.000	0.000	0.000	0.000	0.000	0.000	0.000
28	655	0.000	0.000	0.000	0.000	0.000	0.001	0.000	0.000	0.000	0.000	0.000	0.000
29	720	0.000	0.000	0.000	0.000	0.000	0.000	0.000	0.000	0.000	0.000	0.000	0.000
30	785	0.000	0.000	0.000	0.000	0.000	0.001	0.000	0.000	0.000	0.001	0.000	0.000

TABLE 37

V/AL2O3 VALUES FOR RUN 03, HONDO 5%,760-710, BOTTOM OF BED

Point	Position	Pellet One				Pellet two				Pellet three			
		Trav. 1	Trav. 2	Trav. 3	Trav. 4	Trav. 1	Trav. 2	Trav. 3	Trav. 4	Trav. 1	Trav. 2	Trav. 3	Trav. 4
1	0	0.168	0.317	0.214	0.209	0.583	0.603	0.600	0.279	0.536	0.577	0.507	0.674
2	5	0.159	0.366	0.232	0.228	0.659	0.635	0.562	0.354	0.482	0.561	0.541	0.633
3	10	0.179	0.312	0.214	0.287	0.550	0.607	0.551	0.380	0.536	0.570	0.534	0.647
4	15	0.181	0.283	0.247	0.297	0.506	0.564	0.516	0.347	0.562	0.596	0.550	0.613
5	20	0.146	0.255	0.232	0.261	0.390	0.508	0.500	0.306	0.590	0.523	0.467	0.469
6	25	0.124	0.292	0.191	0.201	0.277	0.400	0.475	0.217	0.525	0.442	0.435	0.433
7	30	0.099	0.201	0.165	0.161	0.283	0.338	0.353	0.174	0.492	0.381	0.347	0.317
8	35	0.073	0.161	0.131	0.127	0.223	0.331	0.270	0.129	0.459	0.339	0.306	0.247
9	40	0.058	0.088	0.116	0.092	0.202	0.241	0.221	0.117	0.319	0.283	0.276	0.202
10	45	0.048	0.089	0.063	0.076	0.181	0.215	0.168	0.085	0.270	0.226	0.211	0.160
11	50	0.041	0.056	0.063	0.056	0.138	0.170	0.132	0.085	0.218	0.183	0.175	0.123
12	85	0.022	0.028	0.026	0.026	0.096	0.089	0.070	0.038	0.122	0.103	0.096	0.070
13	80	0.010	0.014	0.013	0.013	0.043	0.048	0.034	0.017	0.070	0.059	0.057	0.041
14	95	0.005	0.008	0.006	0.007	0.028	0.029	0.017	0.008	0.039	0.032	0.033	0.016
15	110	0.002	0.004	0.003	0.003	0.017	0.016	0.008	0.004	0.019	0.018	0.019	0.010
16	125	0.002	0.003	0.002	0.002	0.008	0.008	0.005	0.002	0.012	0.010	0.013	0.008
17	140	0.001	0.002	0.001	0.001	0.005	0.005	0.002	0.002	0.008	0.008	0.007	0.003
18	155	0.001	0.001	0.001	0.001	0.003	0.003	0.002	0.000	0.005	0.003	0.004	0.002
19	170	0.001	0.001	0.001	0.001	0.002	0.002	0.001	0.001	0.003	0.002	0.003	0.001
20	185	0.001	0.001	0.000	0.000	0.001	0.001	0.001	0.001	0.002	0.001	0.002	0.001
21	200	0.000	0.001	0.001	0.000	0.001	0.001	0.001	0.000	0.001	0.001	0.001	0.000
22	265	0.000	0.001	0.001	0.000	0.000	0.000	0.001	0.000	0.001	0.000	0.001	0.000
23	330	0.000	0.001	0.000	0.000	0.000	0.000	0.000	0.000	0.000	0.000	0.000	0.000
24	395	0.000	0.000	0.000	0.000	0.000	0.000	0.000	0.000	0.000	0.000	0.000	0.000
25	460	0.000	0.000	0.000	0.000	0.000	0.000	0.000	0.000	0.000	0.000	0.000	0.000
26	525	0.000	0.000	0.000	0.000	0.000	0.000	0.000	0.000	0.000	0.000	0.000	0.000
27	590	0.000	0.000	0.000	0.000	0.000	0.000	0.000	0.000	0.000	0.000	0.000	0.000
28	655	0.000	0.001	0.000	0.000	0.000	0.000	0.000	0.000	0.000	0.000	0.000	0.000
29	720	0.000	0.001	0.000	0.000	0.000	0.000	0.000	0.000	0.000	0.000	0.000	0.000
30	785	0.000	0.000	0.000	0.000	0.000	0.000	0.000	0.000	0.000	0.000	0.000	0.000

TABLE 38

V/AL2O3 VALUES FOR RUN 04, HONDO 5%,710-710, TOP OF BED

Point	Position	Pellet One				Pellet two				Pellet three			
		Trav. 1	Trav. 2	Trav. 3	Trav. 4	Trav. 1	Trav. 2	Trav. 3	Trav. 4	Trav. 1	Trav. 2	Trav. 3	Trav. 4
1	0	0.470	0.433	0.468	0.361	0.496	0.662	0.509	0.258	0.491	0.537	0.643	0.570
2	5	0.471	0.435	0.442	0.322	0.543	0.677	0.588	0.275	0.492	0.611	0.693	0.562
3	10	0.544	0.485	0.396	0.360	0.564	0.576	0.641	0.304	0.659	0.620	0.618	0.637
4	15	0.511	0.465	0.322	0.404	0.513	0.477	0.685	0.321	0.646	0.606	0.542	0.545
5	20	0.396	0.346	0.260	0.320	0.398	0.368	0.613	0.358	0.649	0.450	0.392	0.505
6	25	0.315	0.310	0.209	0.253	0.318	0.316	0.519	0.394	0.463	0.354	0.353	0.468
7	30	0.287	0.376	0.150	0.212	0.229	0.248	0.347	0.407	0.354	0.272	0.245	0.314
8	35	0.216	0.311	0.116	0.171	0.190	0.204	0.265	0.388	0.279	0.226	0.197	0.277
9	40	0.170	0.217	0.095	0.140	0.151	0.164	0.193	0.377	0.214	0.181	0.147	0.213
10	45	0.134	0.162	0.069	0.112	0.133	0.121	0.177	0.347	0.196	0.148	0.119	0.188
11	50	0.108	0.143	0.064	0.097	0.094	0.111	0.135	0.293	0.186	0.112	0.097	0.166
12	65	0.066	0.062	0.034	0.052	0.057	0.073	0.084	0.185	0.093	0.069	0.054	0.092
13	60	0.040	0.034	0.022	0.040	0.030	0.045	0.049	0.098	0.057	0.040	0.026	0.056
14	95	0.025	0.017	0.010	0.033	0.015	0.028	0.029	0.057	0.028	0.022	0.015	0.032
15	110	0.013	0.010	0.006	0.017	0.009	0.015	0.016	0.030	0.016	0.011	0.007	0.019
16	125	0.007	0.004	0.003	0.010	0.008	0.009	0.009	0.018	0.009	0.006	0.004	0.010
17	140	0.004	0.003	0.002	0.006	0.003	0.005	0.005	0.009	0.005	0.003	0.002	0.006
18	155	0.003	0.002	0.001	0.004	0.003	0.004	0.003	0.005	0.002	0.002	0.001	0.003
19	170	0.001	0.001	0.001	0.003	0.002	0.002	0.002	0.003	0.001	0.001	0.000	0.002
20	185	0.001	0.001	0.000	0.002	0.001	0.002	0.002	0.002	0.001	0.001	0.000	0.001
21	200	0.001	0.001	0.000	0.002	0.001	0.001	0.001	0.001	0.000	0.001	0.000	0.001
22	265	0.000	0.000	0.000	0.001	0.000	0.000	0.000	0.000	0.000	0.000	0.000	0.000
23	330	0.000	0.000	0.000	0.001	0.000	0.000	0.000	0.000	0.000	0.000	0.000	0.000
24	395	0.000	0.000	0.000	0.000	0.000	0.000	0.000	0.001	0.000	0.000	0.000	0.000
25	460	0.000	0.000	0.000	0.000	0.000	0.000	0.000	0.001	0.000	0.000	0.000	0.000
26	525	0.000	0.000	0.000	0.000	0.000	0.000	0.000	0.000	0.000	0.000	0.000	0.000
27	590	0.000	0.000	0.000	0.000	0.000	0.000	0.000	0.000	0.000	0.000	0.000	0.000
28	655	0.000	0.000	0.000	0.001	0.000	0.000	0.000	0.000	0.000	0.000	0.000	0.000
29	720	0.000	0.000	0.000	0.001	0.000	0.000	0.000	0.000	0.000	0.000	0.000	0.000
30	785	0.000	0.000	0.000	0.000	0.000	0.000	0.000	0.000	0.000	0.000	0.000	0.000

TABLE 39

V/L2O3 VALUES FOR RUN 04, HONDO 5%,710-710, BOTTOM OF BED

Point	Position	Pellet One				Pellet two				Pellet three			
		Trav. 1	Trav. 2	Trav. 3	Trav. 4	Trav. 1	Trav. 2	Trav. 3	Trav. 4	Trav. 1	Trav. 2	Trav. 3	Trav. 4
1	0	0.138	0.163	0.185	0.201	0.229	0.145	0.167	0.204	0.168	0.164	0.158	0.227
2	5	0.150	0.200	0.190	0.228	0.236	0.159	0.188	0.169	0.223	0.196	0.178	0.244
3	10	0.178	0.206	0.221	0.212	0.211	0.168	0.192	0.199	0.209	0.209	0.207	0.233
4	15	0.162	0.181	0.211	0.188	0.191	0.191	0.155	0.189	0.189	0.195	0.213	0.220
5	20	0.136	0.154	0.185	0.145	0.136	0.200	0.128	0.174	0.160	0.156	0.218	0.178
6	25	0.120	0.132	0.162	0.134	0.134	0.157	0.100	0.131	0.114	0.127	0.180	0.148
7	30	0.093	0.109	0.135	0.103	0.121	0.122	0.078	0.120	0.092	0.100	0.140	0.098
8	35	0.078	0.089	0.116	0.084	0.088	0.101	0.065	0.105	0.069	0.087	0.119	0.077
9	40	0.060	0.067	0.088	0.067	0.074	0.078	0.051	0.091	0.056	0.068	0.098	0.063
10	45	0.048	0.058	0.075	0.055	0.060	0.067	0.043	0.076	0.045	0.068	0.078	0.051
11	50	0.041	0.046	0.060	0.043	0.050	0.047	0.036	0.065	0.035	0.051	0.062	0.039
12	65	0.021	0.021	0.031	0.015	0.028	0.020	0.018	0.043	0.021	0.027	0.041	0.020
13	80	0.009	0.014	0.017	0.009	0.014	0.009	0.007	0.028	0.009	0.013	0.021	0.010
14	95	0.005	0.007	0.009	0.005	0.009	0.004	0.004	0.017	0.005	0.007	0.011	0.005
15	110	0.003	0.003	0.005	0.003	0.007	0.002	0.002	0.010	0.002	0.004	0.006	0.003
16	125	0.002	0.002	0.002	0.001	0.003	0.001	0.001	0.007	0.002	0.002	0.004	0.002
17	140	0.001	0.001	0.002	0.001	0.002	0.001	0.001	0.004	0.001	0.001	0.002	0.001
18	155	0.000	0.001	0.001	0.000	0.001	0.000	0.000	0.002	0.001	0.001	0.001	0.001
19	170	0.001	0.001	0.001	0.001	0.001	0.000	0.000	0.002	0.001	0.001	0.001	0.001
20	185	0.000	0.001	0.000	0.000	0.001	0.000	0.000	0.001	0.000	0.000	0.000	0.001
21	200	0.000	0.000	0.000	0.000	0.000	0.000	0.000	0.001	0.000	0.000	0.000	0.000
22	265	0.000	0.000	0.000	0.000	0.000	0.000	0.000	0.000	0.000	0.000	0.000	0.000
23	330	0.000	0.000	0.000	0.000	0.000	0.000	0.000	0.000	0.000	0.000	0.000	0.000
24	395	0.000	0.000	0.000	0.000	0.000	0.000	0.000	0.000	0.000	0.000	0.000	0.000
25	460	0.000	0.000	0.000	0.000	0.000	0.000	0.000	0.000	0.000	0.000	0.000	0.000
26	525	0.000	0.000	0.000	0.000	0.000	0.000	0.000	0.000	0.000	0.000	0.000	0.000
27	590	0.000	0.000	0.000	0.000	0.000	0.000	0.000	0.000	0.000	0.000	0.000	0.000
28	655	0.000	0.000	0.000	0.000	0.000	0.000	0.000	0.000	0.000	0.000	0.000	0.000
29	720	0.000	0.000	0.000	0.000	0.000	0.000	0.000	0.000	0.000	0.000	0.000	0.000
30	785	0.000	0.000	0.000	0.000	0.000	0.000	0.000	0.000	0.000	0.000	0.000	0.000

TABLE 40

V/AL2O3 VALUES FOR RUN 06, ORIENTE 5%,760-710, TOP OF BED

Point	Position	Pellet One				Pellet two				Pellet three			
		Trav. 1	Trav. 2	Trav. 3	Trav. 4	Trav. 1	Trav. 2	Trav. 3	Trav. 4	Trav. 1	Trav. 2	Trav. 3	Trav. 4
1	0	0.383	0.320	0.465	0.476	0.146	0.281	0.357	0.478	0.421	0.320	0.433	0.366
2	5	0.525	0.388	0.516	0.522	0.191	0.321	0.443	0.534	0.440	0.491	0.575	0.505
3	10	0.427	0.514	0.407	0.427	0.155	0.271	0.361	0.375	0.402	0.504	0.362	0.377
4	15	0.323	0.404	0.323	0.297	0.148	0.265	0.301	0.274	0.296	0.348	0.277	0.358
5	20	0.262	0.303	0.219	0.233	0.122	0.258	0.236	0.156	0.268	0.238	1.320	0.348
6	25	0.220	0.237	0.158	0.206	0.105	0.443	0.170	0.164	0.251	0.186	0.207	0.241
7	30	0.167	0.168	0.115	0.155	0.088	0.378	0.118	0.136	0.154	0.150	0.158	0.192
8	35	0.141	0.126	0.088	0.123	0.086	0.187	0.114	0.111	0.114	0.115	0.138	0.162
9	40	0.105	0.106	0.085	0.103	0.071	0.135	0.086	0.086	0.094	0.094	0.106	0.112
10	45	0.085	0.085	0.072	0.075	0.084	0.110	0.070	0.080	0.076	0.083	0.093	0.095
11	50	0.079	0.069	0.056	0.063	0.066	0.090	0.056	0.064	0.064	0.067	0.077	0.080
12	65	0.013	0.046	0.038	0.042	0.041	0.054	0.035	0.045	0.041	0.038	0.058	0.045
13	60	0.039	0.029	0.025	0.026	0.026	0.033	0.024	0.026	0.027	0.024	0.036	0.031
14	95	0.025	0.017	0.016	0.015	0.020	0.021	0.014	0.016	0.018	0.015	0.022	0.021
15	110	0.016	0.012	0.009	0.009	0.013	0.015	0.010	0.012	0.010	0.009	0.016	0.012
16	125	0.011	0.007	0.007	0.008	0.008	0.011	0.005	0.006	0.007	0.007	0.009	0.009
17	140	0.008	0.005	0.004	0.004	0.006	0.008	0.004	0.004	0.004	0.005	0.007	0.005
18	155	0.005	0.004	0.003	0.002	0.003	0.006	0.003	0.003	0.004	0.003	0.004	0.004
19	170	0.004	0.003	0.002	0.003	0.003	0.003	0.002	0.002	0.002	0.003	0.003	0.004
20	185	0.003	0.002	0.001	0.002	0.002	0.003	0.002	0.002	0.002	0.002	0.002	0.002
21	200	0.002	0.002	0.000	0.001	0.002	0.002	0.001	0.001	0.002	0.002	0.002	0.002
22	265	0.001	0.000	0.001	0.001	0.001	0.001	0.000	0.000	0.001	0.001	0.000	0.001
23	330	0.000	0.000	0.000	0.000	0.001	0.001	0.000	0.000	0.000	0.001	0.000	0.000
24	395	0.000	0.000	0.000	0.000	0.001	0.001	0.000	0.000	0.000	0.001	0.000	0.001
25	460	0.000	0.000	0.000	0.000	0.001	0.000	0.000	0.000	0.000	0.001	0.000	0.000
26	525	0.000	0.000	0.000	0.000	0.001	0.000	0.000	0.000	0.000	0.001	0.000	0.000
27	590	0.000	0.000	0.000	0.000	0.000	0.000	0.000	0.000	0.001	0.001	0.000	0.000
28	655	0.000	0.000	0.000	0.000	0.000	0.000	0.000	0.000	0.000	0.000	0.000	0.000
29	720	0.000	0.000	0.000	0.000	0.000	0.000	0.000	0.000	0.000	0.001	0.000	0.000
30	785	0.000	0.000	0.000	0.000	0.000	0.000	0.000	0.000	0.000	0.000	0.000	0.000

TABLE 41

V/L203 VALUES FOR RUN 06, ORIENTE 5%,760-710, BOTTOM OF BED

Point	Position	Pellet One				Pellet two				Pellet three			
		Trav. 1	Trav. 2	Trav. 3	Trav. 4	Trav. 1	Trav. 2	Trav. 3	Trav. 4	Trav. 1	Trav. 2	Trav. 3	Trav. 4
1	0	0.590	0.559	0.560	0.443	0.506	0.403	0.280	0.421	0.666	0.685	0.277	0.604
2	5	0.623	0.532	0.576	0.443	0.547	0.478	0.370	0.418	0.773	0.472	0.325	0.469
3	10	0.539	0.366	0.477	0.375	0.458	0.459	0.583	0.348	0.541	0.380	0.304	0.424
4	15	0.412	0.274	0.391	0.315	0.336	0.303	0.431	0.264	0.384	0.289	0.444	0.275
5	20	0.295	0.203	0.280	0.285	0.269	0.240	0.302	0.214	0.268	0.206	0.416	0.218
6	25	0.209	0.172	0.237	0.259	0.209	0.225	0.233	0.170	0.214	0.158	0.426	0.174
7	30	0.162	0.151	0.188	0.229	0.156	0.177	0.213	0.135	0.167	0.124	0.375	0.139
8	35	0.117	0.125	0.167	0.222	0.136	0.148	0.171	0.119	0.145	0.101	0.298	0.118
9	40	0.104	0.102	0.137	0.212	0.109	0.129	0.127	0.099	0.094	0.089	0.241	0.099
10	45	0.074	0.083	0.136	0.199	0.088	0.109	0.114	0.084	0.097	0.067	0.211	0.085
11	50	0.062	0.066	0.108	0.193	0.075	0.085	0.095	0.065	0.071	0.054	0.170	0.070
12	65	0.032	0.035	0.087	0.166	0.040	0.051	0.057	0.038	0.046	0.028	0.095	0.039
13	80	0.019	0.025	0.070	0.129	0.025	0.030	0.035	0.024	0.028	0.016	0.049	0.024
14	95	0.012	0.013	0.053	0.109	0.015	0.018	0.024	0.015	0.019	0.010	0.024	0.015
15	110	0.008	0.008	0.042	0.081	0.009	0.012	0.014	0.009	0.011	0.006	0.015	0.009
16	125	0.003	0.005	0.035	0.061	0.005	0.007	0.009	0.006	0.007	0.004	0.009	0.006
17	140	0.002	0.003	0.028	0.041	0.004	0.005	0.006	0.004	0.005	0.002	0.005	0.004
18	155	0.001	0.002	0.025	0.019	0.002	0.002	0.004	0.003	0.003	0.002	0.003	0.002
19	170	0.001	0.001	0.018	0.008	0.002	0.001	0.003	0.001	0.002	0.002	0.002	0.001
20	185	0.000	0.001	0.014	0.003	0.001	0.001	0.002	0.002	0.002	0.001	0.002	0.001
21	200	0.000	0.000	0.011	0.002	0.001	0.001	0.001	0.001	0.001	0.001	0.001	0.001
22	265	0.000	0.000	0.002	0.000	0.000	0.000	0.000	0.000	0.000	0.000	0.000	0.000
23	330	0.000	0.000	0.000	0.000	0.000	0.000	0.000	0.000	0.000	0.000	0.000	0.000
24	395	0.000	0.000	0.000	0.000	0.000	0.000	0.000	0.000	0.000	0.000	0.000	0.000
25	460	0.000	0.000	0.000	0.000	0.000	0.000	0.000	0.000	0.000	0.000	0.000	0.000
26	525	0.000	0.000	0.000	0.000	0.000	0.000	0.000	0.000	0.000	0.000	0.000	0.000
27	590	0.000	0.000	0.000	0.000	0.000	0.000	0.000	0.000	0.000	0.000	0.000	0.000
28	655	0.000	0.000	0.000	0.000	0.000	0.000	0.000	0.000	0.000	0.000	0.000	0.000
29	720	0.000	0.000	0.000	0.000	0.000	0.000	0.000	0.000	0.000	0.000	0.000	0.000
30	785	0.000	0.000	0.000	0.000	0.000	0.000	0.000	0.000	0.000	0.000	0.000	0.000

TABLE 42

V/AL2O3 VALUES FOR RUN 07, ORIENTE 5%,710-710, TOP OF BED

Point	Position	Pellet One				Pellet two				Pellet three			
		Trav. 1	Trav. 2	Trav. 3	Trav. 4	Trav. 1	Trav. 2	Trav. 3	Trav. 4	Trav. 1	Trav. 2	Trav. 3	Trav. 4
1	0	0.240	0.194	0.246	0.271	0.391	0.396	0.564	0.425	0.276	0.168	0.243	0.175
2	5	0.178	0.216	0.246	0.227	0.479	0.483	0.625	0.539	0.245	0.192	0.290	0.216
3	10	0.139	0.242	0.211	0.192	0.496	0.441	0.638	0.544	0.172	0.172	0.186	0.174
4	15	0.097	0.201	0.156	0.196	0.463	0.371	0.565	0.485	0.142	0.148	0.149	0.142
5	20	0.076	0.149	0.126	0.176	0.366	0.314	0.363	0.404	0.109	0.141	0.120	0.115
6	25	0.069	0.109	0.103	0.179	0.282	0.244	0.323	0.367	0.092	0.138	0.107	0.100
7	30	0.056	0.091	0.084	0.224	0.209	0.185	0.246	0.270	0.067	0.122	0.080	0.075
8	35	0.045	0.075	0.069	0.215	0.176	0.154	0.222	0.245	0.056	0.100	0.062	0.067
9	40	0.041	0.059	0.065	0.158	0.150	0.130	0.173	0.189	0.046	0.078	0.050	0.052
10	45	0.035	0.055	0.052	0.136	0.132	0.109	0.133	0.164	0.039	0.067	0.041	0.045
11	50	0.019	0.033	0.030	0.105	0.119	0.101	0.118	0.135	0.034	0.068	0.037	0.038
12	65	0.011	0.020	0.018	0.065	0.074	0.062	0.075	0.044	0.019	0.035	0.022	0.022
13	80	0.007	0.010	0.013	0.034	0.048	0.040	0.049	0.038	0.012	0.020	0.013	0.014
14	95	0.005	0.007	0.008	0.022	0.032	0.026	0.030	0.034	0.007	0.015	0.008	0.008
15	110	0.003	0.004	0.004	0.014	0.021	0.019	0.022	0.033	0.005	0.008	0.005	0.006
16	125	0.002	0.003	0.003	0.008	0.013	0.010	0.014	0.029	0.003	0.005	0.003	0.004
17	140	0.001	0.002	0.002	0.007	0.009	0.007	0.010	0.022	0.003	0.004	0.003	0.003
18	155	0.001	0.002	0.001	0.004	0.006	0.004	0.006	0.013	0.002	0.003	0.002	0.002
19	170	0.001	0.001	0.001	0.003	0.004	0.003	0.004	0.009	0.001	0.002	0.001	0.002
20	165	0.001	0.001	0.001	0.002	0.002	0.002	0.003	0.007	0.001	0.001	0.001	0.001
21	200	0.000	0.000	0.001	0.002	0.002	0.002	0.003	0.006	0.000	0.001	0.001	0.001
22	265	0.000	0.001	0.000	0.001	0.000	0.000	0.000	0.002	0.000	0.000	0.000	0.000
23	330	0.000	0.000	0.000	0.001	0.000	0.001	0.000	0.000	0.000	0.001	0.000	0.000
24	395	0.000	0.000	0.000	0.000	0.000	0.000	0.000	0.000	0.000	0.001	0.000	0.000
25	460	0.000	0.000	0.000	0.000	0.000	0.000	0.000	0.000	0.000	0.001	0.000	0.000
26	525	0.000	0.000	0.000	0.000	0.000	0.000	0.000	0.000	0.000	0.000	0.003	0.000
27	590	0.000	0.000	0.000	0.001	0.000	0.000	0.000	0.000	0.001	0.001	0.000	0.000
28	655	0.000	0.000	0.000	0.001	0.000	0.000	0.000	0.000	0.000	0.001	0.000	0.000
29	720	0.000	0.000	0.000	0.000	0.000	0.000	0.000	0.000	0.000	0.000	0.000	0.000
30	785	0.000	0.000	0.000	0.000	0.000	0.000	0.000	0.000	0.000	0.000	0.000	0.000

TABLE 43

VAL203 VALUES FOR RUN 07, ORIENTE 5%,710-710, BOTTOM OF BED

Point	Position	Pellet One				Pellet two				Pellet three			
		Trav. 1	Trav. 2	Trav. 3	Trav. 4	Trav. 1	Trav. 2	Trav. 3	Trav. 4	Trav. 1	Trav. 2	Trav. 3	Trav. 4
1	0	0.441	0.237	0.291	0.402	0.393	0.157	0.278	0.224	0.284	0.291	0.624	0.241
2	5	0.563	0.274	0.550	0.461	0.539	0.203	0.273	0.294	0.382	0.291	0.551	0.228
3	10	0.551	0.283	0.471	0.438	0.491	0.275	0.340	0.268	0.293	0.435	0.438	0.195
4	15	0.458	0.335	0.388	0.426	0.408	0.288	0.313	0.231	0.272	0.466	0.318	0.215
5	20	0.359	0.279	0.272	0.391	0.285	0.281	0.349	0.173	0.212	0.376	0.235	0.263
6	25	0.264	0.254	0.225	0.360	0.228	0.240	0.411	0.160	0.156	0.304	0.194	0.321
7	30	0.228	0.195	0.189	0.308	0.176	0.212	0.297	0.136	0.124	0.198	0.145	0.247
8	35	0.181	0.193	0.169	0.249	0.147	0.178	0.246	0.130	0.112	0.171	0.119	0.228
9	40	0.136	0.155	0.138	0.208	0.125	0.157	0.195	0.105	0.087	0.207	0.092	0.195
10	45	0.100	0.133	0.117	0.210	0.106	0.126	0.157	0.090	0.070	0.109	0.072	0.183
11	50	0.093	0.107	0.096	0.167	0.093	0.113	0.135	0.080	0.063	0.088	0.057	0.162
12	65	0.053	0.071	0.062	0.114	0.060	0.071	0.074	0.048	0.040	0.056	0.038	0.125
13	80	0.031	0.047	0.039	0.080	0.038	0.052	0.044	0.034	0.017	0.031	0.027	0.092
14	95	0.019	0.031	0.024	0.051	0.022	0.033	0.028	0.021	0.014	0.017	0.019	0.072
15	110	0.013	0.023	0.017	0.034	0.014	0.021	0.015	0.014	0.010	0.011	0.014	0.054
16	125	0.008	0.016	0.012	0.022	0.010	0.011	0.010	0.010	0.008	0.008	0.010	0.035
17	140	0.006	0.011	0.008	0.014	0.007	0.008	0.007	0.007	0.006	0.004	0.007	0.022
18	155	0.004	0.009	0.006	0.009	0.005	0.006	0.004	0.005	0.004	0.003	0.005	0.014
19	170	0.003	0.007	0.004	0.006	0.004	0.004	0.004	0.004	0.004	0.002	0.004	0.008
20	185	0.003	0.008	0.003	0.005	0.003	0.004	0.003	0.002	0.003	0.002	0.003	0.005
21	200	0.003	0.008	0.003	0.003	0.002	0.003	0.003	0.002	0.003	0.001	0.002	0.004
22	265	0.001	0.005	0.001	0.002	0.000	0.001	0.001	0.001	0.001	0.001	0.002	0.001
23	330	0.001	0.001	0.001	0.001	0.000	0.001	0.001	0.001	0.001	0.001	0.001	0.000
24	395	0.000	0.001	0.000	0.001	0.000	0.001	0.001	0.000	0.001	0.000	0.000	0.000
25	480	0.002	0.001	0.000	0.000	0.000	0.000	0.000	0.000	0.002	0.000	0.001	0.000
26	525	0.000	0.000	0.000	0.001	0.000	0.000	0.000	0.000	0.001	0.000	0.000	0.000
27	590	0.000	0.000	0.000	0.001	0.000	0.000	0.000	0.000	0.002	0.000	0.001	0.000
28	655	0.000	0.000	0.000	0.001	0.000	0.000	0.000	0.000	0.001	0.000	0.000	0.000
29	720	0.000	0.000	0.000	0.000	0.000	0.000	0.000	0.000	0.001	0.000	0.001	0.001
30	785	0.000	0.000	0.000	0.001	0.000	0.000	0.000	0.000	0.001	0.000	0.001	0.003

TABLE 44

V/L203 VALUES FOR RUN 09, CANO LIMON 5%,760-710, TOP OF BED

Point	Position	Pellet One				Pellet two				Pellet three			
		Trav. 1	Trav. 2	Trav. 3	Trav. 4	Trav. 1	Trav. 2	Trav. 3	Trav. 4	Trav. 1	Trav. 2	Trav. 3	Trav. 4
1	0	0.065	0.071	0.040	0.061	0.044	0.040	0.060	0.043	0.033	0.034	0.072	0.036
2	5	0.069	0.071	0.050	0.119	0.051	0.043	0.043	0.037	0.026	0.029	0.063	0.031
3	10	0.049	0.059	0.048	0.089	0.041	0.040	0.040	0.031	0.024	0.029	0.060	0.032
4	15	0.040	0.061	0.049	0.100	0.040	0.039	0.037	0.029	0.023	0.025	0.055	0.028
5	20	0.042	0.054	0.042	0.089	0.028	0.032	0.031	0.026	0.020	0.020	0.061	0.024
6	25	0.036	0.048	0.040	0.098	0.033	0.032	0.029	0.022	0.015	0.015	0.029	0.017
7	30	0.034	0.037	0.038	0.084	0.025	0.024	0.027	0.019	0.013	0.013	0.053	0.008
8	35	0.039	0.034	0.035	0.096	0.023	0.024	0.022	0.019	0.010	0.010	0.037	0.011
9	40	0.034	0.027	0.027	0.067	0.019	0.018	0.019	0.015	0.009	0.009	0.036	0.010
10	45	0.037	0.026	0.027	0.052	0.018	0.017	0.018	0.011	0.007	0.007	0.034	0.008
11	50	0.034	0.020	0.021	0.043	0.013	0.013	0.016	0.010	0.006	0.006	0.042	0.008
12	85	0.027	0.013	0.014	0.037	0.009	0.009	0.011	0.006	0.004	0.003	0.026	0.004
13	80	0.017	0.007	0.008	0.025	0.005	0.005	0.007	0.005	0.003	0.003	0.015	0.003
14	95	0.011	0.005	0.006	0.017	0.003	0.004	0.005	0.003	0.003	0.002	0.006	0.002
15	110	0.007	0.003	0.004	0.009	0.003	0.003	0.004	0.002	0.001	0.001	0.003	0.001
16	125	0.004	0.002	0.003	0.006	0.002	0.002	0.003	0.002	0.001	0.001	0.001	0.001
17	140	0.003	0.002	0.002	0.004	0.001	0.001	0.002	0.001	0.001	0.001	0.002	0.000
18	155	0.002	0.002	0.001	0.002	0.001	0.001	0.001	0.001	0.000	0.001	0.001	0.000
19	170	0.002	0.001	0.001	0.002	0.001	0.001	0.001	0.001	0.001	0.000	0.001	0.000
20	185	0.001	0.001	0.001	0.001	0.000	0.001	0.001	0.001	0.000	0.000	0.000	0.000
21	200	0.001	0.001	0.000	0.001	0.000	0.000	0.001	0.001	0.000	0.000	0.001	0.000
22	285	0.000	0.000	0.000	0.001	0.000	0.000	0.000	0.000	0.000	0.000	0.000	0.000
23	330	0.000	0.000	0.000	0.000	0.000	0.000	0.000	0.000	0.000	0.000	0.000	0.000
24	395	0.000	0.000	0.000	0.000	0.000	0.000	0.000	0.000	0.000	0.000	0.000	0.000
25	460	0.000	0.000	0.000	0.000	0.000	0.000	0.000	0.000	0.000	0.000	0.000	0.000
26	525	0.000	0.000	0.000	0.000	0.000	0.000	0.000	0.000	0.000	0.000	0.000	0.000
27	590	0.000	0.000	0.000	0.000	0.000	0.000	0.000	0.000	0.000	0.000	0.000	0.000
28	855	0.000	0.000	0.000	0.001	0.000	0.000	0.000	0.000	0.000	0.000	0.000	0.000
29	720	0.000	0.000	0.000	0.000	0.000	0.000	0.000	0.000	0.000	0.000	0.000	0.000
30	785	0.000	0.000	0.000	0.000	0.000	0.000	0.000	0.000	0.000	0.000	0.000	0.000

TABLE 45

WAL203 VALUES FOR RUN 09, CANO LIMON 5%,760-710, BOTTOM OF BED

Point	Position	Pellet One				Pellet two				Pellet three			
		Trav. 1	Trav. 2	Trav. 3	Trav. 4	Trav. 1	Trav. 2	Trav. 3	Trav. 4	Trav. 1	Trav. 2	Trav. 3	Trav. 4
1	0	0.102	0.110	0.104	0.096	0.097	0.106	0.141	0.118	0.082	0.074	0.146	0.092
2	5	0.102	0.105	0.109	0.117	0.105	0.114	0.165	0.126	0.100	0.074	0.081	0.097
3	10	0.115	0.094	0.104	0.101	0.110	0.096	0.164	0.135	0.094	0.071	0.076	0.097
4	15	0.106	0.079	0.094	0.096	0.131	0.107	0.107	0.136	0.104	0.071	0.086	0.088
5	20	0.106	0.082	0.080	0.073	0.135	0.118	0.073	0.137	0.089	0.063	0.081	0.086
6	25	0.100	0.075	0.068	0.064	0.124	0.129	0.063	0.133	0.088	0.056	0.079	0.079
7	30	0.079	0.059	0.054	0.053	0.128	0.136	0.055	0.122	0.083	0.048	0.073	0.065
8	35	0.069	0.060	0.043	0.044	0.111	0.134	0.072	0.117	0.068	0.041	0.065	0.064
9	40	0.058	0.052	0.038	0.031	0.101	0.129	0.078	0.093	0.063	0.034	0.049	0.045
10	45	0.044	0.040	0.033	0.027	0.088	0.121	0.083	0.080	0.053	0.031	0.045	0.038
11	50	0.036	0.034	0.024	0.021	0.076	0.097	0.069	0.070	0.048	0.024	0.035	0.029
12	65	0.023	0.023	0.013	0.014	0.051	0.073	0.046	0.043	0.031	0.015	0.020	0.018
13	80	0.012	0.018	0.007	0.007	0.028	0.041	0.026	0.027	0.017	0.008	0.013	0.010
14	95	0.007	0.008	0.004	0.004	0.018	0.026	0.017	0.016	0.011	0.005	0.008	0.006
15	110	0.005	0.005	0.003	0.002	0.011	0.017	0.009	0.010	0.007	0.003	0.005	0.003
16	125	0.003	0.003	0.002	0.001	0.008	0.010	0.006	0.007	0.004	0.003	0.004	0.002
17	140	0.002	0.002	0.001	0.001	0.005	0.006	0.004	0.004	0.003	0.001	0.002	0.002
18	155	0.001	0.002	0.000	0.001	0.004	0.004	0.003	0.003	0.002	0.001	0.001	0.001
19	170	0.001	0.001	0.000	0.000	0.002	0.003	0.002	0.002	0.001	0.001	0.001	0.001
20	185	0.001	0.001	0.000	0.001	0.002	0.002	0.001	0.002	0.001	0.000	0.001	0.000
21	200	0.000	0.001	0.000	0.000	0.001	0.001	0.001	0.001	0.000	0.000	0.000	0.000
22	265	0.000	0.000	0.000	0.000	0.000	0.001	0.001	0.000	0.000	0.000	0.000	0.000
23	330	0.000	0.000	0.000	0.000	0.000	0.000	0.000	0.000	0.000	0.000	0.000	0.000
24	395	0.000	0.000	0.000	0.000	0.000	0.000	0.000	0.000	0.000	0.000	0.000	0.000
25	460	0.000	0.000	0.000	0.000	0.000	0.000	0.000	0.000	0.000	0.000	0.000	0.000
26	525	0.000	0.000	0.000	0.000	0.000	0.000	0.000	0.000	0.000	0.000	0.000	0.000
27	590	0.000	0.000	0.000	0.000	0.000	0.000	0.000	0.000	0.000	0.000	0.000	0.000
28	655	0.000	0.000	0.000	0.000	0.000	0.000	0.000	0.000	0.000	0.000	0.000	0.000
29	720	0.000	0.000	0.000	0.000	0.000	0.000	0.000	0.000	0.000	0.000	0.000	0.000
30	785	0.000	0.000	0.000	0.000	0.000	0.000	0.000	0.000	0.000	0.000	0.000	0.000

TABLE 46

V/L2O3 VALUES FOR RUN 10, CANO LIMON 5%,710-710, TOP OF BED

Point	Position	Pellet One				Pellet two				Pellet three			
		Trav. 1	Trav. 2	Trav. 3	Trav. 4	Trav. 1	Trav. 2	Trav. 3	Trav. 4	Trav. 1	Trav. 2	Trav. 3	Trav. 4
1	0	0.124	0.114	0.117	0.117	0.054	0.063	0.065	0.073	0.118	0.138	0.124	0.121
2	5	0.101	0.121	0.163	0.129	0.066	0.079	0.057	0.071	0.129	0.165	0.113	0.133
3	10	0.109	0.123	0.133	0.130	0.057	0.068	0.055	0.063	0.143	0.140	0.118	0.150
4	15	0.113	0.128	0.104	0.120	0.058	0.062	0.053	0.057	0.144	0.135	0.132	0.128
5	20	0.112	0.119	0.102	0.116	0.049	0.049	0.047	0.049	0.130	0.113	0.121	0.126
6	25	0.118	0.106	0.104	0.101	0.045	0.044	0.045	0.042	0.136	0.104	0.117	0.118
7	30	0.105	0.098	0.094	0.075	0.037	0.034	0.037	0.032	0.093	0.085	0.107	0.100
8	35	0.085	0.088	0.083	0.062	0.029	0.030	0.033	0.025	0.114	0.085	0.099	0.090
9	40	0.076	0.080	0.065	0.054	0.026	0.025	0.026	0.020	0.093	0.084	0.083	0.081
10	45	0.059	0.065	0.064	0.041	0.020	0.019	0.024	0.017	0.092	0.057	0.077	0.068
11	50	0.053	0.059	0.054	0.040	0.018	0.014	0.019	0.013	0.074	0.049	0.062	0.062
12	65	0.027	0.033	0.026	0.022	0.010	0.009	0.013	0.007	0.043	0.028	0.046	0.037
13	80	0.016	0.018	0.017	0.013	0.006	0.006	0.007	0.004	0.026	0.017	0.028	0.020
14	95	0.008	0.014	0.010	0.009	0.004	0.004	0.005	0.003	0.014	0.011	0.018	0.014
15	110	0.004	0.007	0.007	0.005	0.003	0.002	0.003	0.002	0.008	0.006	0.012	0.008
16	125	0.004	0.005	0.004	0.003	0.002	0.002	0.002	0.001	0.005	0.005	0.008	0.007
17	140	0.002	0.003	0.003	0.002	0.001	0.001	0.001	0.001	0.003	0.002	0.005	0.003
18	155	0.001	0.003	0.002	0.001	0.001	0.001	0.001	0.001	0.002	0.002	0.004	0.002
19	170	0.001	0.002	0.001	0.001	0.001	0.000	0.001	0.001	0.001	0.001	0.002	0.001
20	185	0.001	0.001	0.001	0.001	0.001	0.000	0.000	0.000	0.001	0.000	0.002	0.001
21	200	0.000	0.001	0.001	0.001	0.001	0.000	0.000	0.000	0.001	0.000	0.002	0.001
22	265	0.000	0.000	0.001	0.000	0.000	0.000	0.000	0.000	0.000	0.000	0.000	0.000
23	330	0.000	0.000	0.001	0.000	0.000	0.000	0.000	0.000	0.000	0.000	0.000	0.000
24	395	0.000	0.000	0.001	0.000	0.000	0.000	0.000	0.000	0.000	0.000	0.000	0.000
25	460	0.000	0.000	0.001	0.000	0.000	0.000	0.000	0.000	0.000	0.000	0.000	0.000
26	525	0.000	0.000	0.001	0.000	0.000	0.000	0.000	0.000	0.000	0.000	0.000	0.000
27	590	0.000	0.000	0.000	0.000	0.000	0.000	0.000	0.000	0.000	0.000	0.000	0.000
28	655	0.000	0.000	0.000	0.000	0.000	0.000	0.000	0.000	0.000	0.000	0.000	0.000
29	720	0.000	0.000	0.000	0.000	0.000	0.000	0.000	0.000	0.000	0.000	0.000	0.000
30	785	0.000	0.000	0.000	0.000	0.000	0.000	0.000	0.000	0.000	0.000	0.000	0.000

TABLE 47

VIAL203 VALUES FOR RUN 10, CANO LIMON 5%,710-710, BOTTOM OF BED

Point	Position	Pellet One				Pellet two				Pellet three			
		Trav. 1	Trav. 2	Trav. 3	Trav. 4	Trav. 1	Trav. 2	Trav. 3	Trav. 4	Trav. 1	Trav. 2	Trav. 3	Trav. 4
1	0	0.083	0.084	0.101	0.110	0.198	0.153	0.181	0.191	0.197	0.151	0.174	0.144
2	5	0.063	0.088	0.118	0.090	0.171	0.183	0.158	0.201	0.143	0.156	0.189	0.177
3	10	0.063	0.087	0.110	0.084	0.198	0.191	0.188	0.193	0.172	0.161	0.199	0.182
4	15	0.066	0.085	0.102	0.086	0.223	0.150	0.188	0.206	0.169	0.161	0.178	0.180
5	20	0.068	0.073	0.093	0.080	0.157	0.127	0.160	0.170	0.166	0.151	0.152	0.162
6	25	0.072	0.067	0.076	0.071	0.135	0.104	0.140	0.139	0.158	0.146	0.119	0.141
7	30	0.067	0.064	0.071	0.064	0.106	0.084	0.118	0.105	0.144	0.123	0.088	0.110
8	35	0.060	0.063	0.065	0.058	0.088	0.072	0.093	0.089	0.116	0.117	0.086	0.124
9	40	0.054	0.054	0.056	0.045	0.071	0.055	0.075	0.065	0.102	0.105	0.076	0.100
10	45	0.048	0.047	0.050	0.042	0.058	0.044	0.084	0.056	0.086	0.091	0.072	0.089
11	50	0.043	0.040	0.039	0.033	0.049	0.037	0.067	0.038	0.079	0.081	0.059	0.082
12	65	0.029	0.027	0.024	0.021	0.027	0.020	0.039	0.026	0.046	0.054	0.032	0.046
13	80	0.019	0.017	0.014	0.015	0.016	0.011	0.021	0.015	0.027	0.034	0.019	0.026
14	95	0.012	0.011	0.010	0.009	0.011	0.007	0.016	0.007	0.017	0.020	0.012	0.016
15	110	0.008	0.007	0.006	0.006	0.006	0.004	0.007	0.004	0.010	0.013	0.007	0.009
16	125	0.005	0.006	0.004	0.003	0.004	0.003	0.006	0.003	0.006	0.006	0.004	0.006
17	140	0.004	0.003	0.002	0.003	0.002	0.002	0.003	0.001	0.004	0.004	0.003	0.003
18	155	0.003	0.002	0.002	0.002	0.002	0.001	0.003	0.001	0.003	0.003	0.002	0.002
19	170	0.002	0.002	0.001	0.001	0.001	0.000	0.002	0.000	0.002	0.002	0.001	0.001
20	185	0.001	0.001	0.001	0.001	0.001	0.001	0.002	0.000	0.002	0.001	0.001	0.000
21	200	0.001	0.001	0.000	0.001	0.000	0.001	0.001	0.000	0.001	0.001	0.000	0.000
22	285	0.000	0.000	0.000	0.000	0.000	0.000	0.001	0.000	0.000	0.000	0.000	0.000
23	330	0.000	0.000	0.000	0.000	0.000	0.000	0.000	0.000	0.000	0.000	0.000	0.000
24	395	0.000	0.000	0.000	0.000	0.000	0.000	0.001	0.000	0.000	0.000	0.000	0.000
25	460	0.000	0.000	0.000	0.000	0.000	0.000	0.000	0.000	0.000	0.000	0.000	0.000
26	525	0.000	0.000	0.000	0.000	0.000	0.000	0.000	0.000	0.000	0.000	0.000	0.000
27	590	0.000	0.000	0.000	0.000	0.000	0.000	0.000	0.000	0.000	0.000	0.000	0.000
28	655	0.000	0.000	0.000	0.000	0.000	0.000	0.000	0.000	0.000	0.000	0.000	0.000
29	720	0.000	0.000	0.000	0.000	0.000	0.000	0.000	0.000	0.000	0.000	0.000	0.000
30	785	0.000	0.000	0.000	0.000	0.000	0.000	0.000	0.000	0.000	0.000	0.000	0.000

2
VITA

Raul Adarme Mayorga

Candidate for the Degree of

Doctor of Philosophy

Thesis: EFFECT OF ASPHALTENES ON THE PERFORMANCE OF HDS
CATALYSTS USED IN GRADED BEDS

Major Field: Chemical Engineering

Biographical:

Personal Data: Born in Colombia, South America, July
28, 1961, the son of Efrain and Mery del C.
Adarme.

Education: Graduated from Industrial University of
Santander with an Engineering Degree in June,
1983; Graduated from Oklahoma State University
with a Master of Science Degree in December,
1986; completed requirements for Doctor of
Philosophy Degree at Oklahoma State University in
December, 1989.

Professional Experience: Engineering Trainee at
Ecopetrol Refinery, Cartagena, Colombia, 1981;
Teaching Assistant at Industrial University of
Santander, July, 1983 to July, 1984; Research
Assistant at Oklahoma State University, May, 1985
to July, 1986; Teaching Assistant at Oklahoma
State University, August, 1986 to August, 1988;
Cooperative Graduate Research Student at Phillips
Research Center, Bartlesville, Oklahoma,
September, 1988 to September, 1989; Member, Omega
Chi Epsilon Honor Society; Member, Tau Beta Pi
Honor Society.